CONSTITUTIVE MODELING AND SIMULATION OF THE SUPERELASTIC EFFECT IN SHAPE-MEMORY ALLOYS

Panos Papadopoulos

Department of Mechanical Engineering, University of California, Berkeley

Acknowledgments

T. Duerig, NDC

V. Imbeni, SRI

Y. Jung, PU

J.M. McNaney, LLNL

R.O. Ritchie, UCB

H.-R. Wenk, UCB

OUTLINE OF LECTURES

- Part I: Phenomenology and crystallographics
- Part II: Constitutive modeling
- Part III: Algorithmics

CONTENTS OF PART I

- Superelasticity and the shape-memory effect
- Technological applications
- Crystallography of solid-solid phase transitions
- Texture
- Experimental results

Superelasticity

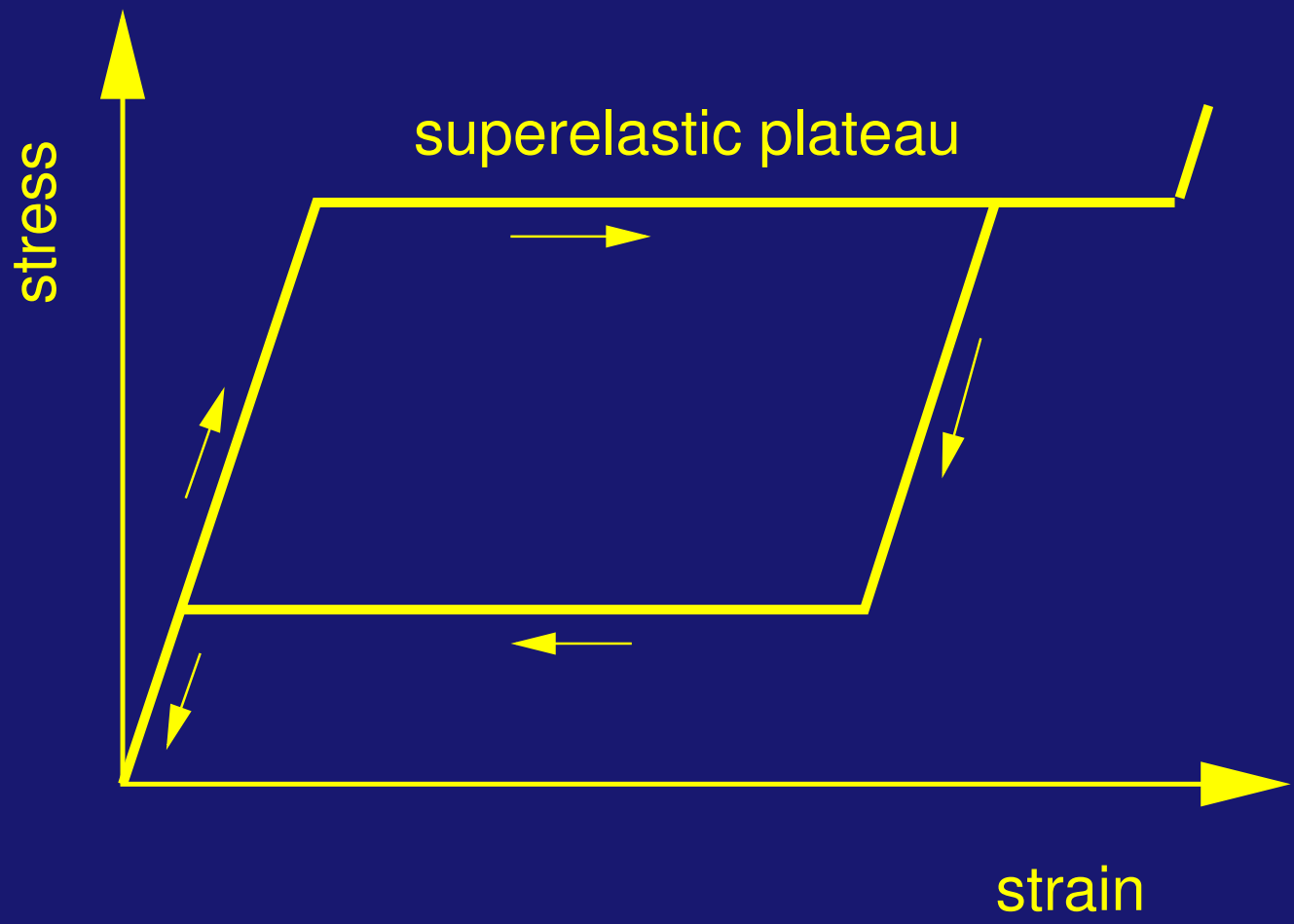

The superelastic effect (at constant temperature)

Superelasticity

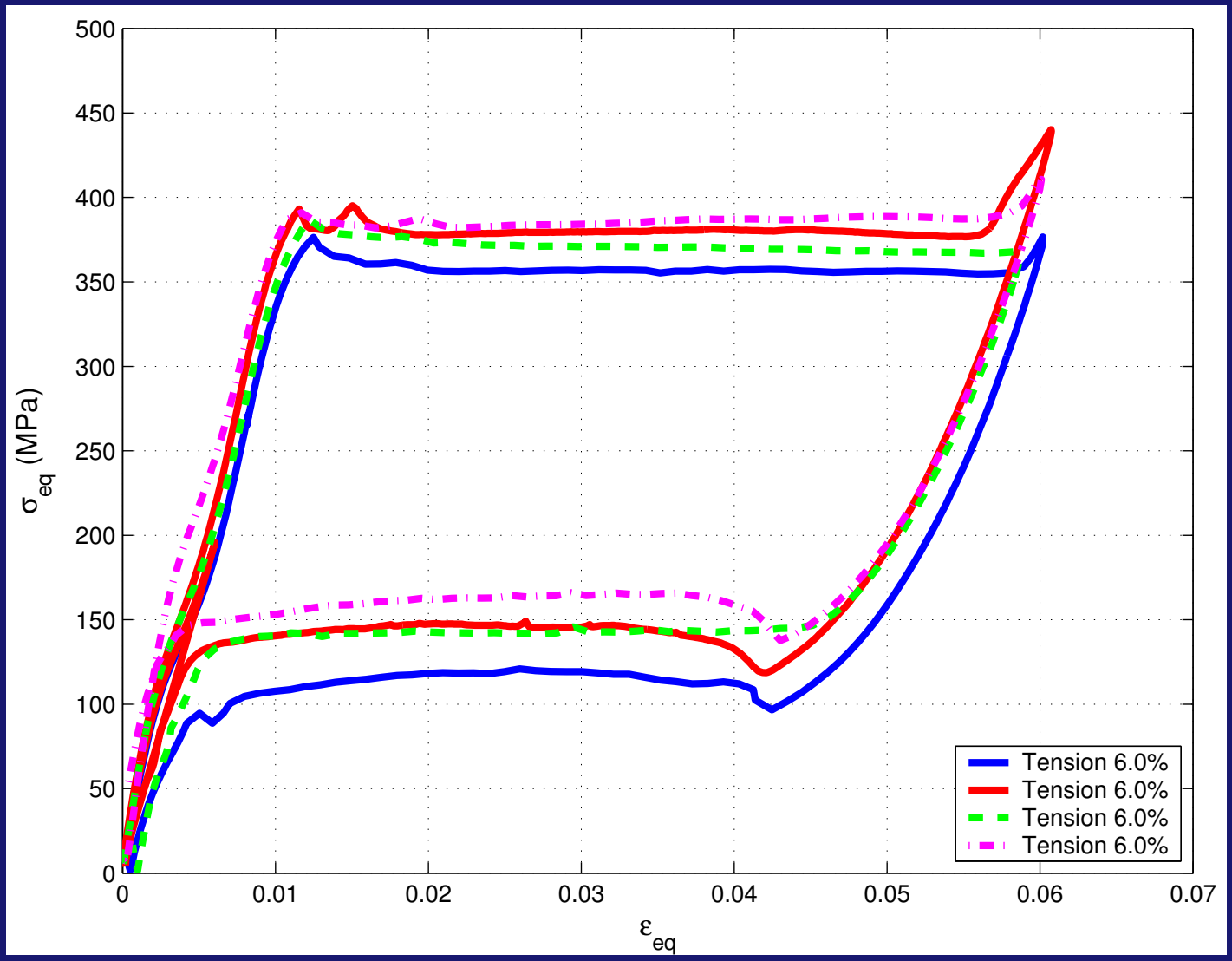

Uniaxial stress-strain plot of polycrystalline superelastic Ni-Ti

Superelasticity

Superelasticity is a property of crystalline materials.

Typical examples of known superelastic materials:

- Ni-Ti

  Nitinol (acronym for Nickel Titanium Naval Ordnance Laboratory) is the most widely used superelastic material.
- Cu-Zn-Al
- Cu-Al-Ni
- Co-Ni-Al
- Fe-Mn-Si

Applications

(Courtesy: NDC Inc.)

Typical biomedical devices made of Nitinol

The superelastic effect is due to the displacive, diffusionless, reversible, solid-solid transformation between an austenitic (highly structured) phase and a martensitic (less structured) phase.

Examine in detail the Ni-Ti crystal:

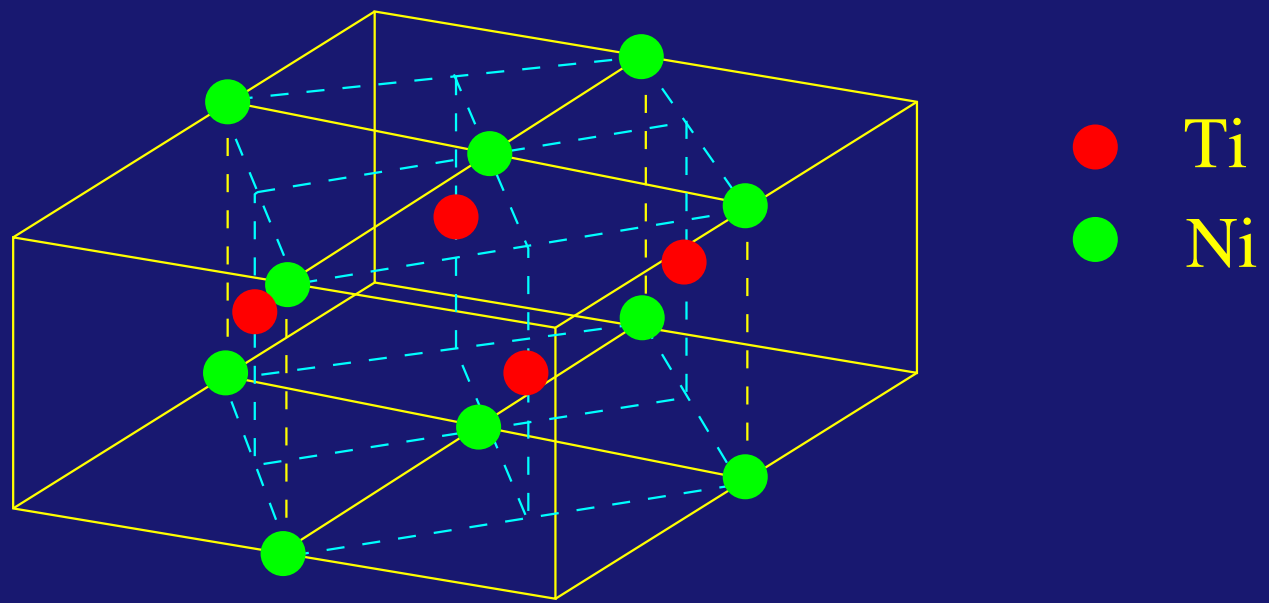

Austenite (body-centered cubic crystal)

The superelastic effect is due to the displacive, diffusionless, reversible, solid-solid transformation between an austenitic (highly structured) phase and a martensitic (less structured) phase.

Examine in detail the Ni-Ti crystal:

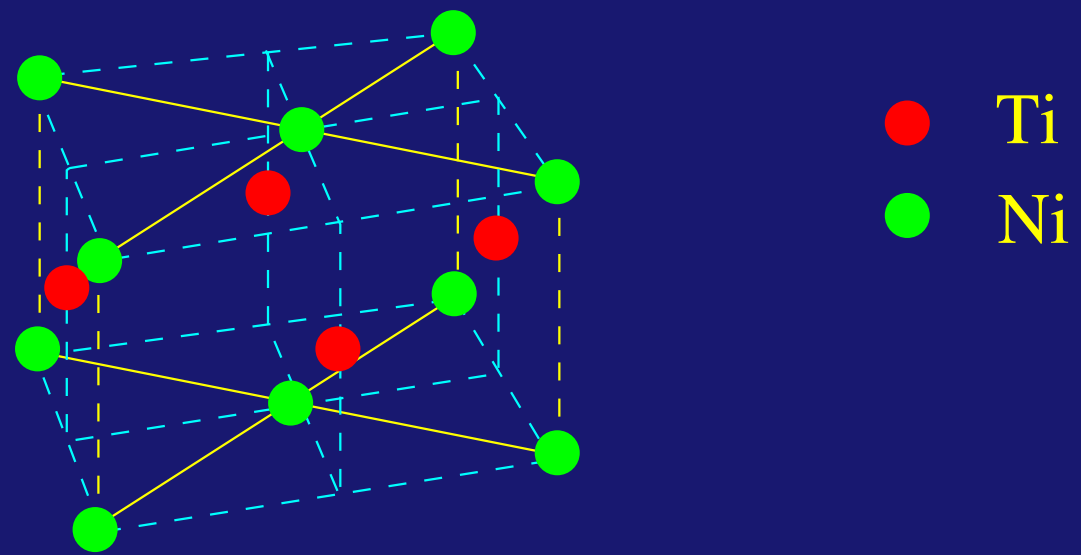

Austenite (body-centered cubic crystal)

The superelastic effect is due to the displacive, diffusionless, reversible, solid-solid transformation between an austenitic (highly structured) phase and a martensitic (less structured) phase.

Examine in detail the Ni-Ti crystal:

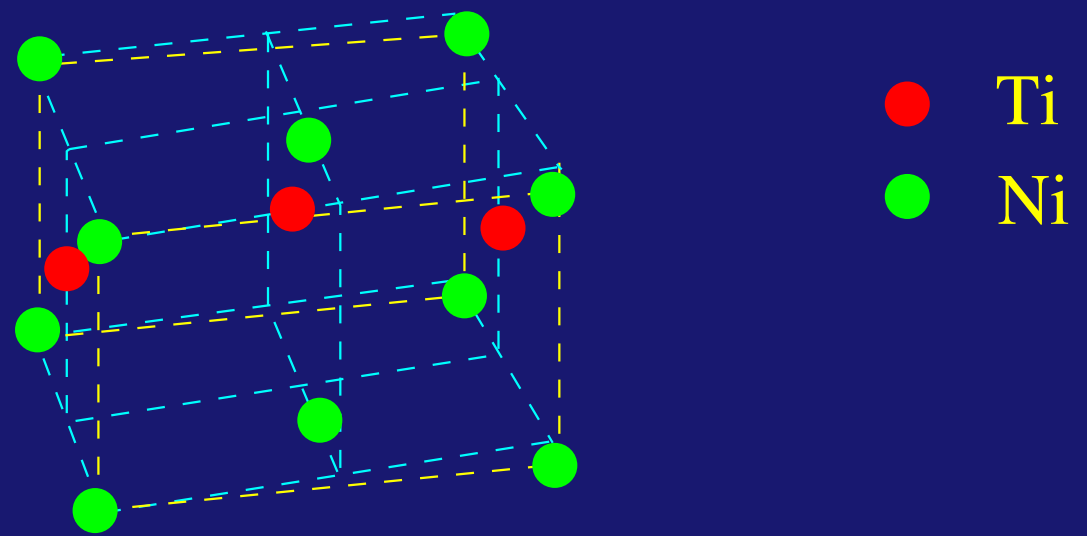

Martensite (monoclinic crystal)

The interface between austenite and martensite is called the habit plane.

How does martensite grow inside an undistorted austenite matrix?

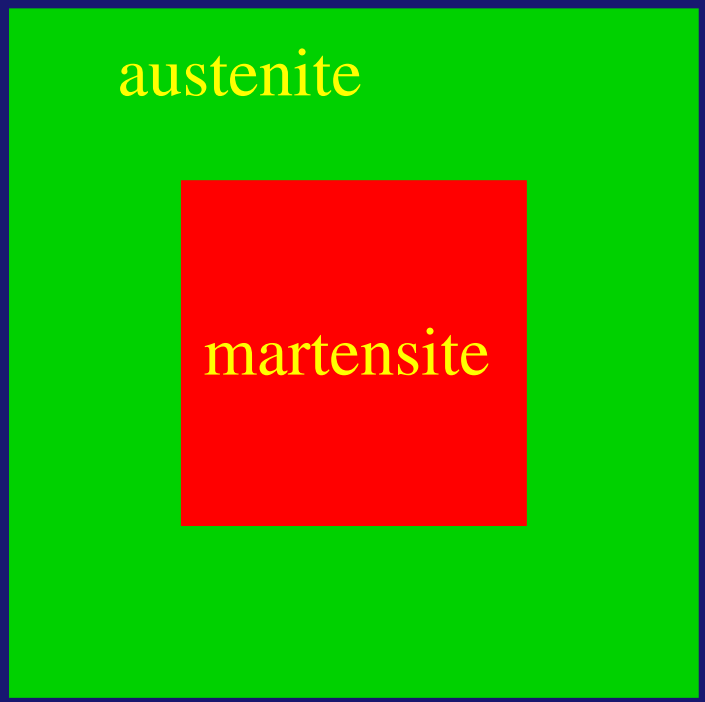

The interface between austenite and martensite is called the habit plane.

How does martensite grow inside an undistorted austenite matrix?

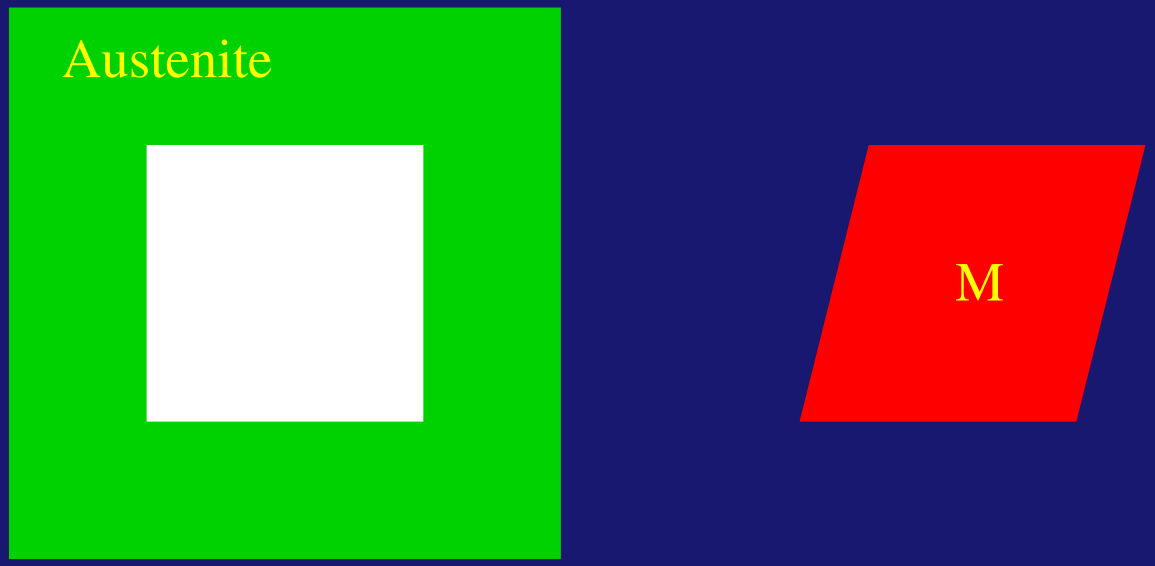

Lattice distortion (incompatible!)

The interface between austenite and martensite is called the habit plane.

How does martensite grow inside an undistorted austenite matrix?

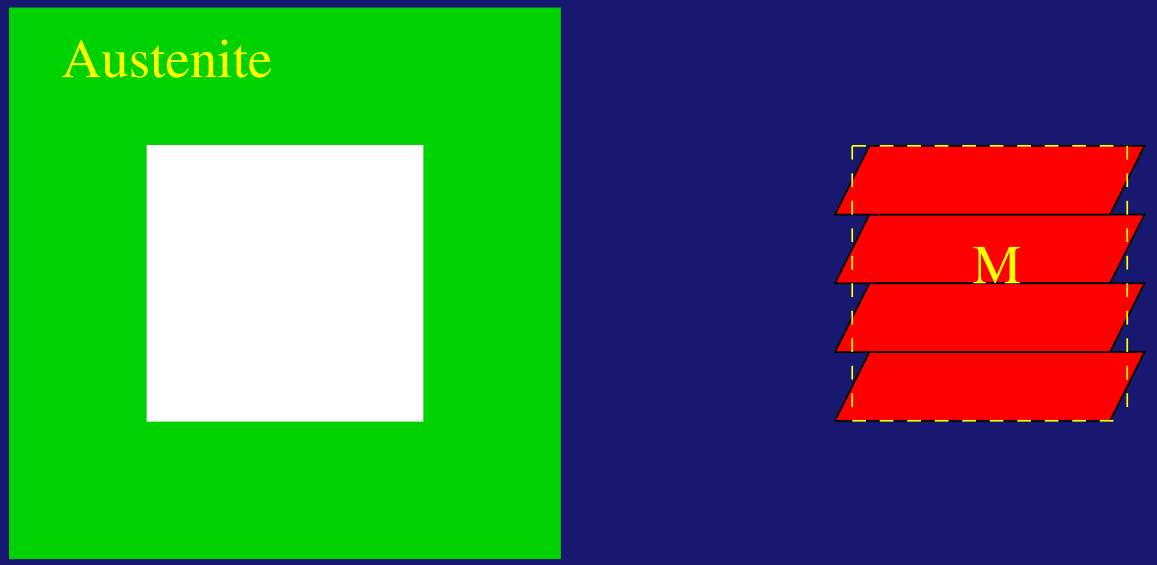

Single martensite with slip (irreversible process)

The interface between austenite and martensite is called the habit plane.

How does martensite grow inside an undistorted austenite matrix?

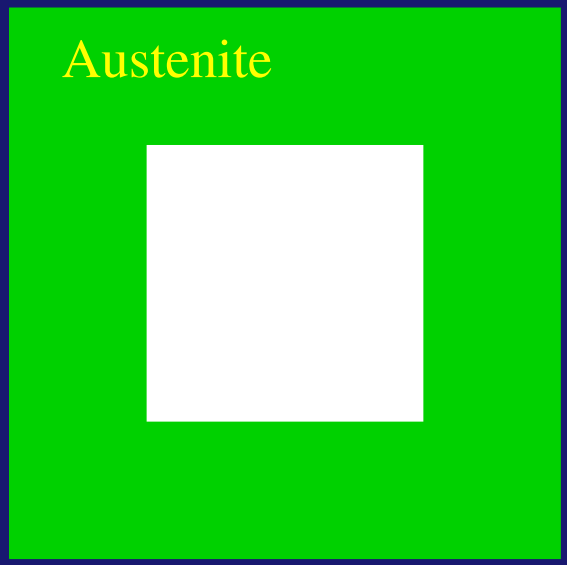

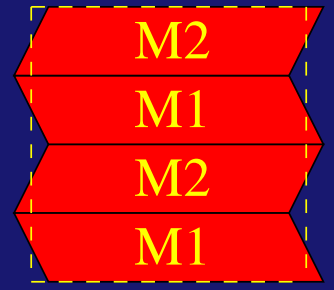

Twin martensite variants (reversible process)

How does martensite grow under imposed shear-like deformation?

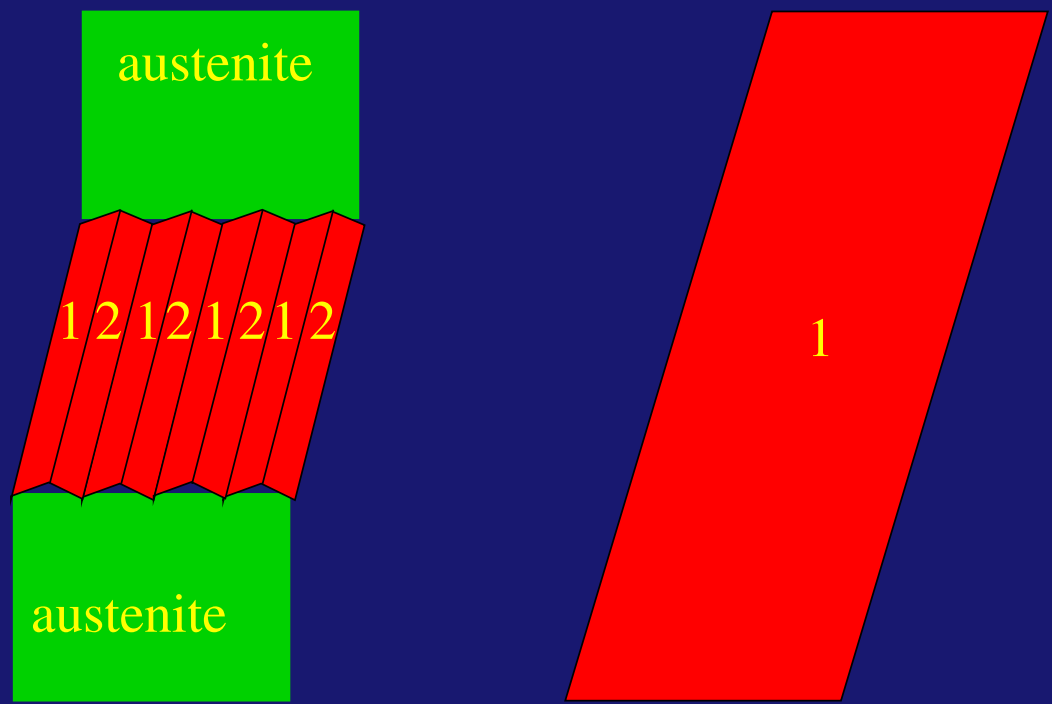

Austenite initially transforms to twinned martensite, which, in turn, gives way to single variant martensite (detwinning).

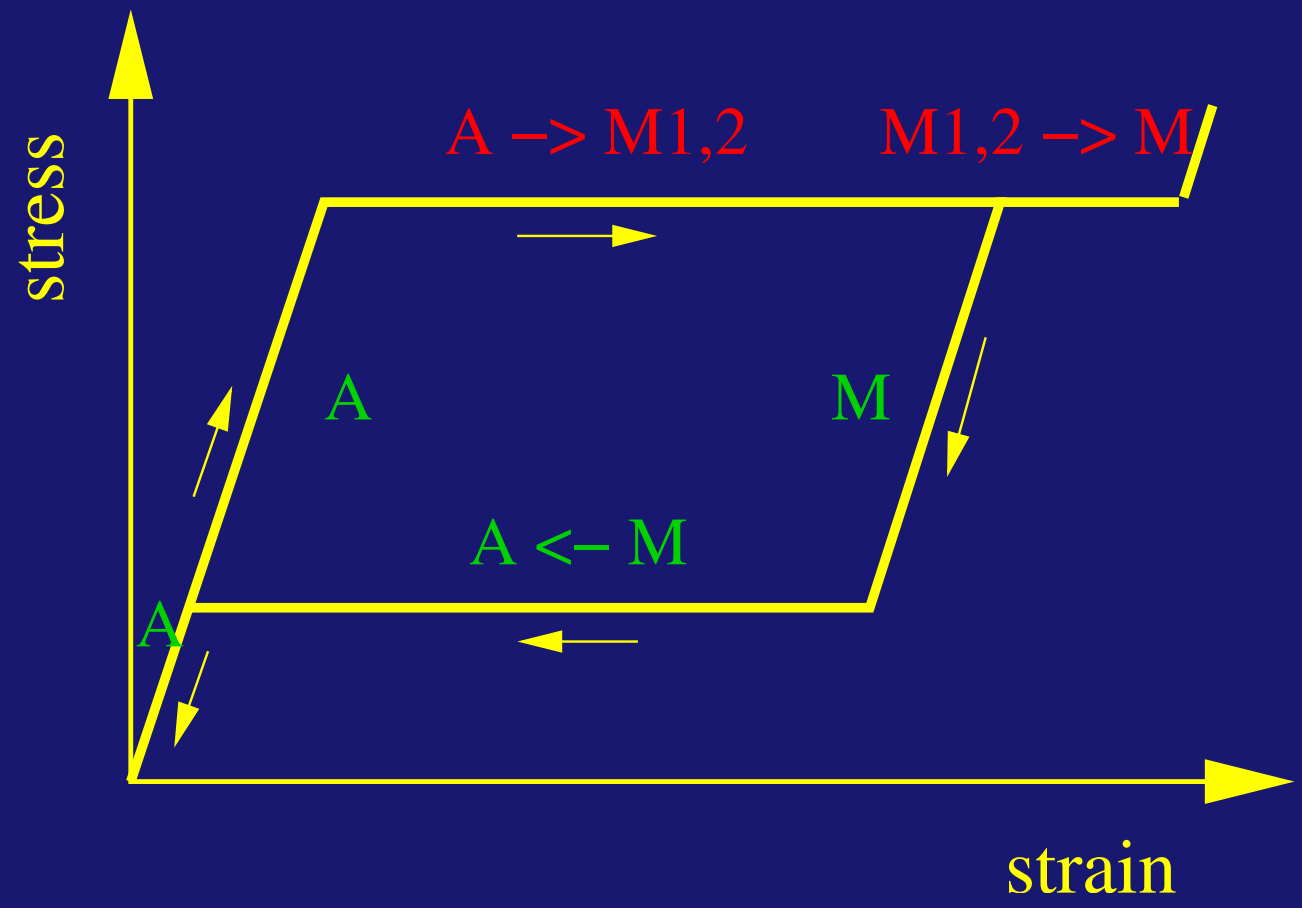

Microstructural interpretation of the superelastic effect

Shape-memory effect

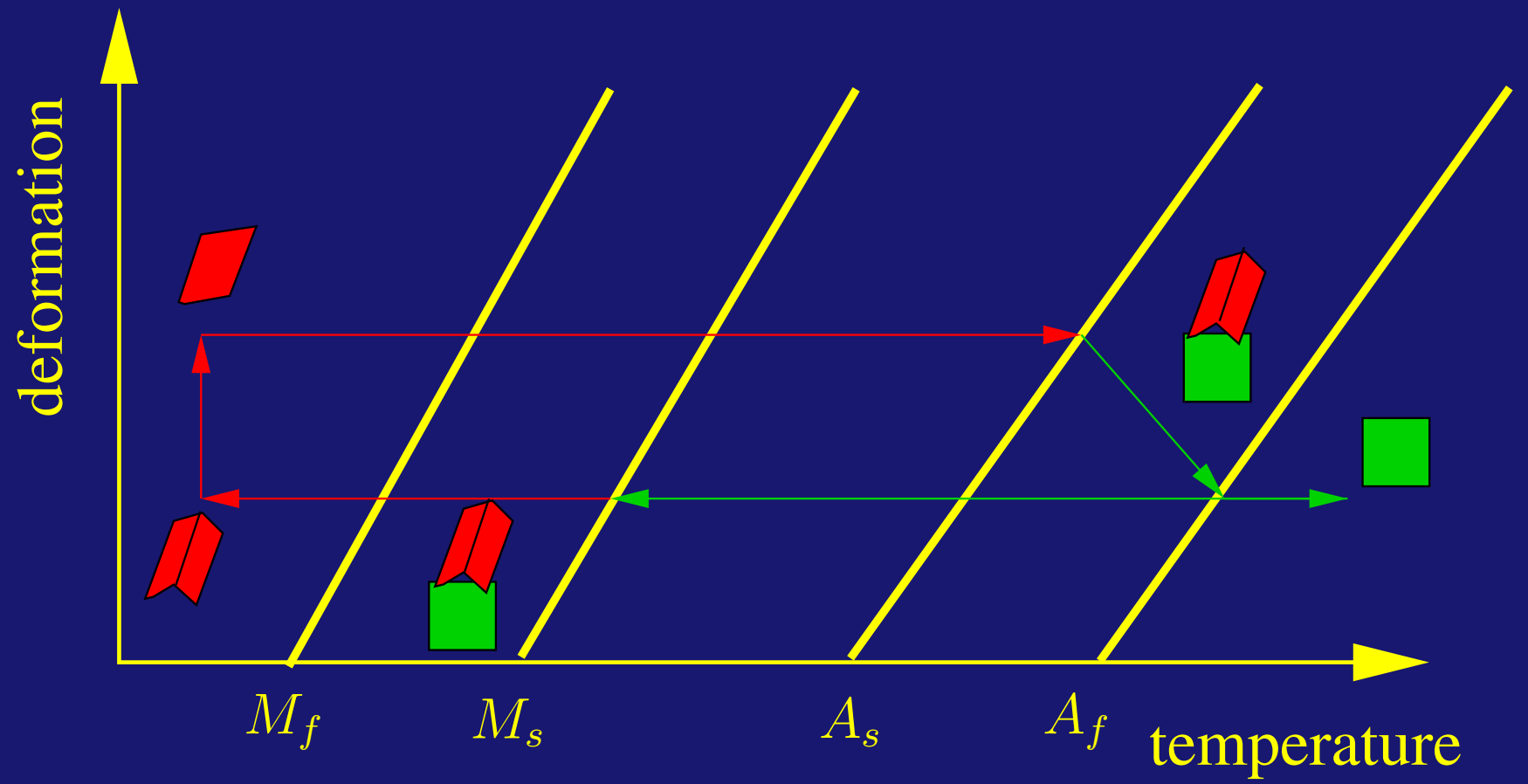

Microstructural interpretation of shape-memory effect

Material

Consider a thin-walled Nitinol tube, which is the starting component for manufacturing various biomedical devices.

Composition: Ti 44.5 wt.%, Ni 55.5 wt.%

Heat-treatment at $485°$C in air (5 min), followed by water-quenching to produce a microstructure that enhances the superelastic properties.

Transformation temperatures:

$$A_s = -6.36°C \quad , \quad A_f = 18.13°C$$
$$M_s = -51.55°C \quad , \quad M_f = -87.43°C$$

Material

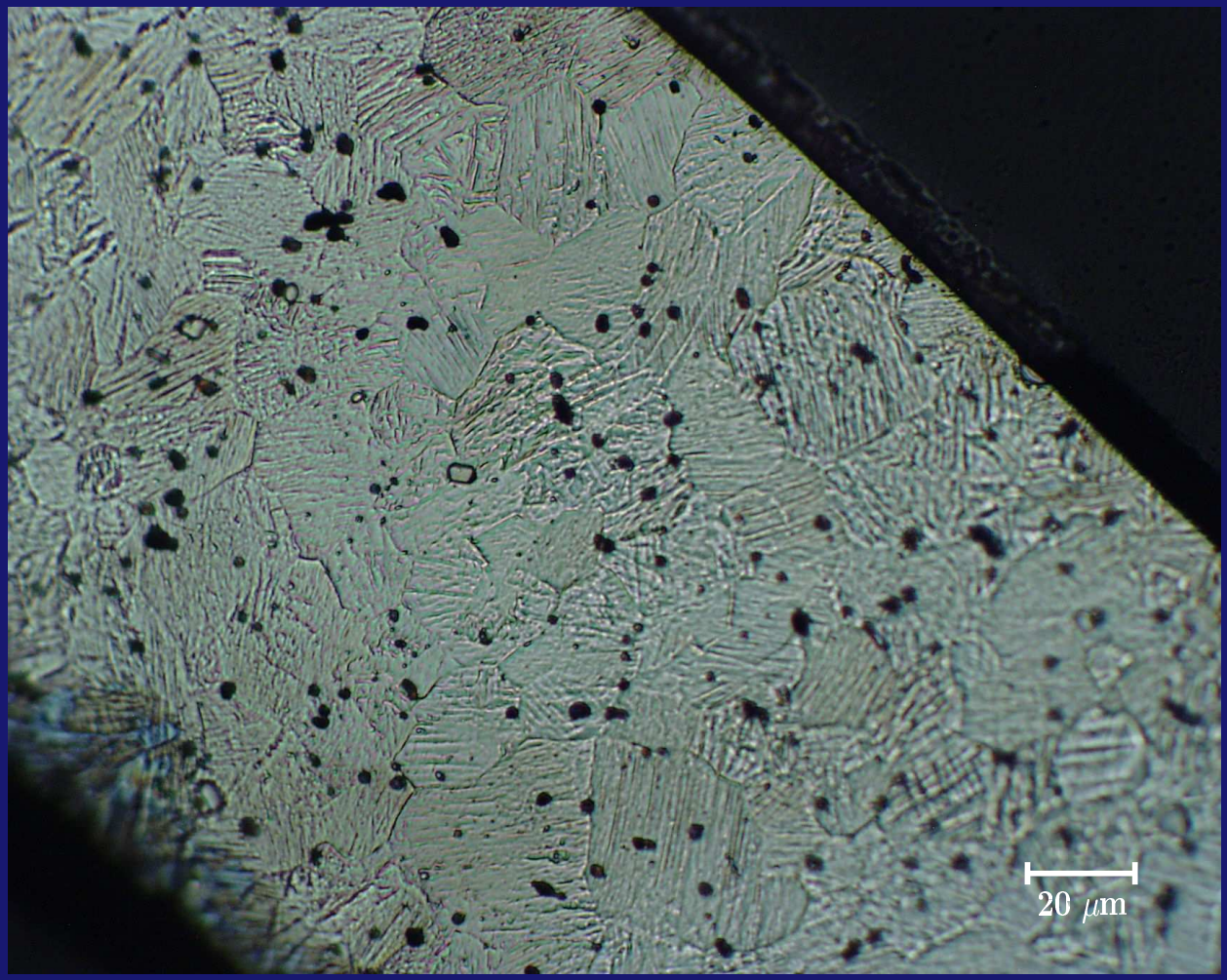

Optical micrograph of a portion of the cross section of a thin-walled Nitinol tube (note the polycrystalline structure)

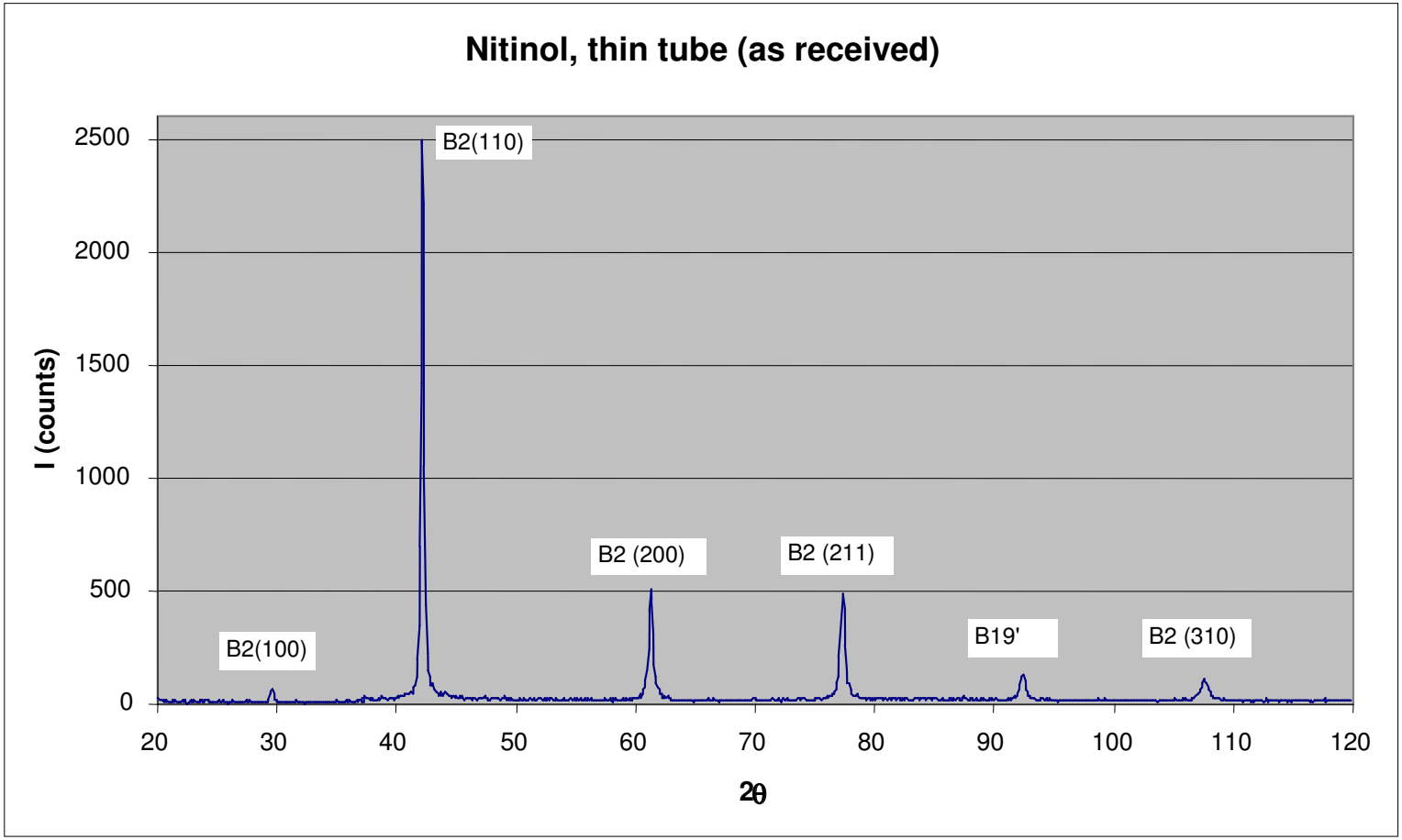

X-ray diffraction analysis of as received Ni-Ti material

Texture

In polycrystalline solids, the overall mechanical response may depend strongly on the preferred lattice orientation of the crystals, i.e., on the texture of the polycrystal.

In superelastic materials, texture may affect the mechanical behavior in two ways:

- By controlling the phase transformation process (i.e., by enabling nucleation of certain variants and not others).
- By inducing anisotropy in the continuum-level elastic response.

Texture measurements can be taken using X-ray or electron diffractometry.

Texture

Texture measurements are represented using stereographic projections of the spherical poles corresponding to the normal to a given crystal plane, when the plane is assumed to pass through the center of the sphere (pole figures).

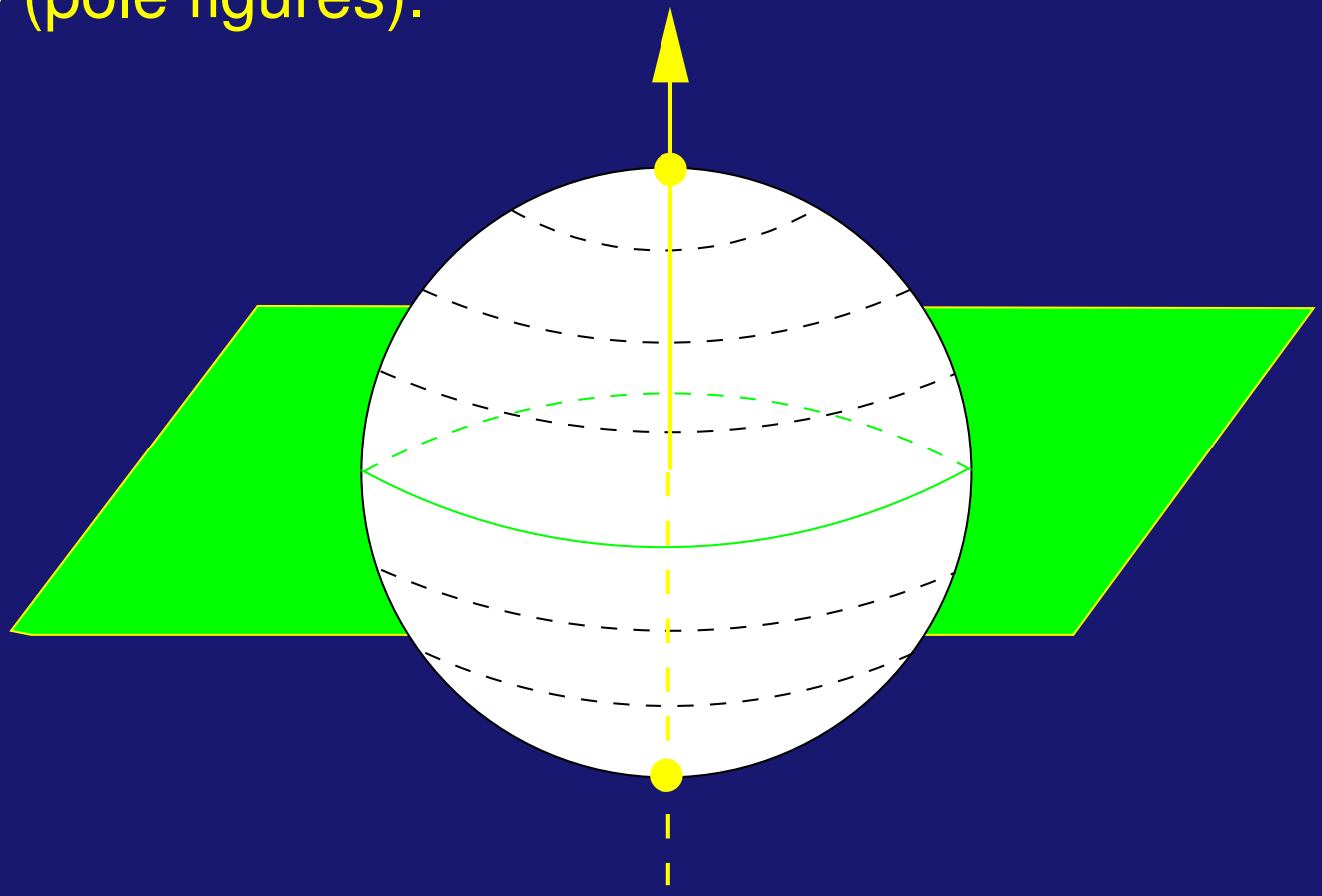

Texture

The tube manufacturing process induces primarily $\langle 111 \rangle \{ 110 \}$-type sheet texture "wrapped" around the cylindrical surface, such that the $\langle 111 \rangle$ austenite lattice direction is aligned with the longitudinal axis of the tube.

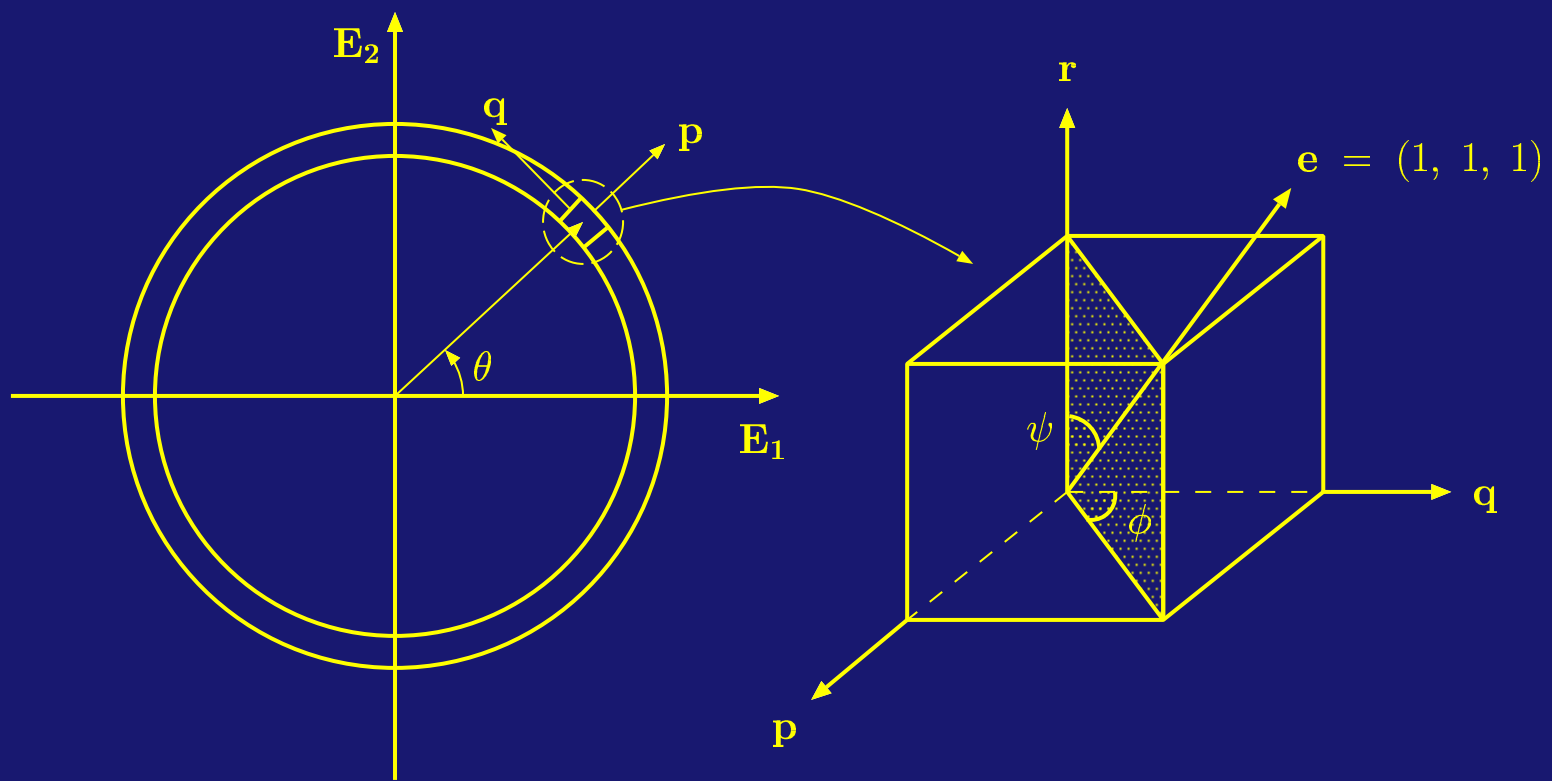

Texture

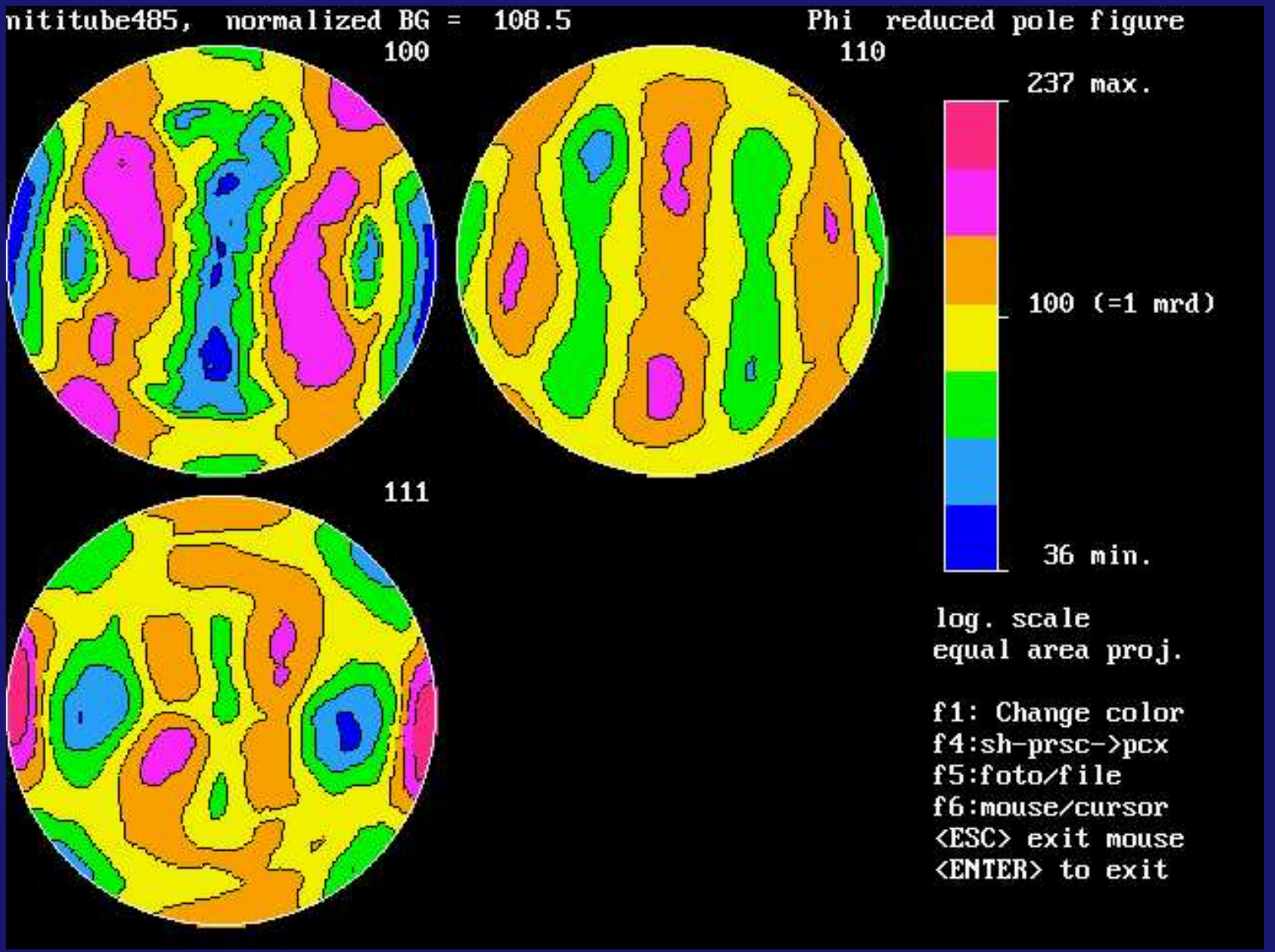

Pole figures for Nitinol tubes (R.D. horizontal, T.D. vertical)

Experiments

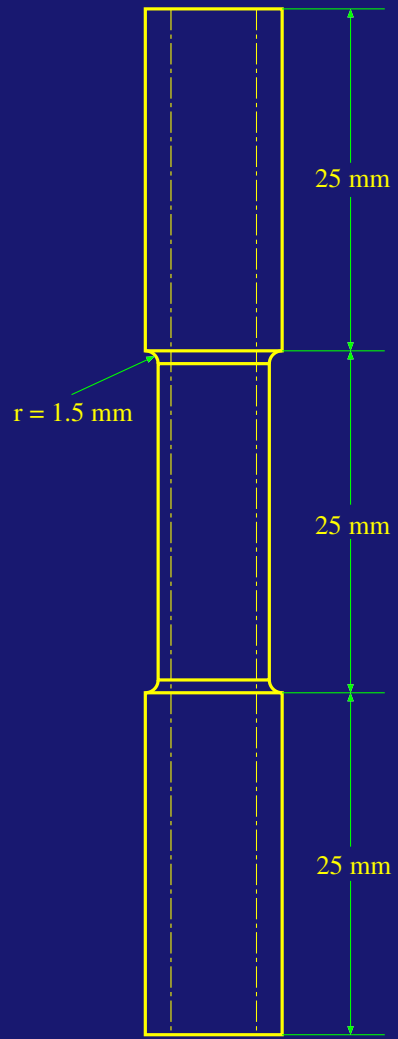

Test section

thickness $= 0.20mm$

outer radius $= 2.15mm$

Gripping sections

thickness $= 0.37mm$

outer radius $= 2.32mm$

Schematic illustration of the NiTi specimen (not to scale)

Experiments

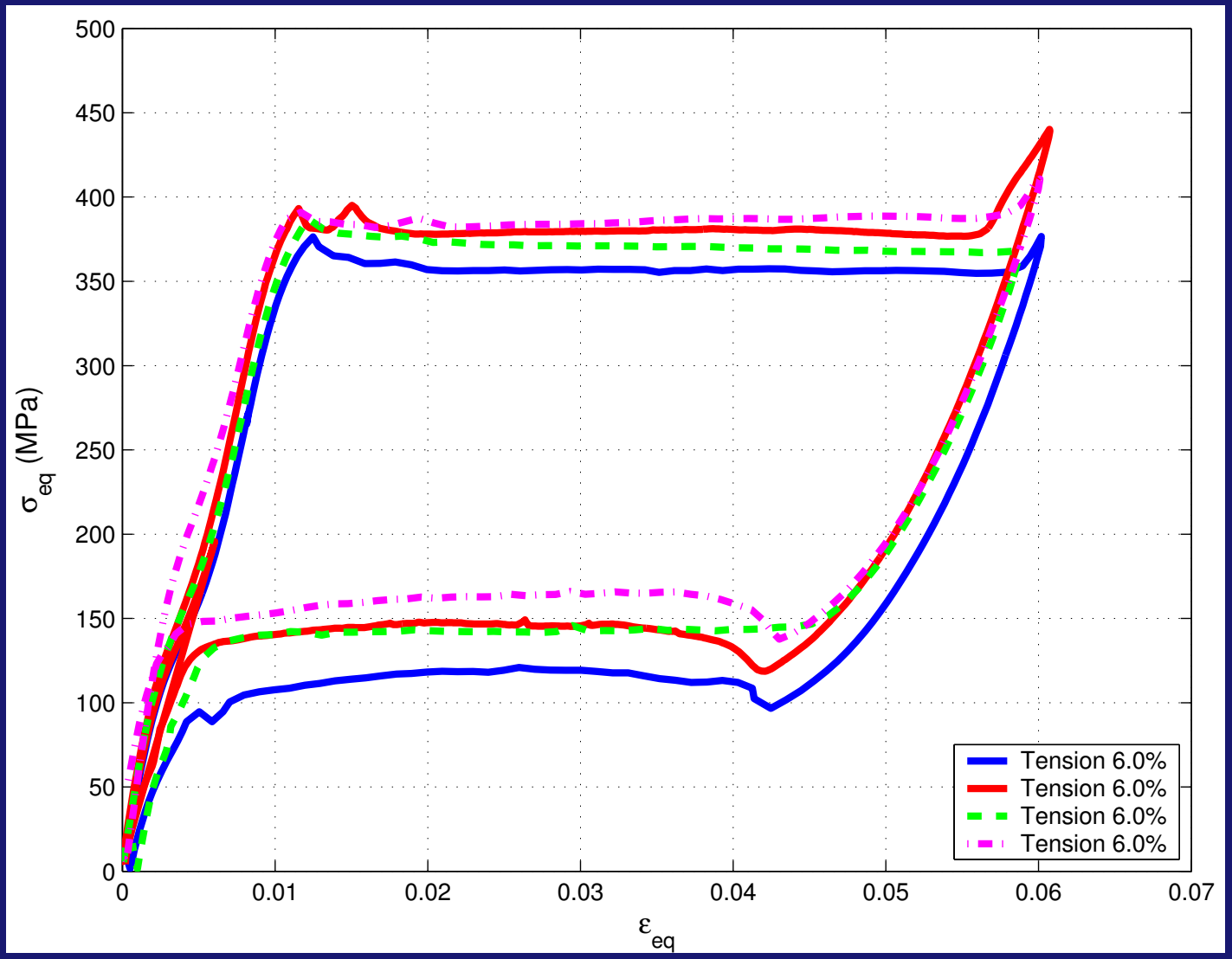

Equivalent stress-strain plot showing repeatability of tension tests

Experiments

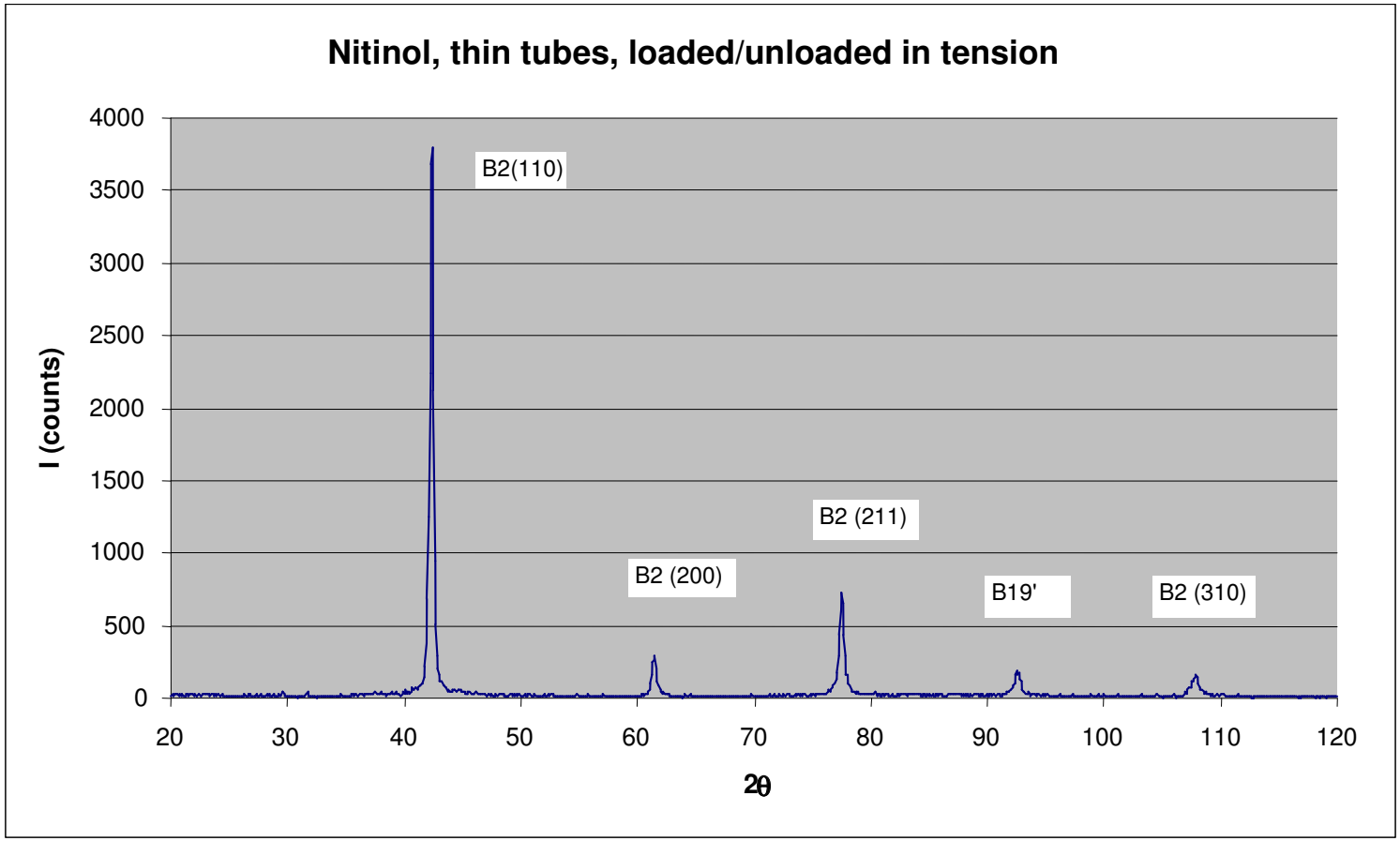

X-ray diffraction after complete tension cycle

Experiments

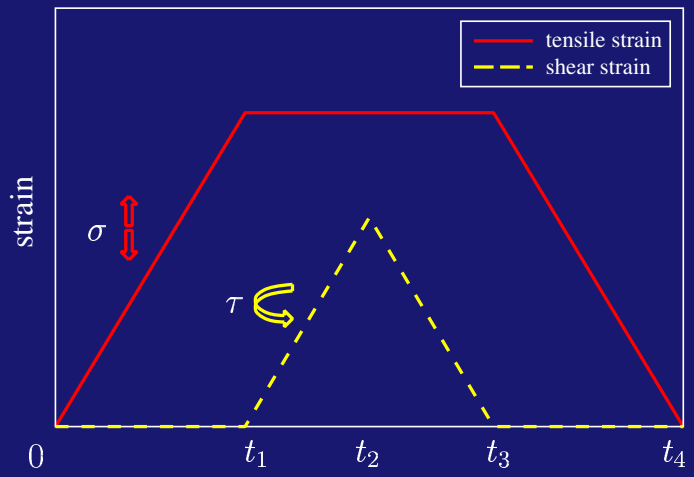

(a) Tension followed by torsion (TYPE I)

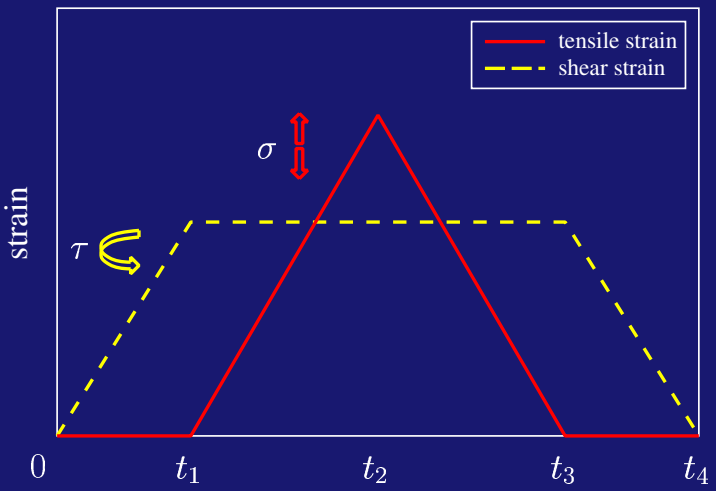

(b) Torsion followed by tension (TYPE II)

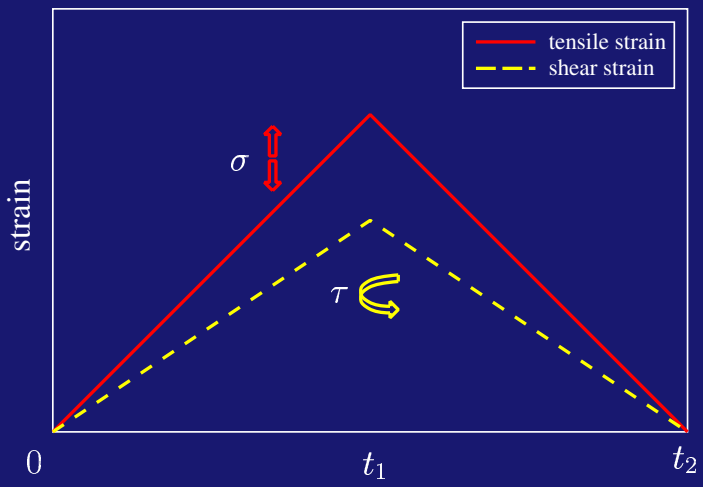

(c) Simultaneous tension-torsion (TYPE III)

Strain/time sequence for TYPE I, II, III loading

Experiments

The experimental setup provided measurements of the equivalent Cauchy (true) stress σ_{eq} versus the equivalent Lagrangian strain ε_{eq}, namely

$$\sigma_{eq} = \sqrt{\sigma_t^2 + 3\sigma_s^2} \quad , \quad \varepsilon_{eq} = \sqrt{\varepsilon_t^2 + \frac{4}{3}\,\varepsilon_s^2}\,,$$

where σ_t and σ_s denote the tensile and shearing stress, while ε_t and ε_s denote the tensile and shearing strain.

Strain rates were imposed in the 10^{-5}/s to 10^{-4}/s were used for both the tensile and torsional loading.

Experiments

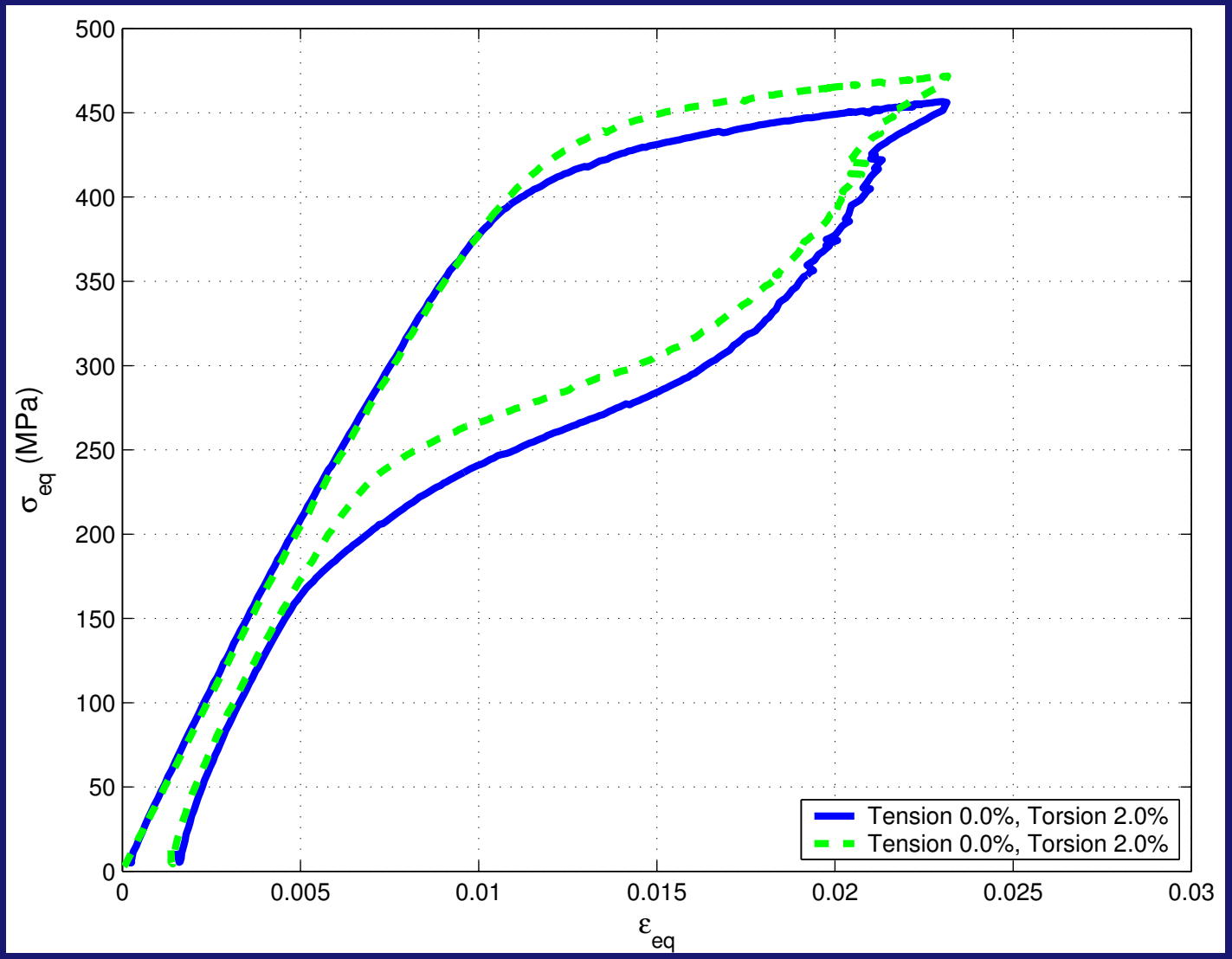

Equivalent stress-strain plot showing repeatability of torsion tests

Experiments

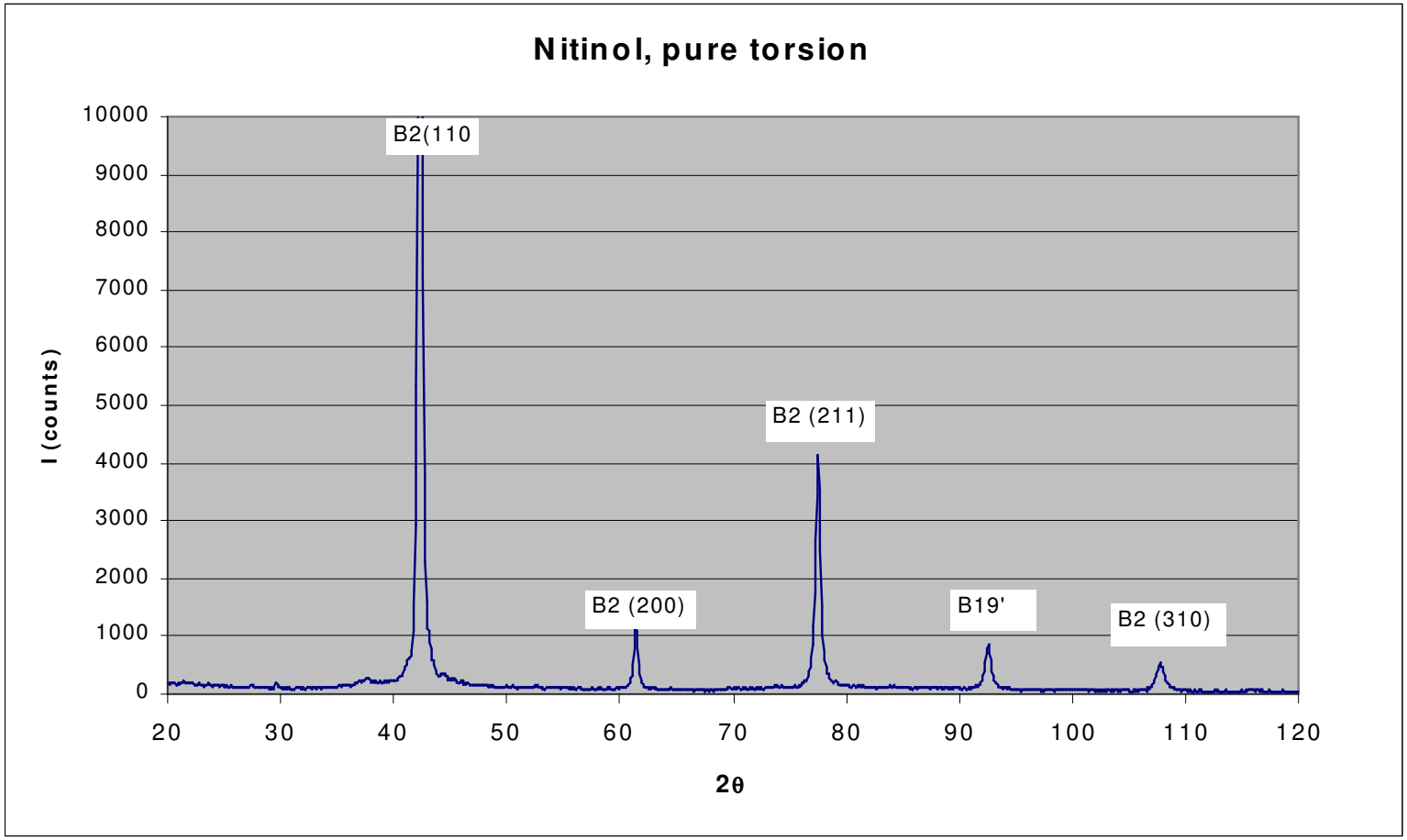

X-ray diffraction after complete torsion cycle

Experiments

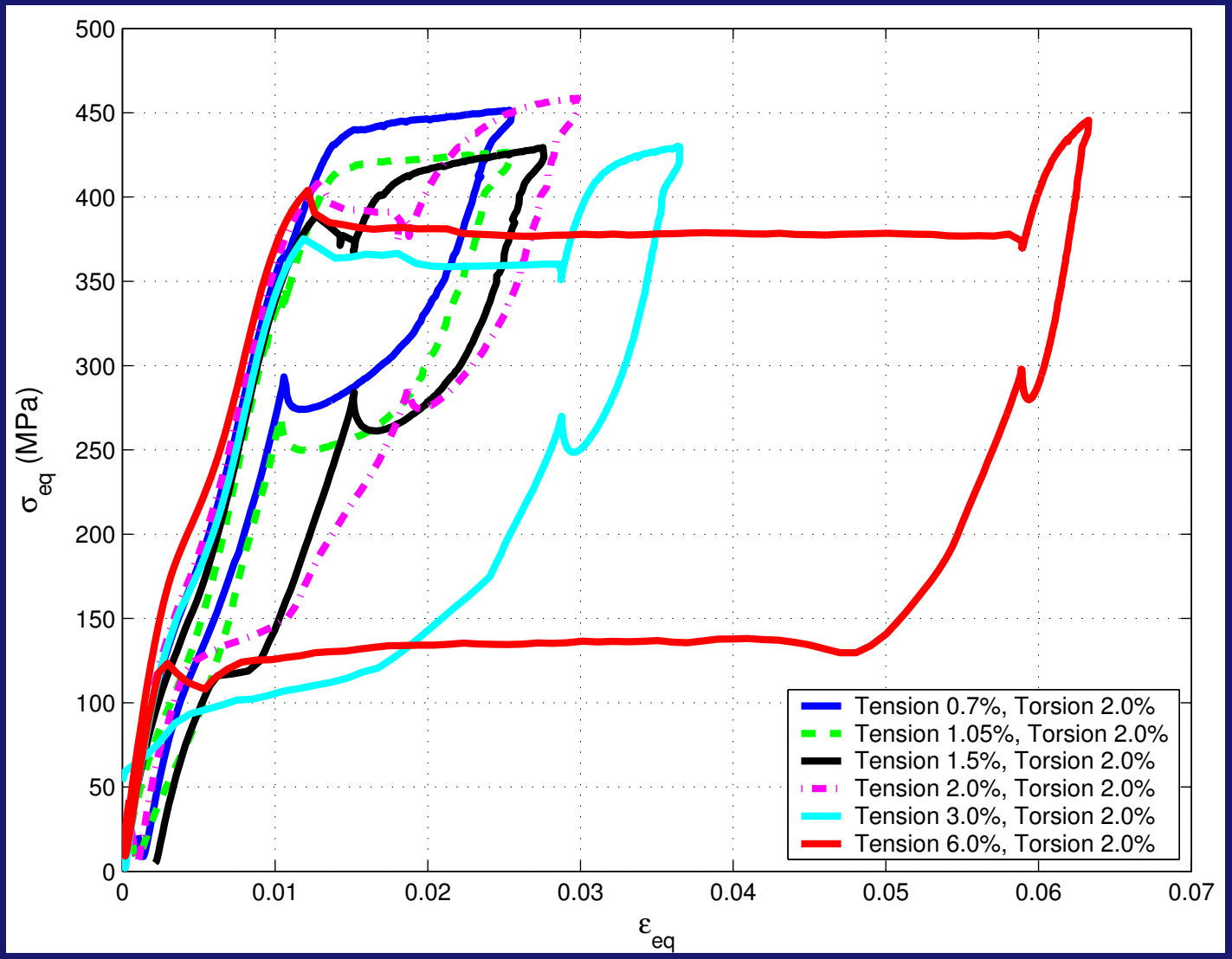

Equivalent stress-strain plot of tension followed by torsion (TYPE I)

Experiments

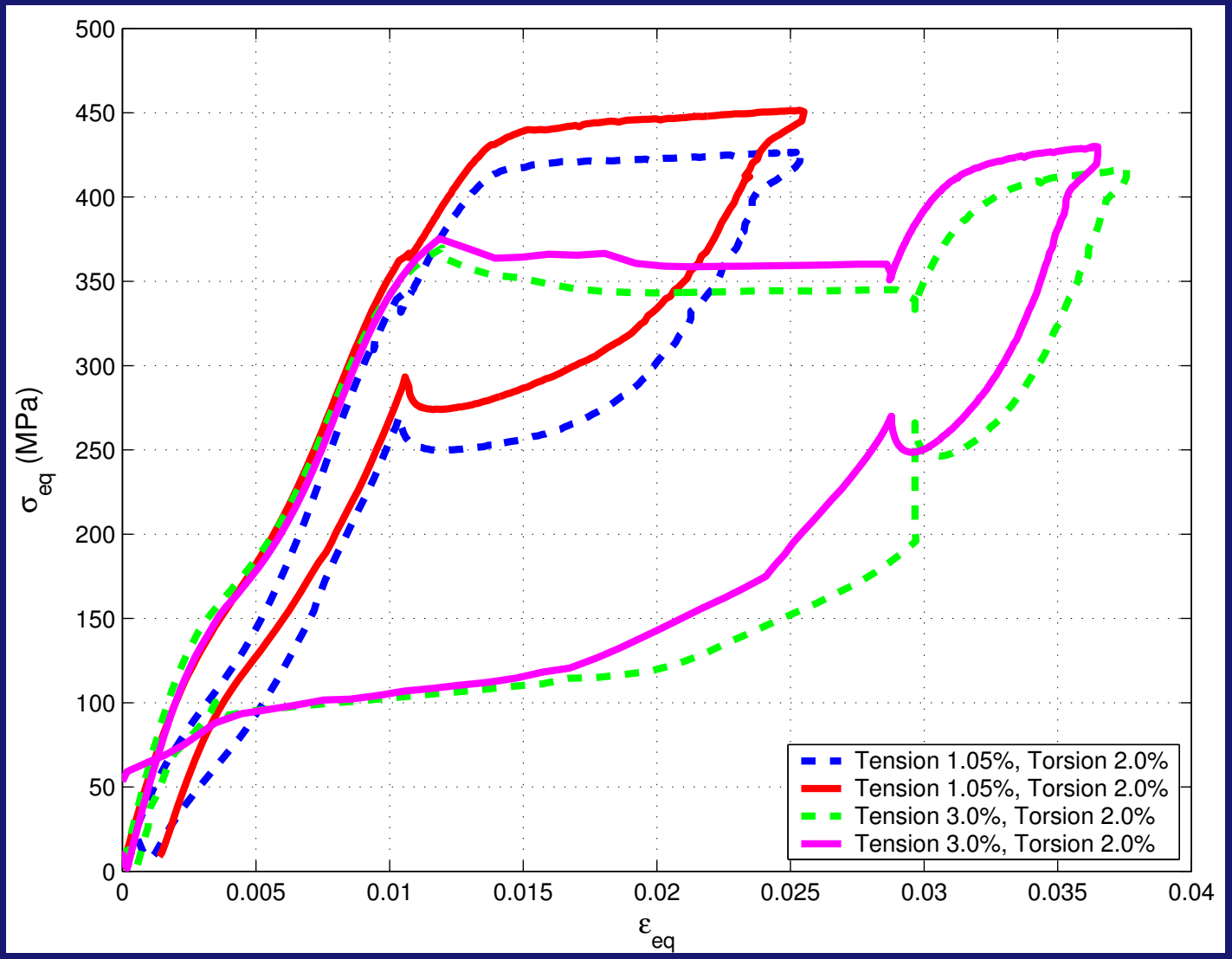

Equivalent stress-strain plot showing repeatability of TYPE I tests

Experiments

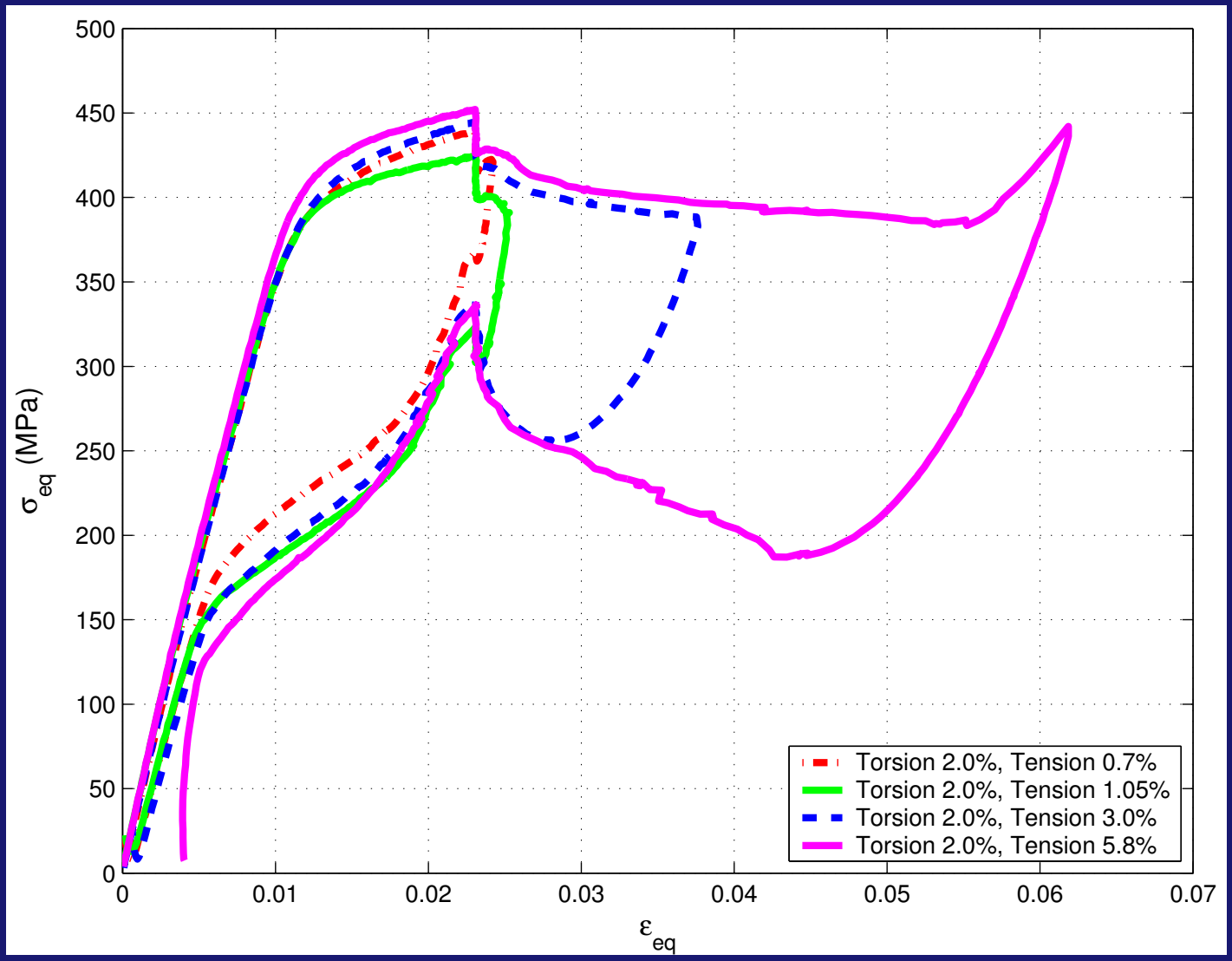

Equivalent stress-strain plot of torsion followed by tension (TYPE II)

Experiments

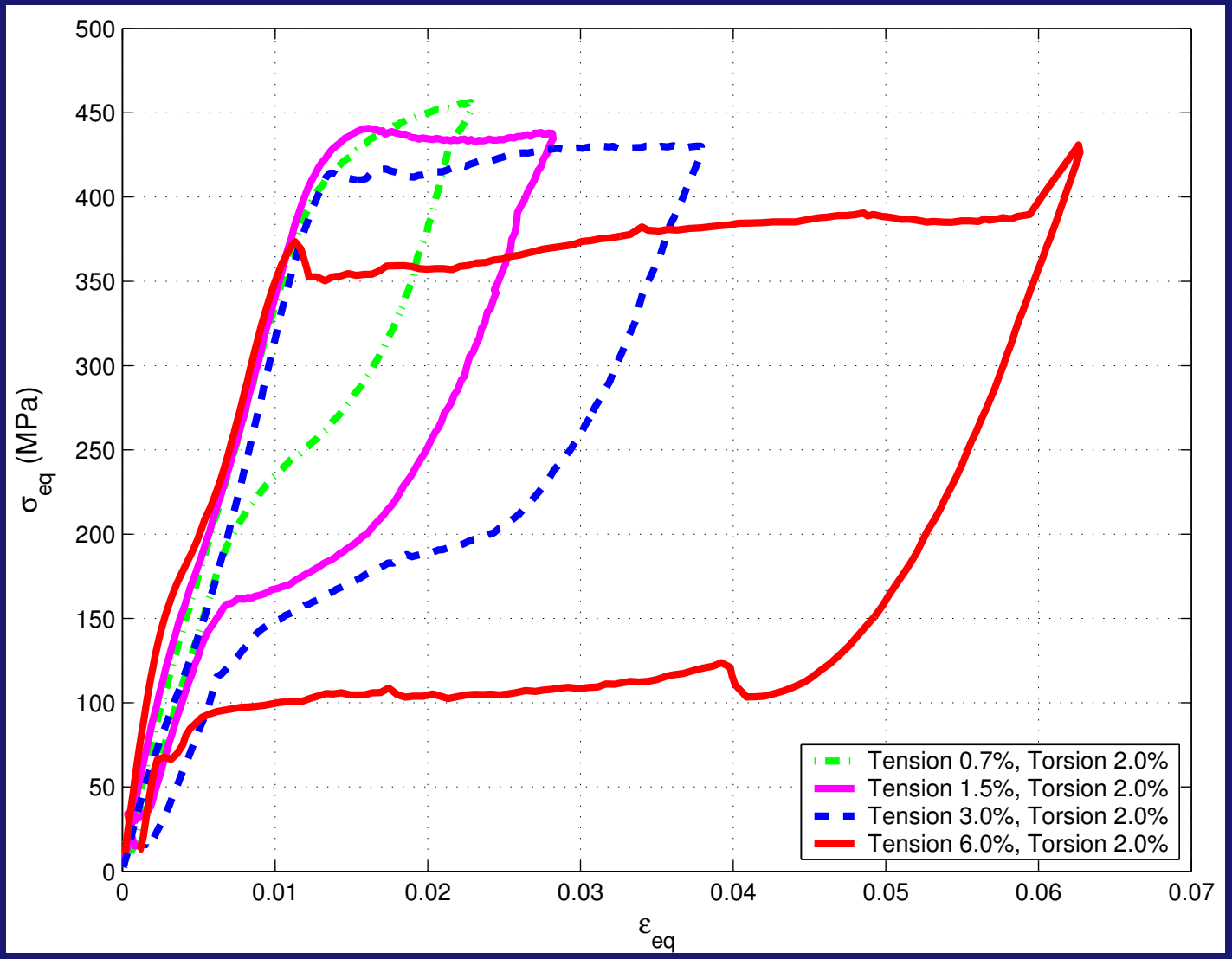

Equivalent stress-strain plot of simultaneous tension-torsion (TYPE III)

Closure

- In superelastic materials, austenite-to-martensite phase transformation occurs by nucleation of martensite twins, followed by detwinning.
- The stress-strain response is rich and complex, especially under non-proportional loading.
- The response to torsion defies the classical metal plasticity paradigm.
- The modeling of the mechanical response of superelastic materials leads to a multiscale problem.

  Martensite laminates, crystal grains, continuum

References

1. J.M. Ball and R.D. James, *Arch. Rat. Mech. Anal.*, **100**, pp. 13-52, (1987) [Non-linearly elastic theory of martensitic transformation].

2. K.F. Hane and T.W. Shield, *Acta Mater.*, **47**, pp. 2603-17, (1999) [Exhaustive description of the microstructure in NiTi phase transition].

3. K. Gall and H. Sehitoglu, *Int. J. Plast.*, **15**, pp. 69-92, (1999) [Role of texture in NiTi].

4. T.W. Duerig, A. Pelton and D. Stöckel, *Mater. Sci. Engrg.*, **A273-275**, pp. 149-160, (1999) [A review of biomedical applications of Nitinol].

5. J.M. McNaney, V. Imbeni, Y. Jung, P. Papadopoulos and R.O. Ritchie, *Mech. Mat.*, **35**, pp. 969-986, (2003) [Multiaxial experiments on polycrystal NiTi].

CONTENTS OF PART II

- Continuum modeling at the crystal grain level
- Loading and transformation criteria
- Connection between continuum and microstructural modeling
- A constrained optimization problem
- Twinned and detwinned martensite

Nomenclature:

$\mathbf{F}$	:	deformation gradient
$\mathbf{E}$	:	Lagrangian strain tensor
$\mathbf{U}$	:	Right stretch tensor
$\boldsymbol{\epsilon}$	:	Infinitesimal strain tensor
$\mathbf{P}$	:	1st (unsymmetric) Piola-Kirchhoff stress tensor
$\mathbf{S}$	:	2nd (symmetric) Piola-Kirchhoff stress tensor
$\boldsymbol{\sigma}$	:	Infinitesimal stress tensor
$\mathbf{Q}$	:	general rotation tensor
$\mathbf{I}$	:	second-order identity tensor

Consider constitutive modeling at the crystal grain level.

The total deformation induced by the martensitic transformation can be expressed in the form:

$$\mathbf{F} = \mathbf{F}_1\mathbf{F}_2\mathbf{R}_3 \ ,$$

where

- $\mathbf{F}_1$: lattice deformation
- $\mathbf{F}_2$: twinning deformation
- $\mathbf{R}_3$: rigid rotation

Of the three deformation components, $\mathbf{F}_1$ is dominant.

Modeling

There are three basic modeling choices at the crystal grain level:

- Model the transformation of austenite to detwinned martensite.

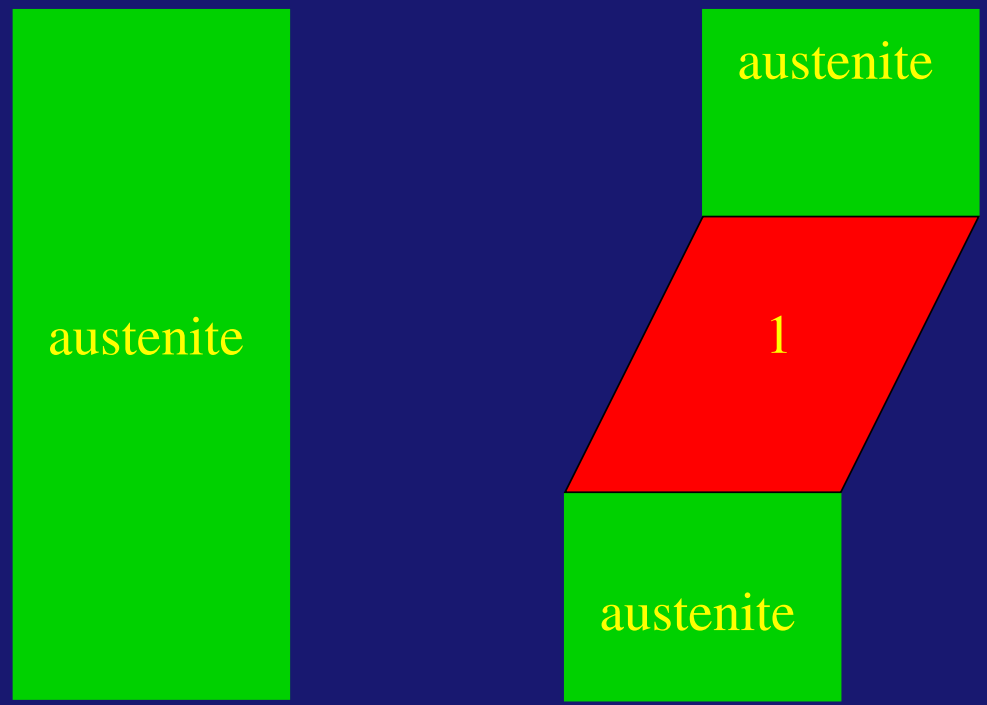

There are three basic modeling choices at the crystal grain level:

- Model the transformation of austenite to twinned martensite.

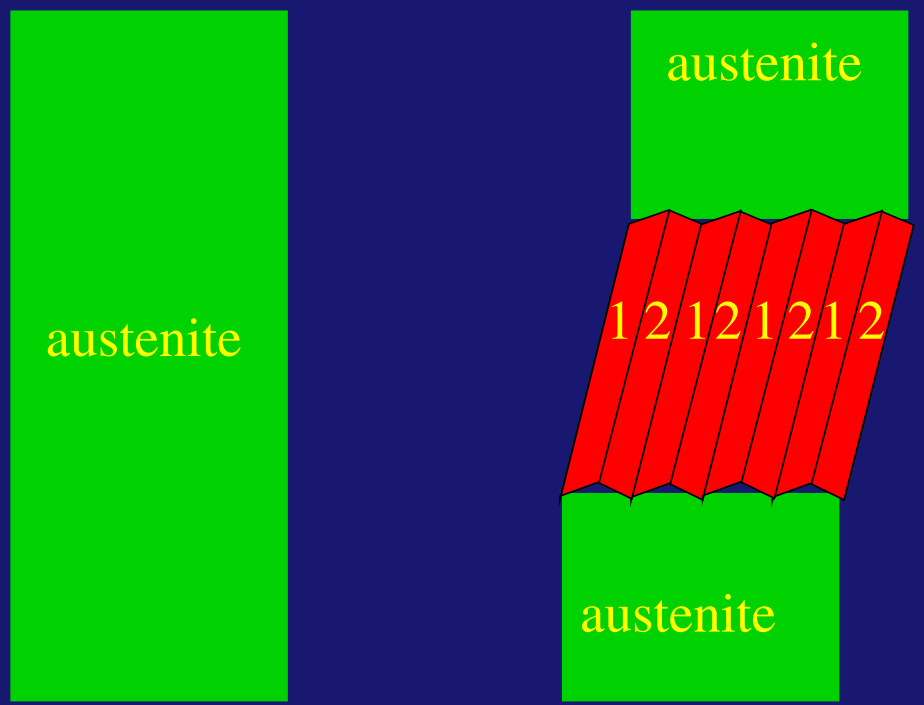

Modeling

There are three basic modeling choices at the crystal grain level:

- Model the transformation of austenite first to twinned martensite, then to detwinned martensite.

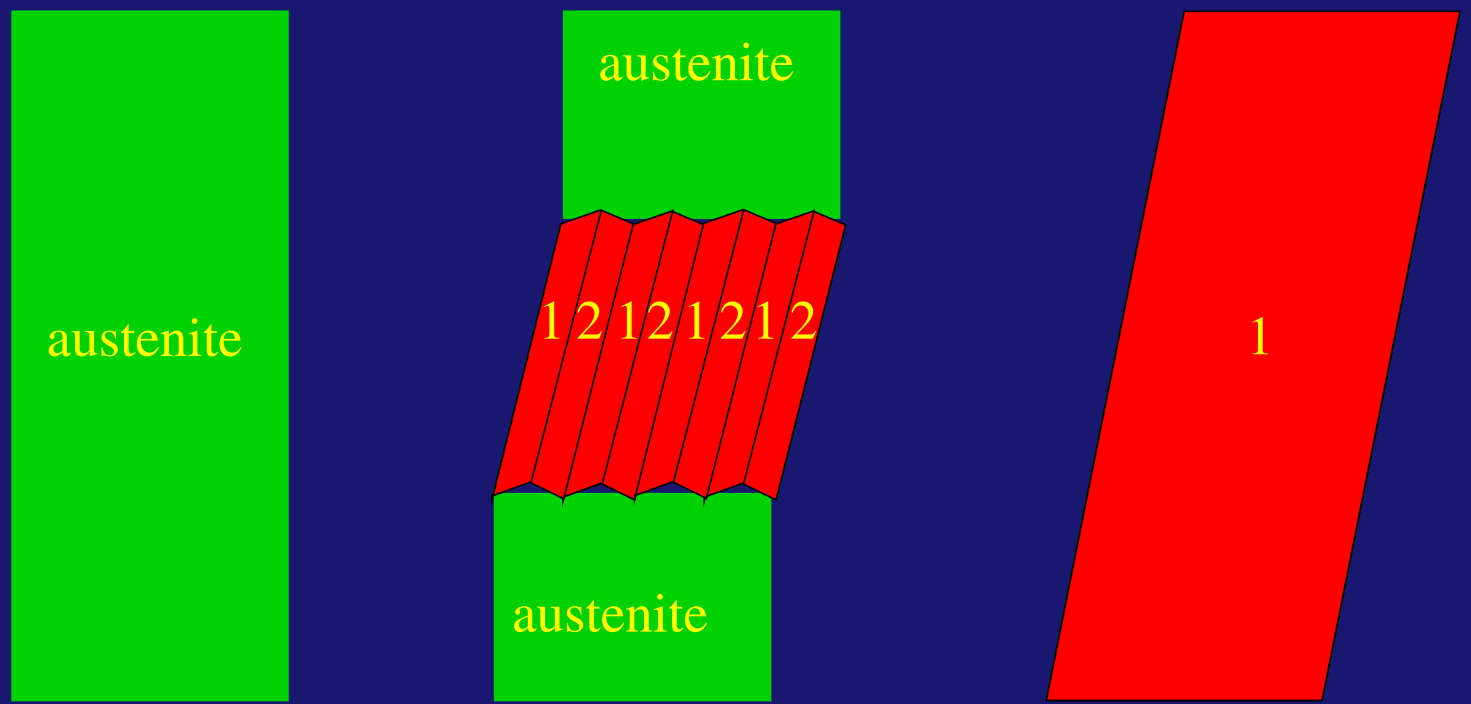

Consider first modeling the transformation of austenite to detwinned martensite. In the case of Ni-Ti (cubic to monoclinic transformation), there are a total of 12 martensite "lattice correspondence variants", i.e.,

$$\mathbf{F}_{1,i} \;=\; \mathbf{R}(\mathbf{Q}_i \mathbf{U} \mathbf{Q}_i^T) \;,\; i = 1, \ldots, 12 \;.$$

In the above polar decompositions, $\mathbf{R}$ is the rotation tensor, $\mathbf{U}$ is the unique stretch tensor, and $\mathbf{Q}_i$ are the 12 rotations corresponding to the 12 ways in which a cube maps onto itself.

The tensor $\mathbf{U}$ can be deduced from the crystallography of the austenite-martensite transformation.

Modeling

Consider next modeling the transformation of austenite to twinned martensite.

In the case of Ni-Ti (cubic to monoclinic transformation), one may expect up to 66x8 = 528 martensite “habit plane variants”.

Compatibility requirements reduce this number to 192 feasible habit plane variants. These variants can be obtained by an energy minimization method.

Of the 192 feasible habit plane variants, only 24 are experimentally observed to be dominant.

In the case of a typical habit plane variant α, the microscopic deformation gradient takes the form

$$\mathbf{F}_{12,\alpha} \;=\; \mathbf{I} + g\mathbf{m}_\alpha \otimes \mathbf{n}_\alpha \;,$$

where g is the transformation displacement, $\mathbf{m}_\alpha$ is the unit vector in the transformation direction, and $\mathbf{n}_\alpha$ is the outward unit normal to the habit plane.

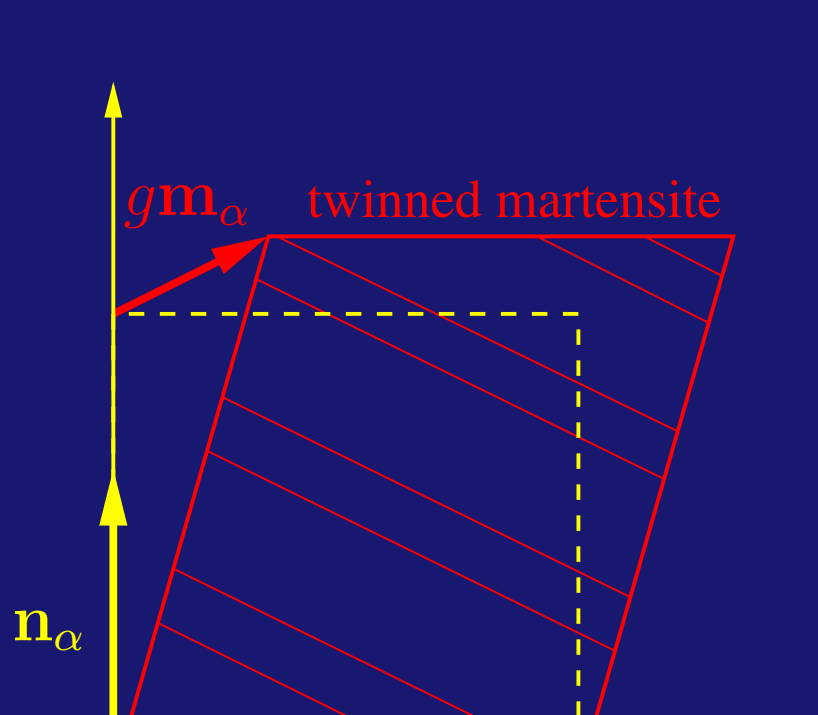

Modeling

Proceed with modeling by analogy to the theory of elastic-plastic materials.

A plastic (resp. phase-tranforming) material can be views as an elastic material whose response is parametrized by the plastic (resp. transformation) variables.

Two key differences:

- Martensitic transformation is fully reversible.
- Loading conditions in multi-surface plasticity are determined per surface, while in martensitic transformation they are cumulative.

Micromechanically-motivated constitutive assumptions:

1. Existence of a Lagrangian transformation strain $\mathbf{E}^t$ depending on the martensitic volume fractions

$$\{\xi_\alpha\} \;=\; \left\{(\xi_1, \xi_2, \cdots, \xi_{nv}) \quad | \quad \sum_{\beta=1}^{nv} \xi_\beta \leq 1 \;,\; \xi_\beta \geq 0 \right\},$$

   such that $\mathbf{E}^t = \hat{\mathbf{E}}^t\left(\{\xi_\alpha\}\right)$, where nv stands for the number of potentially present variants.

   Homogeneity condition: $\hat{\mathbf{E}}^t(\{0\}) \;=\; \mathbf{0}$.

   Note the analogy (and contrast) with plasticity theory.

2. Admittance of a Helmholtz free energy $\Psi = \rho_0(\epsilon - \eta\theta)$, where $\Psi = \hat{\Psi}(\mathbf{E}, \{\xi_\alpha\}, \theta)$. Here, ρ_0 is the mass density, ϵ is the internal energy per unit mass, η is the entropy, and θ the absolute temperature.

   Recall the local form of the energy equation

$$\rho_0\dot{\epsilon} \;=\; \rho_0 r - \mathrm{Div}\mathbf{q}_0 + \mathbf{S}\cdot\dot{\mathbf{E}}\;,$$

   where r is the heat supply per unit mass and $\mathbf{q}_0$ the referential heat flux vector.

   Also recall the Clausius-Duhem inequality

$$\rho_0\dot{\eta}\theta \;\geq\; \rho_0 r - \mathrm{Div}\mathbf{q}_0 + \frac{\mathbf{q}_0\cdot\mathrm{Grad}\,\theta}{\theta}\;.$$

For any homothermal superelastic process,

$$\left(\mathbf{S} - \frac{\partial \hat{\Psi}}{\partial \mathbf{E}}\right) \cdot \dot{\mathbf{E}} - \sum_{\alpha=1}^{nv} \frac{\partial \hat{\Psi}}{\partial \xi_\alpha} \cdot \dot{\xi}_\alpha \;\geq\; 0 \,.$$

Since $\mathbf{E}$ and $\{\xi_\alpha\}$ can be varied independently, a standard process leads to

$$\mathbf{S} \;=\; \frac{\partial \hat{\Psi}}{\partial \mathbf{E}} \,,$$

while the Clausius-Duhem inequality further implies that

$$\dot{D} \;=\; \sum_{\alpha=1}^{nv} \left(-\frac{\partial \hat{\Psi}}{\partial \xi_\alpha}\right) \dot{\xi}_\alpha \;\geq\; 0 \,.$$

3. Existence of functions $\hat{Y}_\alpha^f$ and $\hat{Y}_\alpha^r$ in the form

$$Y_\alpha^f = \hat{Y}_\alpha^f(\mathbf{E}, \{\xi_\beta\}, \theta) \quad , \quad Y_\alpha^r = \hat{Y}_\alpha^r(\mathbf{E}, \{\xi_\beta\}, \theta)$$

associated with the forward and reverse transformation of variant α, respectively, where $\hat{Y}_\alpha^f < \hat{Y}_\alpha^r$.

$Y_\alpha^f = 0 \quad \Leftrightarrow \quad$ variant α active in forward transformation

$Y_\alpha^r = 0 \quad \Leftrightarrow \quad$ variant α active in reverse transformation

Forward and reverse transformation active sets:

$$\mathcal{J}^f(\mathbf{E}, \theta) = \{\alpha \mid \hat{Y}_\alpha^f(\mathbf{E}, \{\xi_\beta\}, \theta) = 0, \xi_\alpha > 0\} ,$$
$$\mathcal{J}^r(\mathbf{E}, \theta) = \{\alpha \mid \hat{Y}_\alpha^r(\mathbf{E}, \{\xi_\beta\}, \theta) = 0, \xi_\alpha > 0\} .$$

Modeling

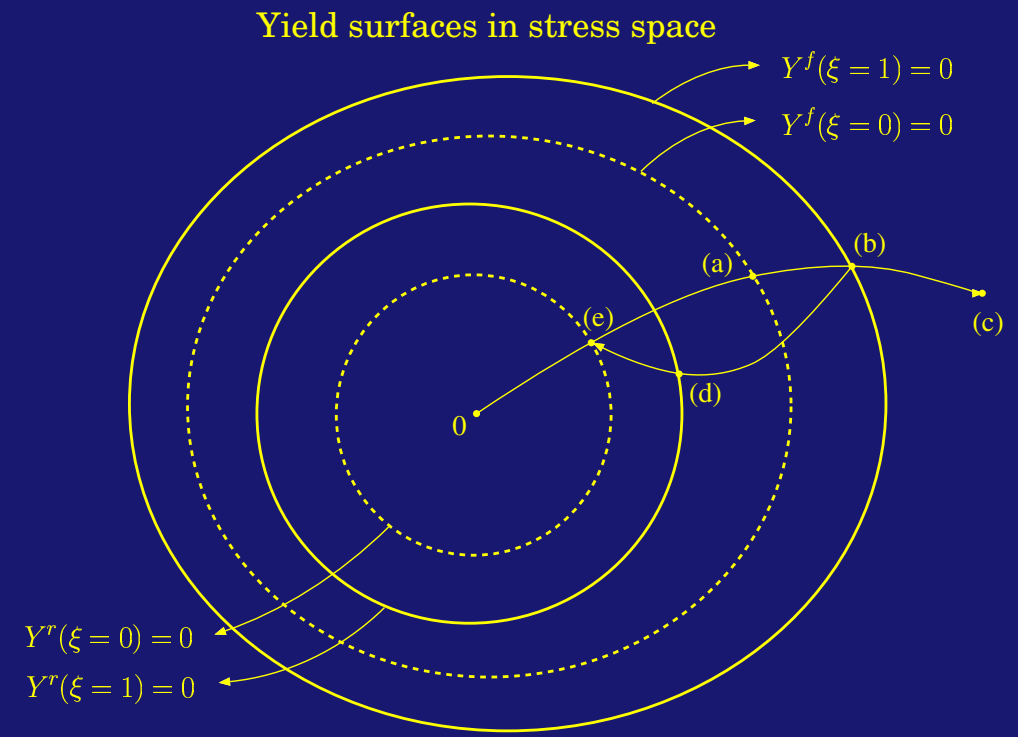
Yield surfaces in stress space
$Y^f(\xi = 1) = 0$
$Y^f(\xi = 0) = 0$
(a)
(b)
(c)
(d)
(e)
0
$Y^r(\xi = 0) = 0$
$Y^r(\xi = 1) = 0$

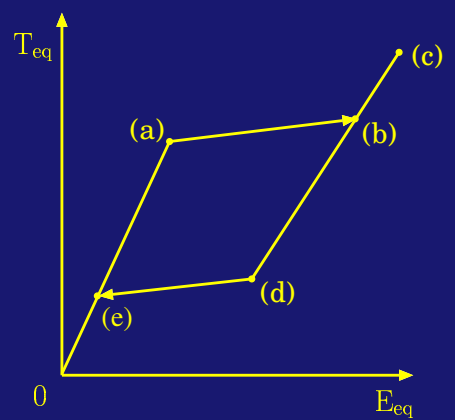
T_{eq}
(a)
(b)
(c)
(d)
(e)
0
E_{eq}

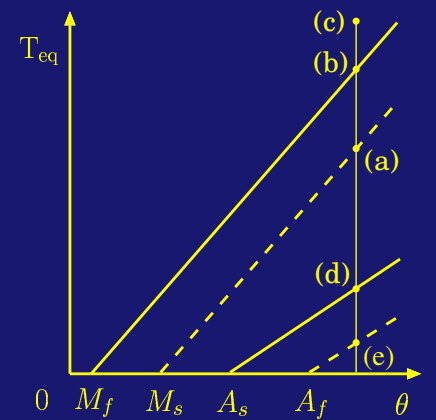
T_{eq}
(c)
(b)
(a)
(d)
(e)
0
M_f
M_s
A_s
A_f
θ

Persistency of a forward-active variant α,

$$\dot{Y}^f_\alpha \;=\; \frac{\partial \hat{Y}^f_\alpha}{\partial \mathbf{E}} \cdot \dot{\mathbf{E}} - \sum_{\beta \in \mathcal{J}^f} Q_{\alpha\beta} \dot{\xi}_\beta \;=\; 0 \;,$$

where $Q^f_{\alpha\beta} = -\dfrac{\partial \hat{Y}^f_\alpha}{\partial \xi_\beta}$ are the components of the forward coupling matrix (assumed invertible) which quantifies the coupling between variants during forward transformation.

It follows that during forward transformation of variant α,

$$\dot{\xi}_\alpha \;=\; \sum_{\beta \in \mathcal{J}^f} Q^{f\,-1}_{\beta\alpha} \frac{\partial \hat{Y}^f_\beta}{\partial \mathbf{E}} \cdot \dot{\mathbf{E}} \;.$$

This is a rate-type, rate-independent equation (note connection with rate-independent plasticity).

4. Stipulate of forward and reverse transformation criteria.

From a state of a forward transformation ($\mathcal{J}^f \neq \emptyset$):

$$\sum_{\alpha \in \mathcal{J}^f} W_\alpha^f \frac{\partial \hat{Y}_\alpha^f}{\partial \mathbf{E}} \cdot \dot{\mathbf{E}} \begin{cases} > 0 & \Leftrightarrow \text{ forward transformation} \\ = 0 & \Leftrightarrow \text{ neutral forward transformation} \\ < 0 & \Leftrightarrow \text{ elastic unloading} \end{cases} .$$

From a state of a reverse transformation ($\mathcal{J}^f = \emptyset$, $\mathcal{J}^r \neq \emptyset$):

$$\sum_{\alpha \in \mathcal{J}^r} W_\alpha^r \frac{\partial \hat{Y}_\alpha^r}{\partial \mathbf{E}} \cdot \dot{\mathbf{E}} \begin{cases} > 0 & \Leftrightarrow \text{ elastic reloading} \\ = 0 & \Leftrightarrow \text{ neutral reverse transformation} \\ < 0 & \Leftrightarrow \text{ reverse transformation} \end{cases} .$$

To determine the weight function W_α^f, note that during forward transformation

$$\sum_{\alpha \in \mathcal{J}^f} (-Y_\alpha^f - \frac{\partial \hat{\Psi}}{\partial \xi_\alpha}) \dot{\xi}_\alpha \geq 0 \, .$$

Recalling the equation for $\dot{\xi}_\alpha$, it follows that

$$\sum_{\alpha \in \mathcal{J}^f} \sum_{\beta \in \mathcal{J}^f} Q_{\alpha\beta}^{f\,-1} (-Y_\beta^f - \frac{\partial \hat{\Psi}}{\partial \xi_\beta}) \frac{\partial \hat{Y}_\alpha^f}{\partial \mathbf{E}} \cdot \dot{\mathbf{E}} \geq 0 \, ,$$

which implies that

$$W_\alpha^f = \sum_{\beta \in \mathcal{J}^f} Q_{\alpha\beta}^{f\,-1} (-Y_\beta^f - \frac{\partial \hat{\Psi}}{\partial \xi_\beta}) \, .$$

A similar analysis applies to W_α^r.

Consider an alternative option: postulate a single forward transformation function of the form

$$Y^f \;=\; \| - \frac{\partial \hat{\Psi}}{\partial \xi_\alpha} \|_q - \mathcal{F}_c \;,$$

where $\|(\cdot)\|_q$ denotes the standard vector q-norm.

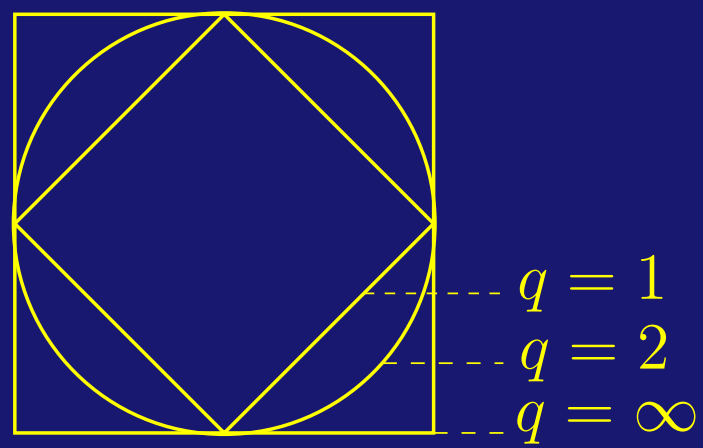

Note analogy to yield functions in plasticity theory.

Why use non-smooth transformation criteria?

How to incorporate microstructural information into the crystal grain constitutive model?

Homogenize the kinematics and kinetics of the microstructure over a representative referential volume element (RVE) $\mathcal{V}$ that characterizes the physics of the martensitic transformation.

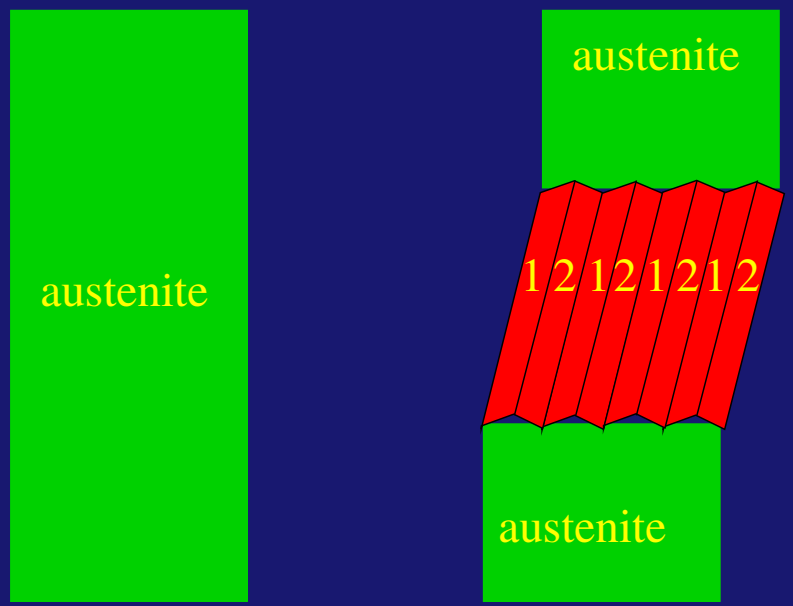

"Descend" into the limiting case of infinitesimal deformations and let the mechanical part of the Helmholtz free energy be of the form

$$\psi(\boldsymbol{\epsilon}, \{\xi_\alpha\}) = \underbrace{\sum_{\alpha=}^{nv+1} \xi_\alpha \frac{1}{2}(\boldsymbol{\epsilon} - \boldsymbol{\epsilon}_\alpha^t) \cdot \mathbb{C}(\boldsymbol{\epsilon} - \boldsymbol{\epsilon}_\alpha^t)}_{\text{single phases}} + \underbrace{\psi_m(\{\xi_\alpha\})}_{\text{mixing}},$$

where $\mathbb{C}$ is the elasticity tensor (assumed phase-invariant).

Subsequently, write the mechanical part of the Gibbs free energy of the mixture as

$$\gamma(\boldsymbol{\sigma}, \{\xi_\alpha\}) = \sum_{\alpha=1}^{nv} \frac{1}{2}\boldsymbol{\sigma} \cdot \mathbb{C}^{-1}\boldsymbol{\sigma} + \sum_{\alpha=1}^{nv} \xi_\alpha \boldsymbol{\sigma} \cdot \boldsymbol{\epsilon}_\alpha^t + \dots$$

Assume a spatially homogeneous stress $\boldsymbol{\sigma}^0$ over the ensemble and employ a Legendre transformation to write

$$\sup_{\sigma_0} \int_{\mathcal{V}} \left[-\gamma(\boldsymbol{\sigma}^0, \{\xi_\alpha\}) + \sigma^0 \cdot \boldsymbol{\epsilon} \right] \, dV \;=\; \int_{\mathcal{V}} \psi_R(\boldsymbol{\epsilon}, \{\xi_\alpha\}) \, dV \;,$$

where ψ_R is the Reuss (lower) bound to the mechanical part of the free energy.

It follows from the above that the Reuss bound is

$$\psi_R(\bar{\boldsymbol{\epsilon}}, \{\xi_\alpha\}) \;=\; \frac{1}{2}(\bar{\boldsymbol{\epsilon}} - \sum_{\alpha=1}^{nv} \xi_\alpha \boldsymbol{\epsilon}_\alpha^t) \cdot \mathbb{C}(\bar{\boldsymbol{\epsilon}} - \sum_{\alpha=1}^{nv} \xi_\alpha \boldsymbol{\epsilon}_\alpha^t)$$

in terms of the volume-averaged strain $\bar{\boldsymbol{\epsilon}} = \dfrac{1}{\text{vol}(\mathcal{V})} \displaystyle\int_{\mathcal{V}} \epsilon \, dV$.

Alternatively, assume a spatially homogeneous strain ϵ^0 over the ensemble and again homogenize the elastic part of the Helmholtz free energy to find that

$$\psi_V(\bar{\boldsymbol{\epsilon}}, \{\xi_\alpha\}) \;=\; \frac{1}{2}(\bar{\boldsymbol{\epsilon}} - \sum_{\alpha=1}^{nv} \xi_\alpha \boldsymbol{\epsilon}_\alpha^t) \cdot \mathbb{C}(\bar{\boldsymbol{\epsilon}} - \sum_{\alpha=1}^{nv} \xi_\alpha \boldsymbol{\epsilon}_\alpha^t) - \frac{1}{2} \sum_{\alpha=1}^{nv} \tilde{\boldsymbol{\sigma}} \cdot \xi_\alpha \boldsymbol{\epsilon}_\alpha^t \;,$$

where $\tilde{\sigma}$ is the self-equilibrated zero-mean fluctuation stress.

One may estimate the contribution of the fluctuation stress, although the existing estimates are generally not very accurate.

Motivated by the micromechanical model, let the Helmholtz free energy be written as

$$\Psi \;=\; \hat{\Psi}(\mathbf{E}, \{\xi_\alpha\}, \theta) \;=\; \underbrace{\frac{1}{2}\left(\mathbf{E}-\mathbf{E}^t\right)\cdot\mathbb{C}\left(\mathbf{E}-\mathbf{E}^t\right)}_{\text{mechanical}} + \underbrace{B(\theta-\theta_0)\sum_{\alpha=1}^{nv}\xi_\alpha}_{\text{chemical}} \;.$$

where $\mathbf{E}^t$ is the cumulative transformation strain, B is a chemical energy constant (latent heat of transformation), and θ_0 is the equilibrium temperature.

Note that the strains are moderate (typically, less than 6-10%).

The cummulative transformation strain is now defined as

$$\mathbf{E}^t \;=\; \sum_{\alpha=1}^{nv} \xi_\alpha \mathbf{E}^t_\alpha \;,$$

where the variant transformation strain $\mathbf{E}^t_\alpha$ is given by

$$\mathbf{E}^t_\alpha \;=\; \frac{1}{2}\, g(\mathbf{m}_\alpha \otimes \mathbf{n}_\alpha + \mathbf{n}_\alpha \otimes \mathbf{m}_\alpha + g\mathbf{n}_\alpha \otimes \mathbf{n}_\alpha) \;,$$

in terms of the microscopic deformation gradient

$$\mathbf{F}_\alpha \;=\; \mathbf{I} + g\mathbf{m}_\alpha \otimes \mathbf{n}_\alpha \;.$$

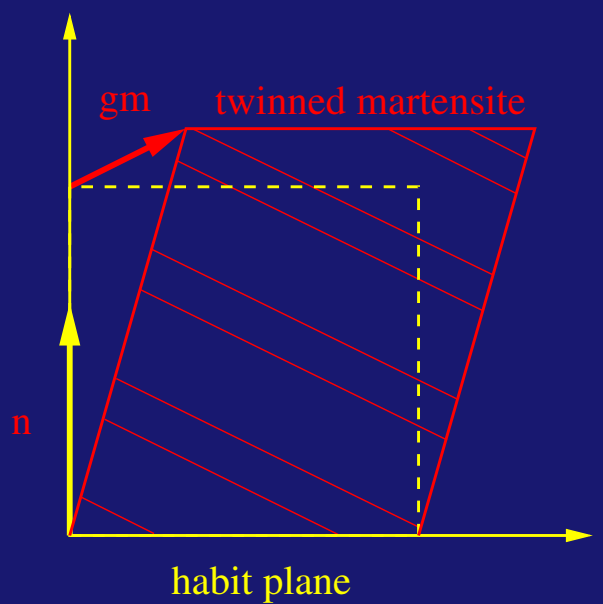

Further, admit critical thermodynamic force-based transformation functions

$$Y_\alpha^f \;=\; -\frac{\partial \hat{\Psi}}{\partial \xi_\alpha} - \mathcal{F}^c \qquad , \qquad Y_\alpha^r \;=\; -\frac{\partial \hat{\Psi}}{\partial \xi_\alpha} + \mathcal{F}^c \;,$$

to characterize forward and reverse transformation, respectively.

Given the particular form of the Helmholtz free energy,

$$Y_\alpha^f \;= \hat{Y}_\alpha^f(\mathbf{E}, \{\xi_\beta\}, \theta) = \; \mathbb{C}\big(\mathbf{E} - \sum_{\beta=1}^{nv} \xi_\beta \mathbf{E}_\beta^t\big) \cdot \mathbf{E}_\alpha^t - \big(B(\theta - \theta_0) + \mathcal{F}^c\big) \;,$$

$$Y_\alpha^r \;= \hat{Y}_\alpha^r(\mathbf{E}, \{\xi_\beta\}, \theta) = \; \mathbb{C}\big(\mathbf{E} - \sum_{\beta=1}^{nv} \xi_\beta \mathbf{E}_\beta^t\big) \cdot \mathbf{E}_\alpha^t - \big(B(\theta - \theta_0) - \mathcal{F}^c\big) \;.$$

During elastic loading or forward transformation, the loading conditions simplify to

$$\sum_{\alpha \in \mathcal{J}^f} \dot{\xi}_\alpha \;\geq\; 0 \,,$$

namely, the total production of martensite is non-negative.

Recalling further the form of the forward transformation criterion, it follows that during elastic loading or forward transformation

$$\sum_{\alpha \in \mathcal{J}^f} \Big(-\frac{\partial \hat{\Psi}}{\partial \xi_\alpha} - \mathcal{F}^c\Big)\dot{\xi}_\alpha \;=\; 0 \,.$$

An analogous result applies to reverse transformation.

Note that here

$$\frac{\partial^2 \hat{\Psi}}{\partial \xi_\alpha \partial \xi_\beta} \;=\; Q_{\alpha\beta} \;=\; \mathbf{E}^t_\alpha \cdot \mathbb{C}\mathbf{E}^t_\beta \;,$$

where the $nv \times nv$ coupling matrix $[Q_\alpha\beta]$ is symmetric and of rank at most 6. This implies that for $nv > 6$, the matrix $[Q_{\alpha\beta}]$ is necessarily positive semi-definite.

Recalling again that

$$\sum_{\alpha \in \mathcal{J}^f} \big(-\frac{\partial \hat{\Psi}}{\partial \xi_\alpha} - \mathcal{F}^c\big)\dot{\xi}_\alpha \;=\; 0 \;,$$

it follows that the identification of active variants and volume fractions can be cast as a constrained optimization problem at fixed strain and temperature.

Specifically, in the case of forward transformation, the martensitic content $\{\xi_\alpha\}$ satisfies

$$\{\xi_\alpha\} \;=\; \underset{\{\xi_\gamma\}\in\mathcal{J}^f}{\operatorname{argmin}}\; \Phi^f \;,$$

subject to inequality constraints

$$-\xi_\alpha \;\leq\; 0 \qquad , \qquad \sum_{\alpha=1}^{nv} \xi_\alpha \;\leq\; 1 \;.$$

where the functional Φ^f is defined as

$$\Phi^f = \Psi + \sum_{\alpha\in\mathcal{J}^f} \mathcal{F}^c \xi_\alpha \;,$$

and may attain multiple minima. A similar conclusion applies to reverse transformation for the functional $\Phi^r = \Psi - \sum_{\alpha\in\mathcal{J}^r} \mathcal{F}^c \xi_\alpha$.

How to model detwinning?

The twinned and detwinned variants may coexist, so that

$$\Psi \;=\; \hat{\Psi}(\mathbf{E}, \{\xi_\alpha^{hab}, \xi_\beta^{lat}\}, \theta) \;=$$

$$\frac{1}{2}\left(\mathbf{E}-\mathbf{E}^t\right)\cdot\mathbb{C}\left(\mathbf{E}-\mathbf{E}^t\right) + B(\theta-\theta_0)\sum_{\alpha=1}^{nv}\xi_\alpha \;,$$

where now

$$\mathbf{E}^t \;=\; \sum_{\alpha=1}^{nvh}\xi_\alpha^{hab}\mathbf{E}_\alpha^t + \sum_{\beta=1}^{nvl}\xi_\beta^{lat}\mathbf{E}_\beta^t \;.$$

In the above, nvh and and nvl denote the total number of habit and lattice correspondence variants, respectively.

Closure

- Plasticity theory can be used as a guide toward the development of superelastic constitutive models.
- It is possible to motivate continuum formulations of superelasticity using micromechanics.
- It is sensible to consolidate the loading criteria, while keeping the transformation criteria separate.
- Under certain assumptions, superelasticity can be cast as a constraint minimization problem.
- The role of interaction energy between variants remains an open question.

References

1. J.G. Boyd and D.C. Lagoudas, *Int. J. Plast.*, **12**, pp. 805-842, (1996) [Phenomenological modeling of phase transformation].

2. S. Leclercq and C. Lexcellent, *Int. J. Mech Phys Sol.*, **44**, pp. 953-980, (1996) [Phenomenological modeling of phase transformation including detwinning].

3. M. Huang and L.C. Brinson, *J. Mech. Phys. Sol.*, **46**, pp. 1379-1409, (1998) [Micromechanically motivated model for single crystal]

4. N. Siredey, E. Patoor, M. Berveiller and A. Eberhardt, *Int. J. Sol. Struct.*, **36**, pp. 4289-4315, (1999) [Micromechanically motivated multivariant modeling]

CONTENTS OF PART III

- Operator-split algorithms at the crystal grain level
- Optimization-based algorithms at the crystal grain level
- Modeling of textured polycrystals
- Experiments and simulation
- An application to the design of biomedical devices

Algorithmic treatment

Within the finite element paradigm, the algorithmic problem for a single crystal is set up as follows:

"Given the state at time t_n, and the total displacement $\mathbf{u}_{n+1}$ at time t_{n+1}, determine the state at time t_{n+1}."

The preceding problem is iteratively nested inside the global momentum balance problem.

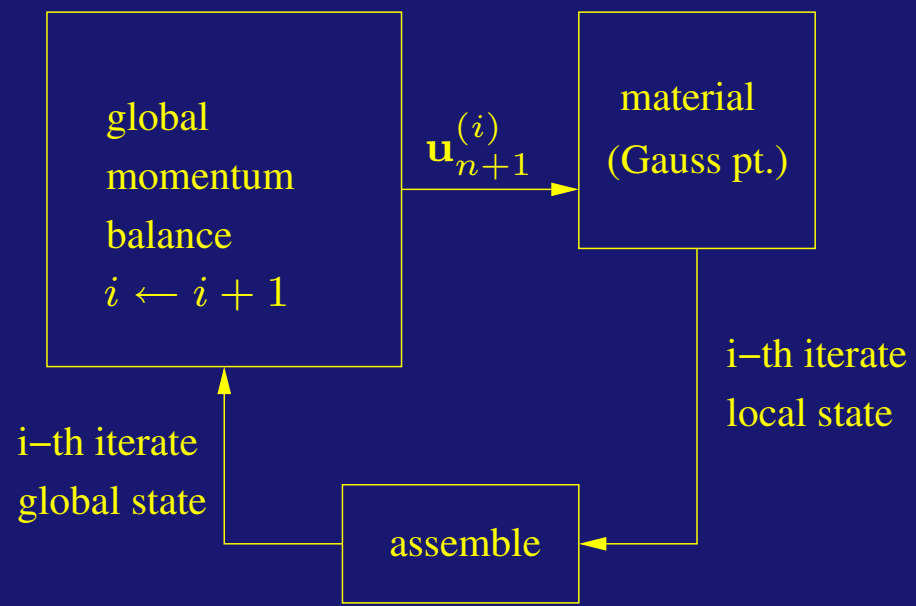

Algorithmic treatment

Two potential approaches:

- Unified approach

  Determine the phase state by solving a constrained optimization problem.

  Unified treatment of transforming and non-transforming states

- Operator-split approach

  Analogy with computational plasticity for rate-independent materials

  Different treatment of transforming and non-transforming states

Unified approach

Treat elastic loading/forward transformation in a unified manner.

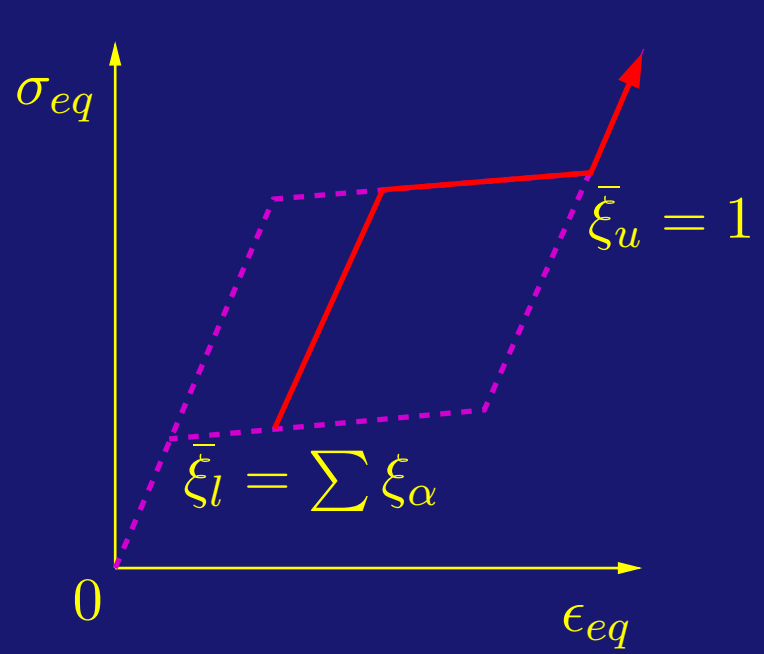

Express the constraint conditions as

$$-\xi_\alpha \leq 0 \quad , \quad \bar{\xi}_l - \sum_{\alpha=1}^{nv} \xi_\alpha \leq 0 \quad , \quad \bar{\xi}_u \leq 1 \, ,$$

where $\bar{\xi}_l$ and $\bar{\xi}_u$ are lower and upper values of the total martensitic volume fraction.

Unified approach

Treat elastic unloading/reverse transformation in a unified manner.

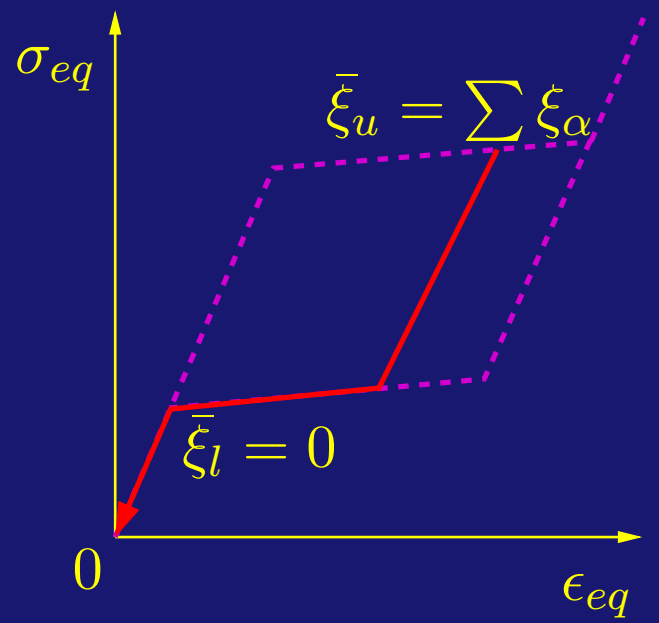

Express the constraint conditions as

$$-\xi_\alpha \;\leq\; 0 \qquad , \qquad \sum_{\alpha=1}^{nv} \xi_\alpha - \bar{\xi}_u \;\leq\; 0 \qquad , \qquad 0 \;\leq\; \bar{\xi}_l \;,$$

where $\bar{\xi}_l$ and $\bar{\xi}_u$ are lower and upper values of the total martensitic volume fraction.

Unified approach

Forward transformation

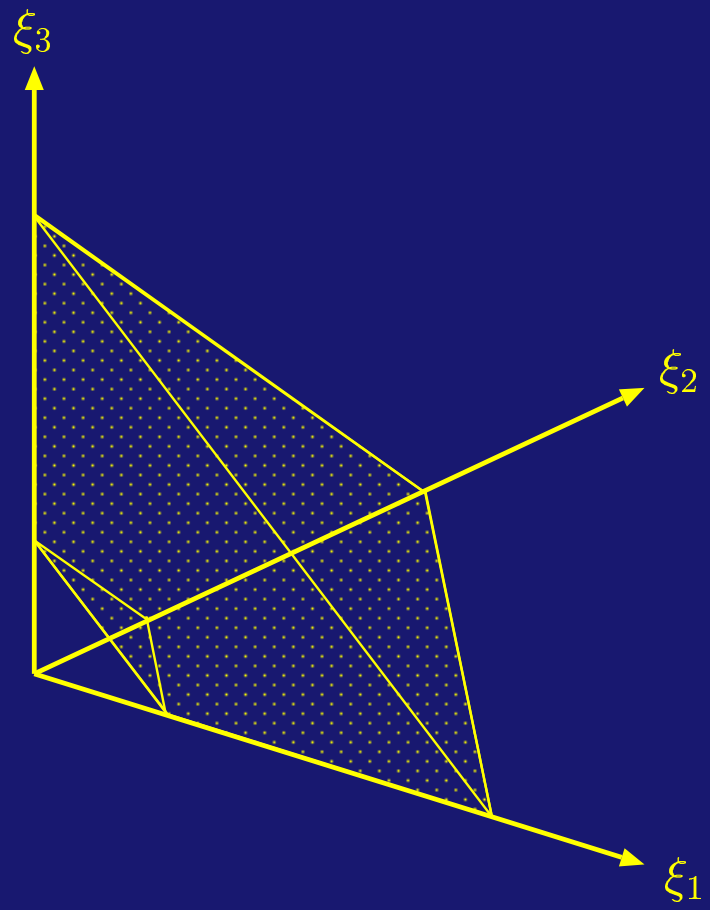

Reverse transformation

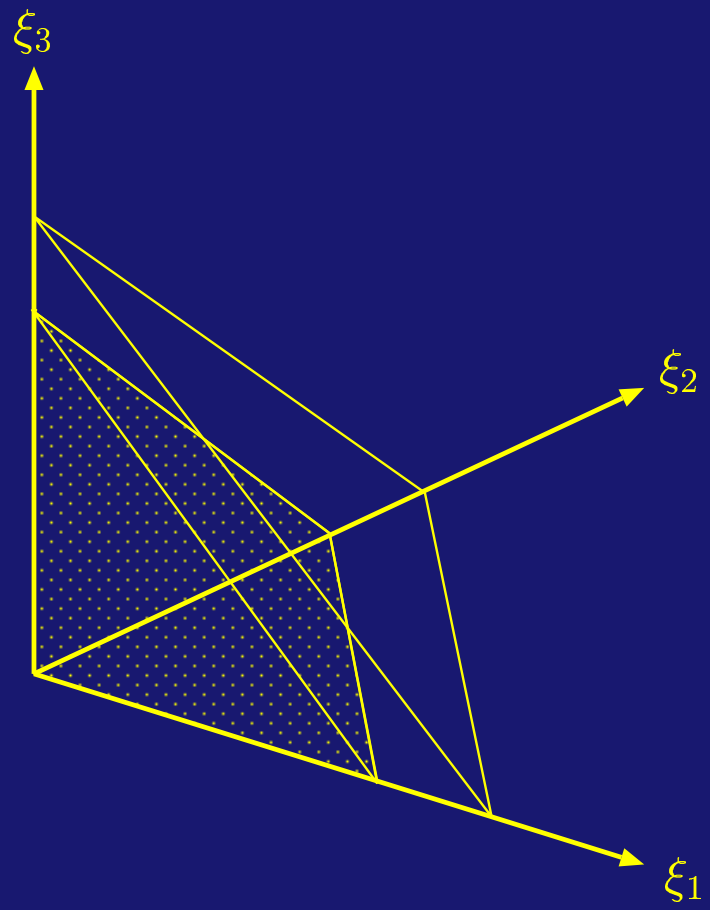

The polytope constraints for $nv = 3$

Recall that the forward transformation problem can be cast in the form

$$\{\xi_\alpha\} \;=\; \underset{\{\xi_\gamma\}\in\mathcal{J}^f}{\operatorname{argmin}}\; \Phi^f \;,$$

subject to the preceding polytope constraints.

Introduce Lagrange multipliers $\{\lambda_\alpha,\ \alpha = 1, \ldots, nv\}$, λ_l, and λ_u, and write

$$\frac{\partial \Phi^f}{\partial \xi_\alpha} + \lambda_\alpha + \lambda_l - \lambda_u \;=\; 0 \;,$$

where

$$\sum_{\alpha=1}^{nv} \lambda_\alpha(-\xi_\alpha) + \lambda_l(\bar{\xi}_l - \sum_{\alpha=1}^{nv} \xi_\alpha) + \lambda_u(\sum_{\alpha=1}^{nv} \xi_\alpha - \bar{\xi}_u) \;=\; 0 \;.$$

Unified approach

Three key algorithmic tasks:

- Identify the state as “loading” (forward transforming) or “unloading” (reverse transforming).
- Identify the set $\mathcal{C}$ of potentially active variants.

  Select up to 6 such variants from the set of all nv habit plane variants.
- Identify the variants from the set $\mathcal{C}$ that are active.

All three tasks are deformation-dependent (albeit history-independent) and generally need to be performed in each loading step!

Recall that the functional Φ^f is defined as

$$\Phi^f \;=\; \frac{1}{2}\left(\mathbf{E}-\mathbf{E}^t\right)\cdot\mathbb{C}\left(\mathbf{E}-\mathbf{E}^t\right)B(\theta-\theta_0)\sum_{\alpha=1}^{nv}\xi_\alpha+\sum_{\alpha\in\mathcal{J}^f}\mathcal{F}^c\xi_\alpha\;,$$

hence is quadratic in $\{\xi_\alpha\}$, and the 24×24 Hessian $\dfrac{\partial^2\Phi^f}{\partial\xi_\alpha\partial\xi_\beta}$ is at most of rank 6. This leads to a semi-definite quadratic programming problem.

To "relax" this problem, identify a set $\mathcal{C}$ of 6 candidate active variants at each step.

Subsequently, a standard active set strategy of positive-definite quadratic programming is applied to determine the active variants and volume fractions.

Unified approach

There are several ways to identify a "reasonable" set $\mathcal{C}$ of 6 candidate active variants. One possibility is to first determine the extrema of Φ^f with respect to each variant separately, i.e., solve

$$\hat{Y}^f_\alpha(\mathbf{E}, \xi_\alpha, \theta) \;=\; \frac{\partial \hat{\Phi}^f}{\partial \xi_\alpha} \;=\; 0 \;,$$

for each ξ_α, $\alpha = 1, \ldots, 24$. Subsequently, select the 6 variants that correspond to the lowest values of $\Phi^f = \hat{\Phi}^f(\mathbf{E}, \xi_\alpha, \theta)$.

Alternatively, one may perform a pair-wise minimization to determine 3 pairs of potentially active variants, as motivated by experiments.

The set of active variants depends crucially on the load.

Unified approach

Given the set $\mathcal{C}$ of candidate variants, express the discrete counterpart of the first-order conditions

$$\frac{\partial \Phi^f}{\partial \xi_\alpha} + \lambda_\alpha + \lambda_l - \lambda_u \;=\; 0 \;,$$

$$\sum_{\alpha=1}^{nv} \lambda_\alpha(-\xi_\alpha) + \lambda_l(\bar{\xi_l} - \sum_{\alpha=1}^{nv} \xi_\alpha) + \lambda_u(\sum_{\alpha=1}^{nv} \xi_\alpha - \bar{\xi_u}) \;=\; 0$$

in matrix form as

$$\begin{aligned} [Q][\xi_{n+1}] + [\Pi_{n+1}]^T[\lambda_{n+1}] &= [c_{n+1}] \;, \\ [\Pi_{n+1}][\xi_{n+1}] &= [h_{n+1}] \;. \end{aligned}$$

This system possesses a unique solution, as $[Q]$ is positive-definite and $[\Pi_{n+1}]$ has full row-rank.

Unified approach

Use an active set strategy starting from any feasible initial guess of volume fractions and active variants (working set).

1. Solve the first-order equations and determine new values of $[\xi_{n+1}]$ and $[\lambda_{n+1}]$.
2. If one or more of the inactive constraints are violated, then add the most offending constraint to the working set and go to step 1.
3. If one or more of the Lagrange multipliers become negative, then drop from the working set the constraint that corresponds to the lowest value over all multipliers and go to step 1.

Slow, but reliable!

The discrete counterparts of the loading criteria from a forward transformation state at $t = t_{n+1}$ are

$$\sum_{\alpha \in \mathcal{C}} (\xi^f_{\alpha,n+1} - \xi_{\alpha,n}) \begin{cases} > 0 & \Leftrightarrow \text{ forward transformation} \\ = 0 \text{ and } \lambda_l = 0 & \Leftrightarrow \text{ neutral forward transformation} \\ = 0 \text{ and } \lambda_l > 0 & \Leftrightarrow \text{ elastic unloading} \end{cases},$$

where $\xi^f_{\alpha,n+1}$ is calculated by constrained minimization of Φ^f.

Note that the latter two conditions are modified in order to account for the explicit enforcement of the constraint $\bar{\xi}_l - \sum_{\alpha \in \mathcal{C}} \xi_\alpha \leq 0$.

Unified approach

The discrete counterparts of the loading criteria from a reverse transformation state at $t = t_{n+1}$ are

$$\sum_{\alpha \in \mathcal{C}} (\xi^r_{\alpha,n+1} - \xi_{\alpha,n}) \begin{cases} < 0 & \Leftrightarrow \text{ reverse transformation} \\ = 0 \text{ and } \lambda_u = 0 & \Leftrightarrow \text{ neutral reverse transformation} \\ = 0 \text{ and } \lambda_u > 0 & \Leftrightarrow \text{ elastic reloading} \end{cases},$$

where $\xi^r_{\alpha,n+1}$ is calculated by constrained minimization of Φ^r.

Note that the first two conditions are modified in order to account for the explicit enforcement of the constraint $\sum_{\alpha \in \mathcal{C}} \xi_\alpha - \bar{\xi}_u \leq 0$.

Unified approach

In the unified approach, there is no distinction in the treatment of elastic or transforming states. This implies that one only needs to check whether the state is “forward” or “reverse”.

Use a flag to handle the characterization (set initially to “forward”). and resolve all possible combinations of forward/reverse loading:

$\Delta\xi_n^r$ \ $\Delta\xi_n^f$	$+$	0
$-$	!flag	‘reverse’
0	‘forward’	flag

Unified approach

The unified approach is also applicable for problems that lead to non-linear programming. For example, assume

$$\Psi \quad = \quad \frac{1}{2}\left(\mathbf{E}-\mathbf{E}^t\right)\cdot\bar{\mathbb{C}}\left(\mathbf{E}-\mathbf{E}^t\right) \quad + \quad B(\theta-\theta_0)\sum_{\alpha=1}^{nv}\xi_\alpha \ ,$$

where, using the rule of mixtures,

$$\bar{\mathbb{C}}=\left(1-\sum_{\alpha=1}^{nv}\xi_\alpha\right)\mathbb{C}_a+\sum_{\alpha=1}^{nv}\mathbb{C}_m \ .$$

Use non-linear programming with active set strategy or reduce the problem to one of quadratic programming by using time-lagging estimates of $\bar{\mathbb{C}}$.

Operator-split approach

Examine the operator-split approach in connection with the preceding model.

Given the state at t_n (i.e., $\{\xi_{\beta,n}\}$), the temperature θ_{n+1}, and the $i-$th iterate of the displacement $\mathbf{u}_{n+1}^{(i)}$:

1. Assume that the total strain $\mathbf{E}_{n+1}^{(i)}$ is elastic, i.e., there is no phase forward transformation.

2a. If $\hat{Y}_\alpha^f(\mathbf{E}_{n+1}^{(i)}, \{\xi_{\beta,n}\}, \theta_{n+1}) < 0$ for all variants α, then the process in $(t_n, t_{n+1}]$ is elastic.

2b. If $\hat{Y}_\alpha^f(\mathbf{E}_{n+1}^{(i)}, \{\xi_{\beta,n}\}, \theta_{n+1}) \geq 0$ for some variant(s) α, then there is some phase transformation.

Operator-split approach

As in the unified approach, one again needs to determine:

- The set $\mathcal{C}$ of potentially active variants.
- The variants from the set $\mathcal{C}$ that are active.

The operator-split approach is popular in computational plasticity because of the simplicity of the elastic predictor and the physical interpretation of the plastic corrector.

Are these attractive features preserved in the case of micromechanically motivated phase transition models?

Operator-split approach

The operator-split approach has two complications:

1. It is not readily obvious how to effect the "plastic" (i.e., transformation) correction. It is sometimes assumed that

$$\dot{\xi}_\alpha \;=\; \kappa\,\frac{\partial Y^f_\alpha}{\partial \xi_\alpha}\;,$$

which corresponds to an "associated" flow rule.

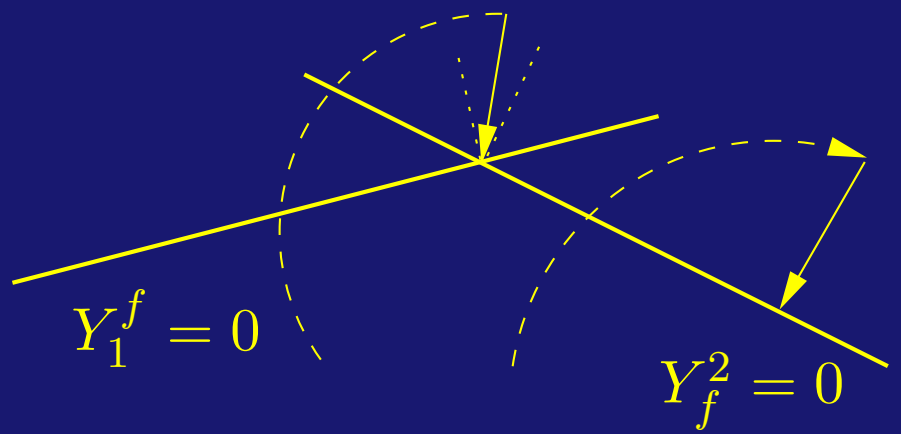

There is no constitutive justification for this assumption!

2. The evolution of the variants is subject to the polytope constraints.

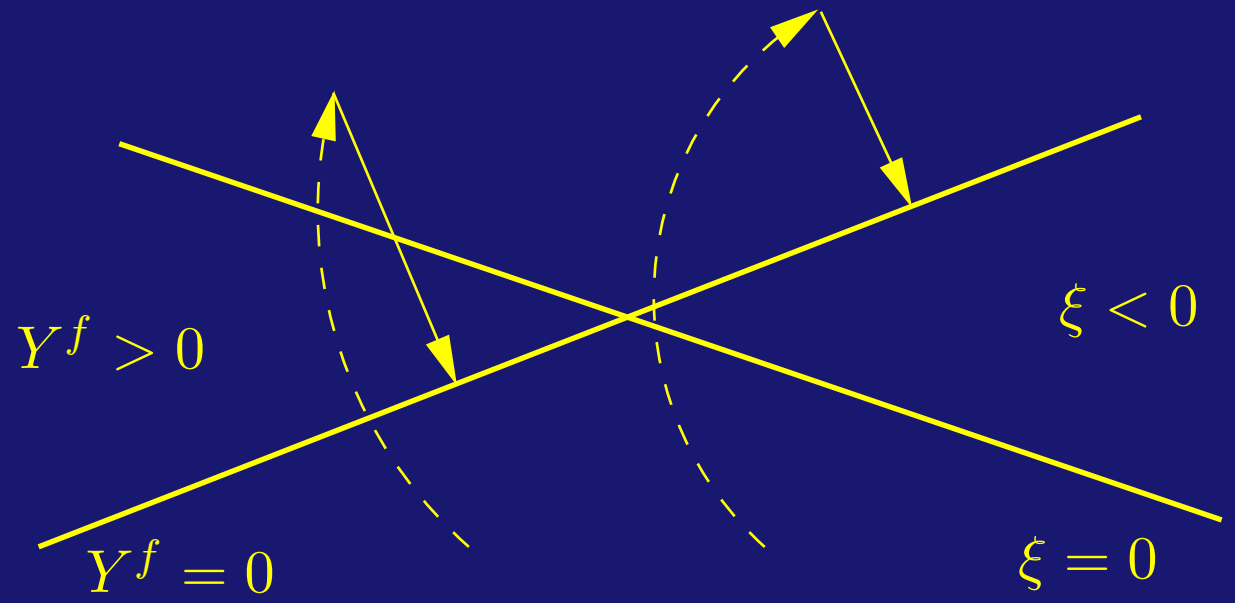

One needs to perform constrained projections in multi-dimensional space. In some cases, the projections indicate unsuitable selection of potentially active variants.

Polycrystal modeling

Texture can potentially play a pivotal role in the mechanical response of polycrystalline superelastic alloys.

Two ways to model the textured polycrystal structure:

- Direct simulation

  Resolve the polycrystal structure using individual finite elements. This is a simple, but potentially expensive approach.

- Two-scale analysis

  Solve fine-scale boundary-value problem on a representative domain and extract volume-averaged stress to be used in a continuum-level simulation. This approach can radically reduce the computational cost.

To conduct either direct simulation or two-scale analysis, one needs to utilize the texture information.

As an example, consider the Nitinol tubes described earlier. Here, the manufacturing process induces primarily $\langle 111 \rangle \{ 110 \}$-type sheet texture "wrapped" around the cylindrical surface, such that the $\langle 111 \rangle$ austenite lattice direction is aligned with the longitudinal axis of the tube.

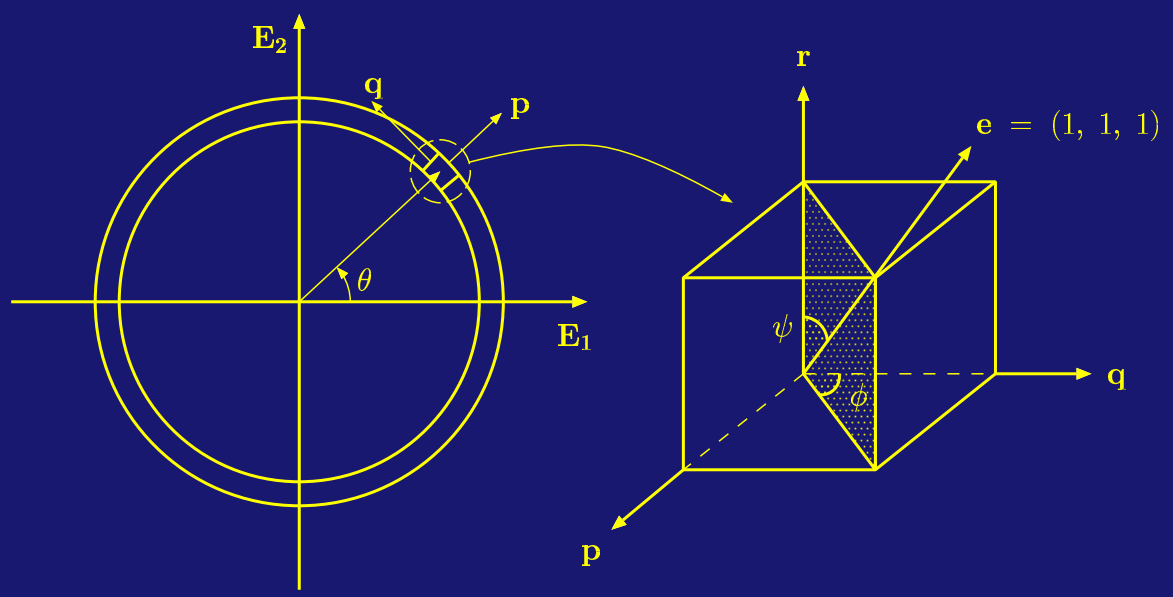

Polycrystal modeling

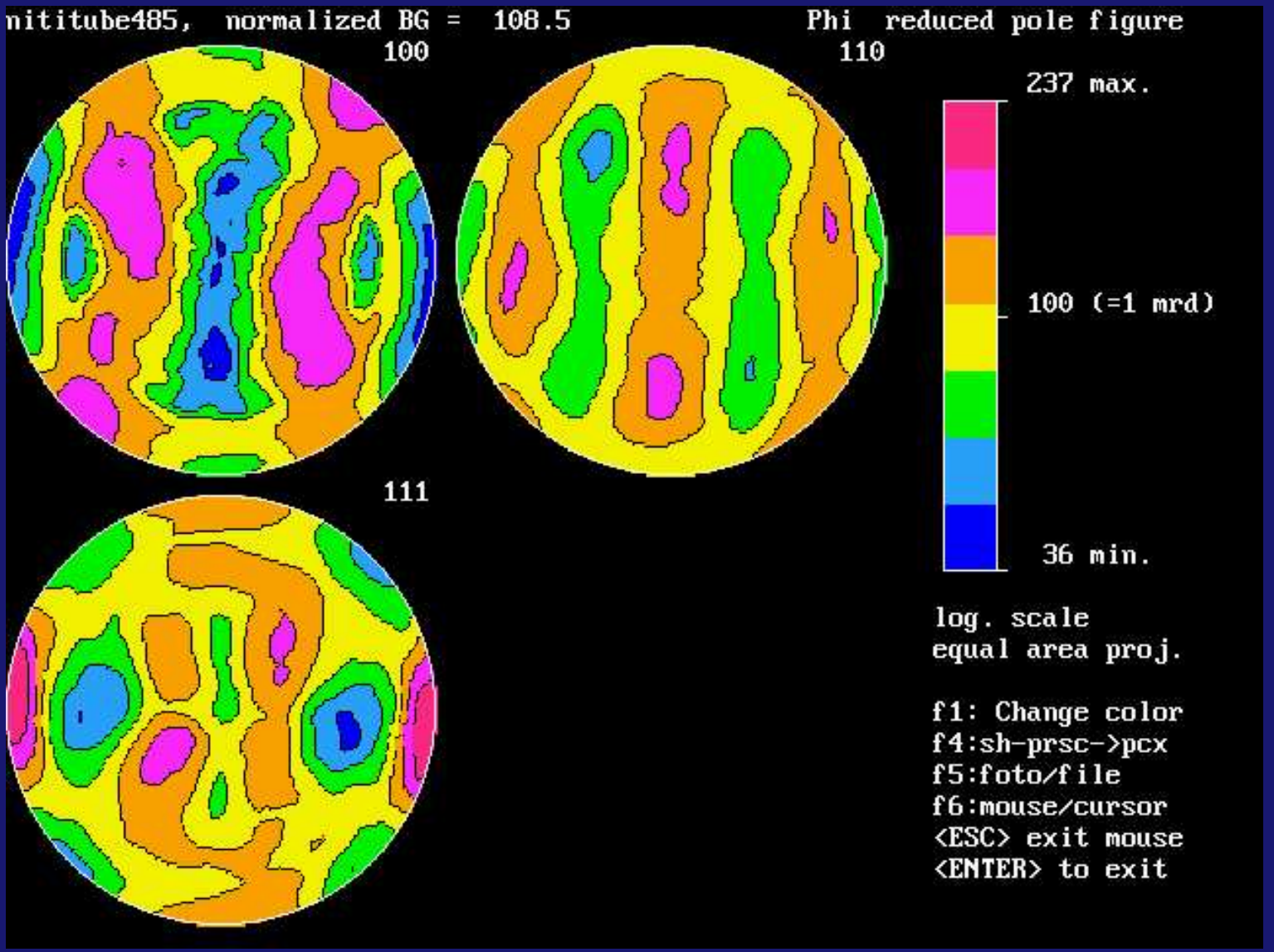

Pole figures for Nitinol tubes (R.D. horizontal, T.D. vertical)

Generally, pole figure data are directly processed by the software that handles crystallographic data acquisition.

Relevant software: BEARTEX, LaboTex, popLA, etc.

Typical software output:

$\omega_1^{(1)}$	$\omega_2^{(1)}$	$\omega_3^{(1)}$	$q^{(1)}$
$\omega_1^{(2)}$	$\omega_2^{(2)}$	$\omega_3^{(2)}$	$q^{(2)}$
$\dots$	$\dots$	$\dots$	$\dots$

,

where $\omega_I^{(i)}$, $I = 1, 2, 3$, are orientation-defining angles for the i-th bin and $q^{(i)}$ is the corresponding diffraction intensity.

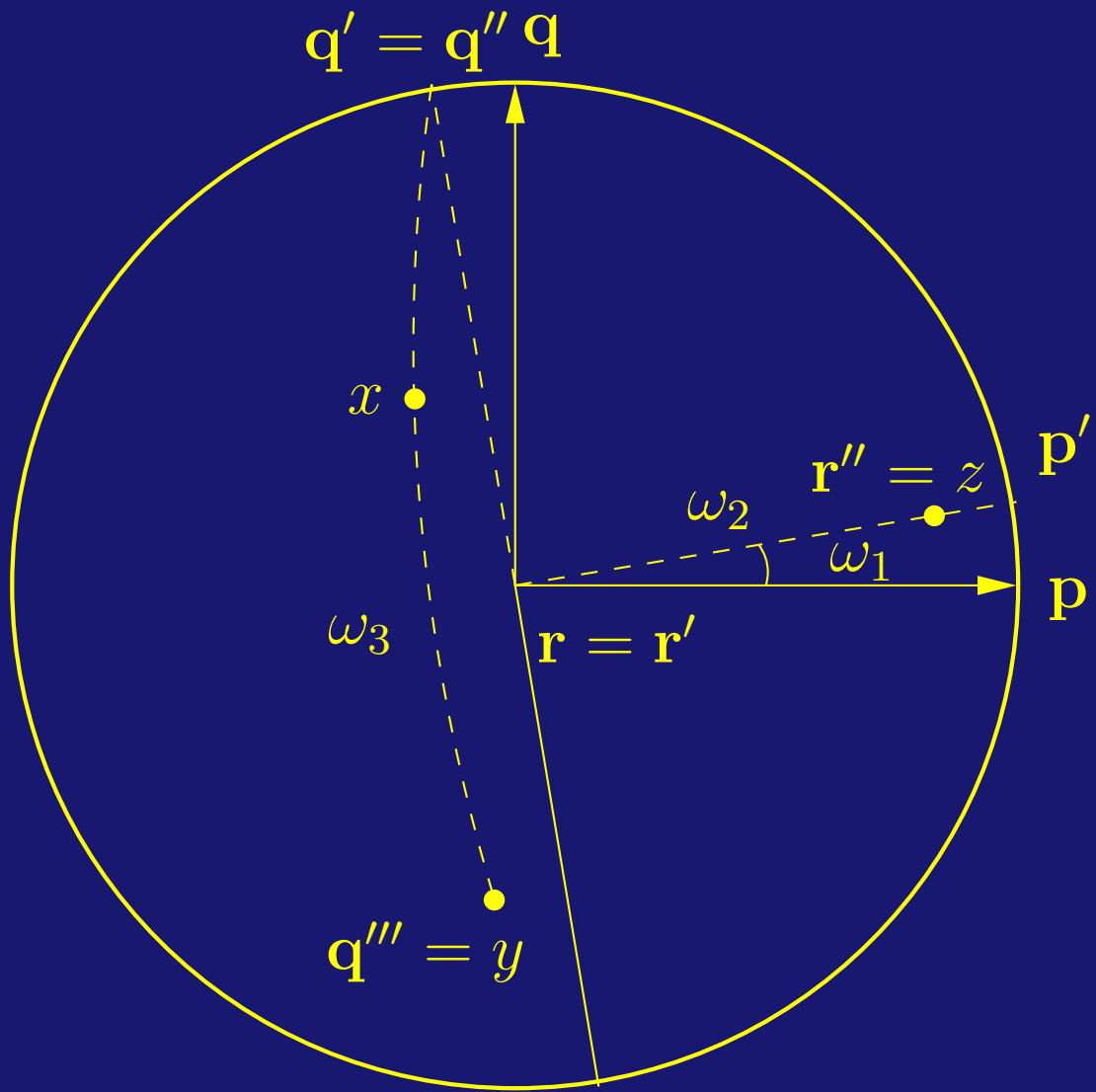

Matthies-Roe angle convention $(\mathbf{p}, \mathbf{q}, \mathbf{r}) \rightarrow (x, y, z)$

Also, recall that the austenite is wrapped around the tube.

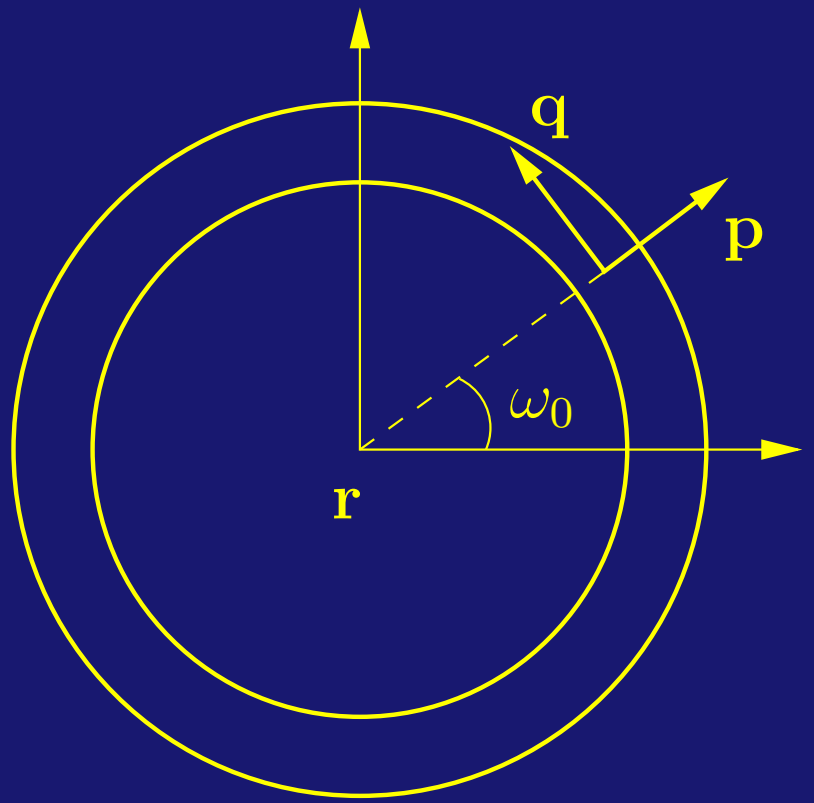

This induces an initial rotation ω_0 of the cubic crystals relative to the $\mathbf{r}$ axis.

In summary, the total rotation $\mathbf{Q}$ that characterizes the texture can be expressed as

$$\mathbf{Q} \;=\; \mathbf{Q}_3\mathbf{Q}_2\mathbf{Q}_1\mathbf{Q}_0 \;,$$

where

$\mathbf{Q}_0$: rotation by ω_0 relative to $\mathbf{r}$,
$\mathbf{Q}_1$: rotation by ω_1 relative to $\mathbf{r}$,
$\mathbf{Q}_2$: rotation by ω_2 relative to $\mathbf{q}'$,
$\mathbf{Q}_3$: rotation by ω_2 relative to $\mathbf{r}''$.

To obtain a matrix representation of the rotation, recall the Rodrigues formula for rotation in $\{\mathbf{p}, \mathbf{q}, \mathbf{r}\}$ by ω with respect to $\mathbf{p}$:

$$\mathbf{Q}_r \;=\; \mathbf{p}\otimes\mathbf{p} + \cos\omega(\mathbf{q}\otimes\mathbf{q} + \mathbf{r}\otimes\mathbf{r}) - \sin\theta(\mathbf{q}\otimes\mathbf{r} - \mathbf{r}\otimes\mathbf{q}) \;.$$

For any given grain, the angles ω_I, $I = 1, 2, 3$, are picked from the pole figure data using a random processes weighted by the diffraction intensities.

The angle ω_0 is computed directly as a function of the location of the grain on the tube.

Once the cumulative rotation $\mathbf{Q}$ is known, the habit plane transformation strains $\{\mathbf{E}^t_\alpha\}$ of a typical crystal grain are expressed as

$$\mathbf{E}^t_{a,tex} \;=\; \mathbf{Q}\mathbf{E}^t_\alpha\mathbf{Q}^T \;,$$

where $\mathbf{E}^t_\alpha$ are the transformation strains relative to the austenite (cubic) frame.

Polycrystal modeling

The direct simulation approach is straightforward.

The two-scale approach requires the solution of a boundary-value problem at each Gauss point:

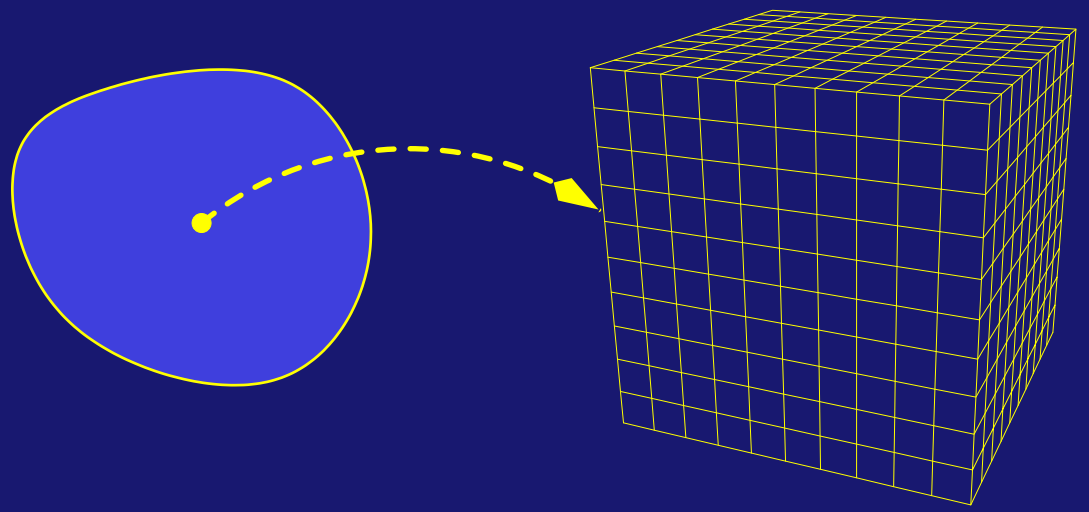

Use the macro-scale deformation as input for the fine-scale problem, determine the mean stress, and use it to define the constitutive behavior in the macro-scale problem.

Polycrystal modeling

Use Taylor assumption, i.e., impose constant deformation gradient field $\bar{\mathbf{F}} = \mathbf{F}$ in the fine-scale problem.

Recalling the Hill-Mandel averaging theorem, compute and output the mean 1st Piola-Kirchhoff stress $\bar{\mathbf{P}}$.

Interesting issues:

- Size of the fine-scale problem (convergence of the microstructure)
- Implicit global solution options (Newton's method and its variants)
- Other consistent averaging options

Material parameters:

Austenite Young's modulus	:	$E = 38.0$ GPa
Martensite Young's modulus	:	$E = 10.0$ GPa
Poisson's ratio	:	$\nu = 0.3$
Chemical energy constant	:	$B = 0.607$ MPa$/^\circ C$
Temperature	:	$\theta - \theta_0 = 22.3^\circ C$
Critical force	:	$\mathcal{F}^c = 7.5$ MPa.

The crystallographic vectors are taken to have components

$$[n] = [-0.88888,\ 0.21523,\ 0.40443]^T$$
$$[m] = [0.43448,\ 0.75743,\ 0.48737]^T\ ,$$

relative to the austenite lattice, while $g = 0.13078$.

Numerical simulations

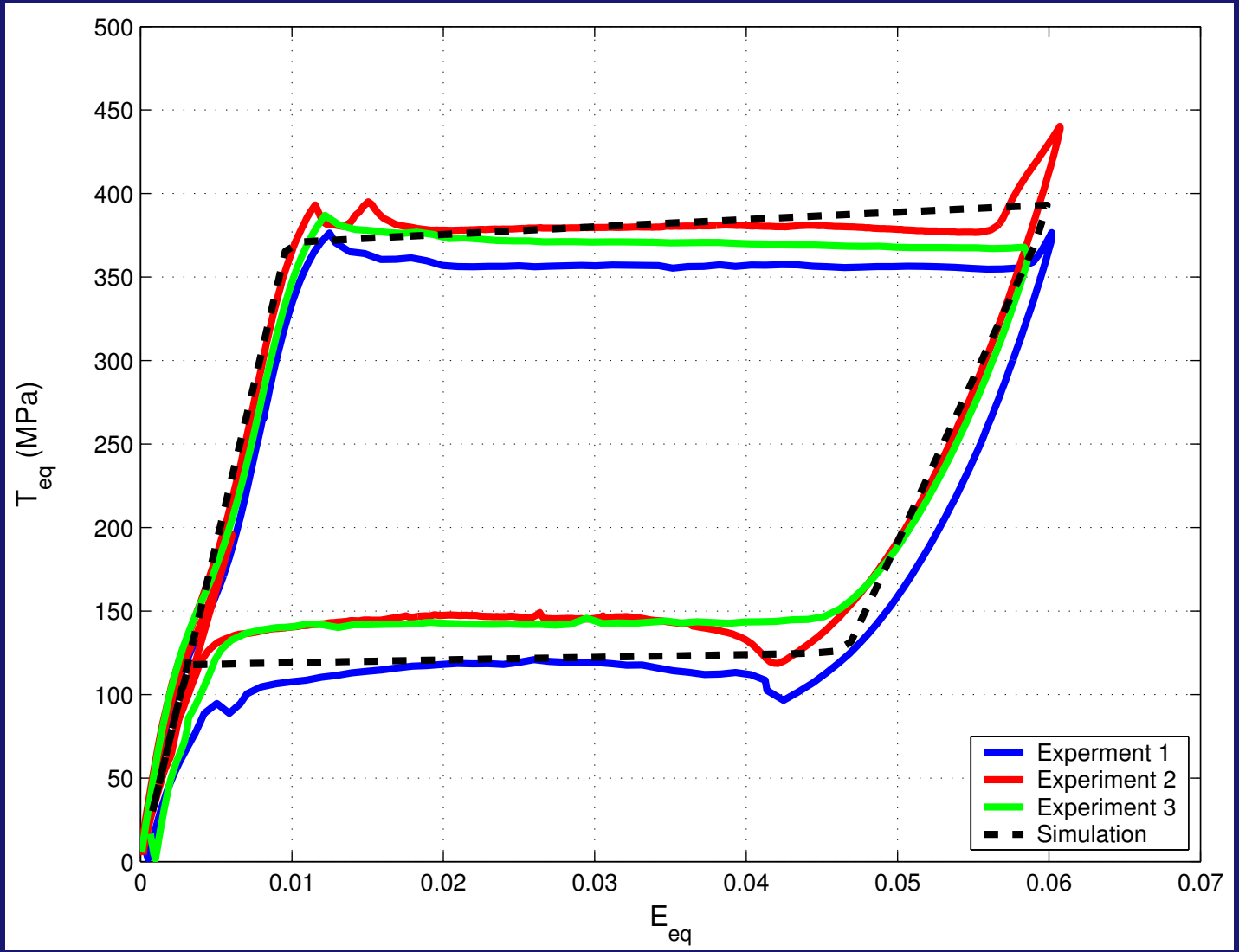

Equivalent stress-strain plot for pure tension

Numerical simulations

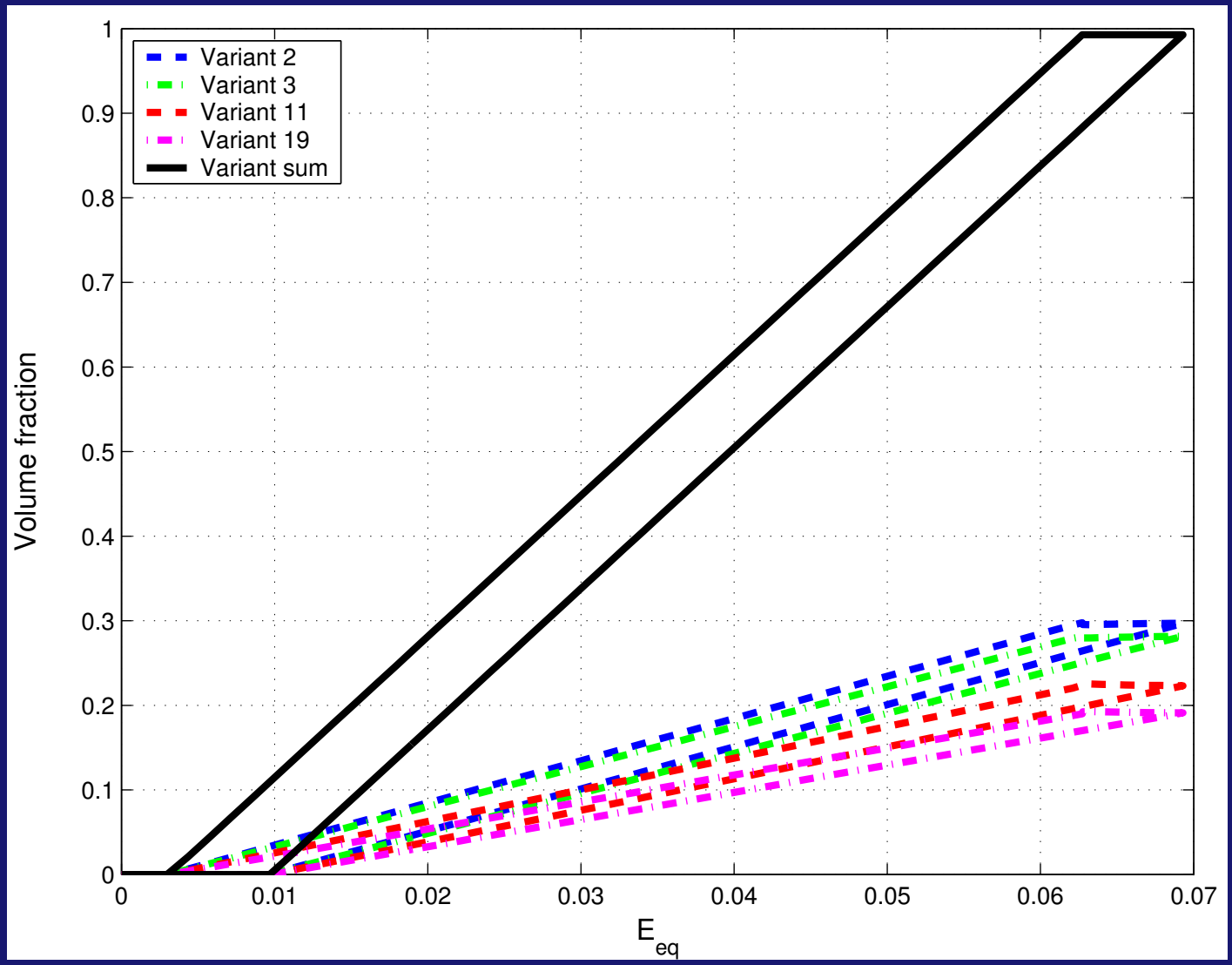

Volume fraction vs. equivalent strain for pure tension

Numerical simulations

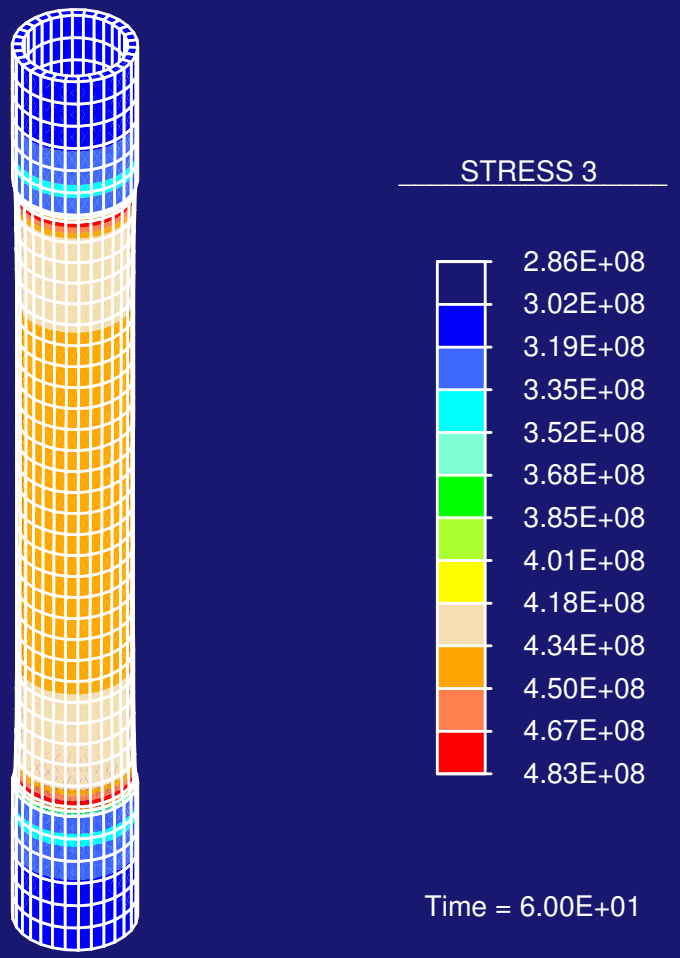

T_{33} stress distribution for pure tension at 6 % strain

Numerical simulations

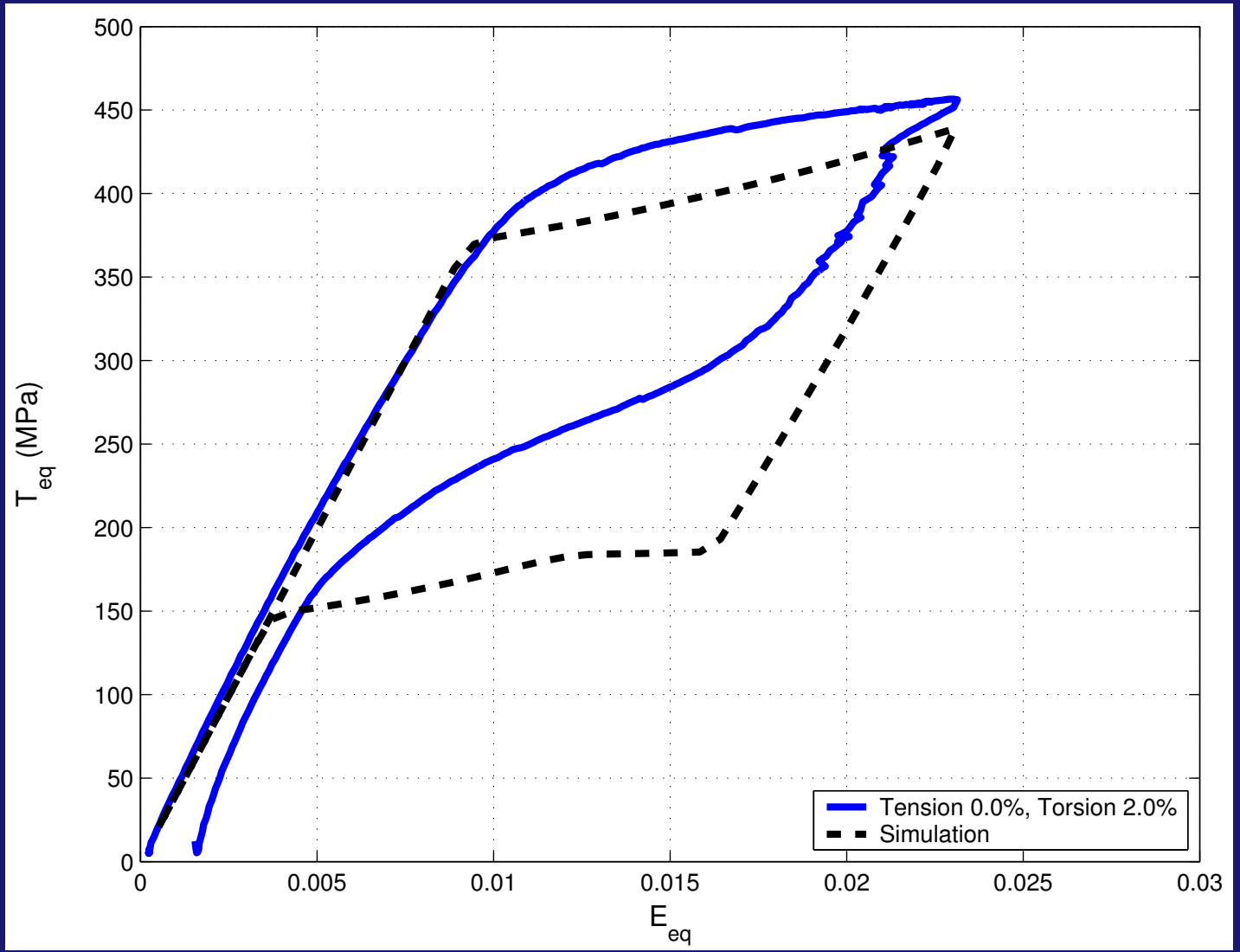

Equivalent stress-strain plot for pure torsion

Numerical simulations

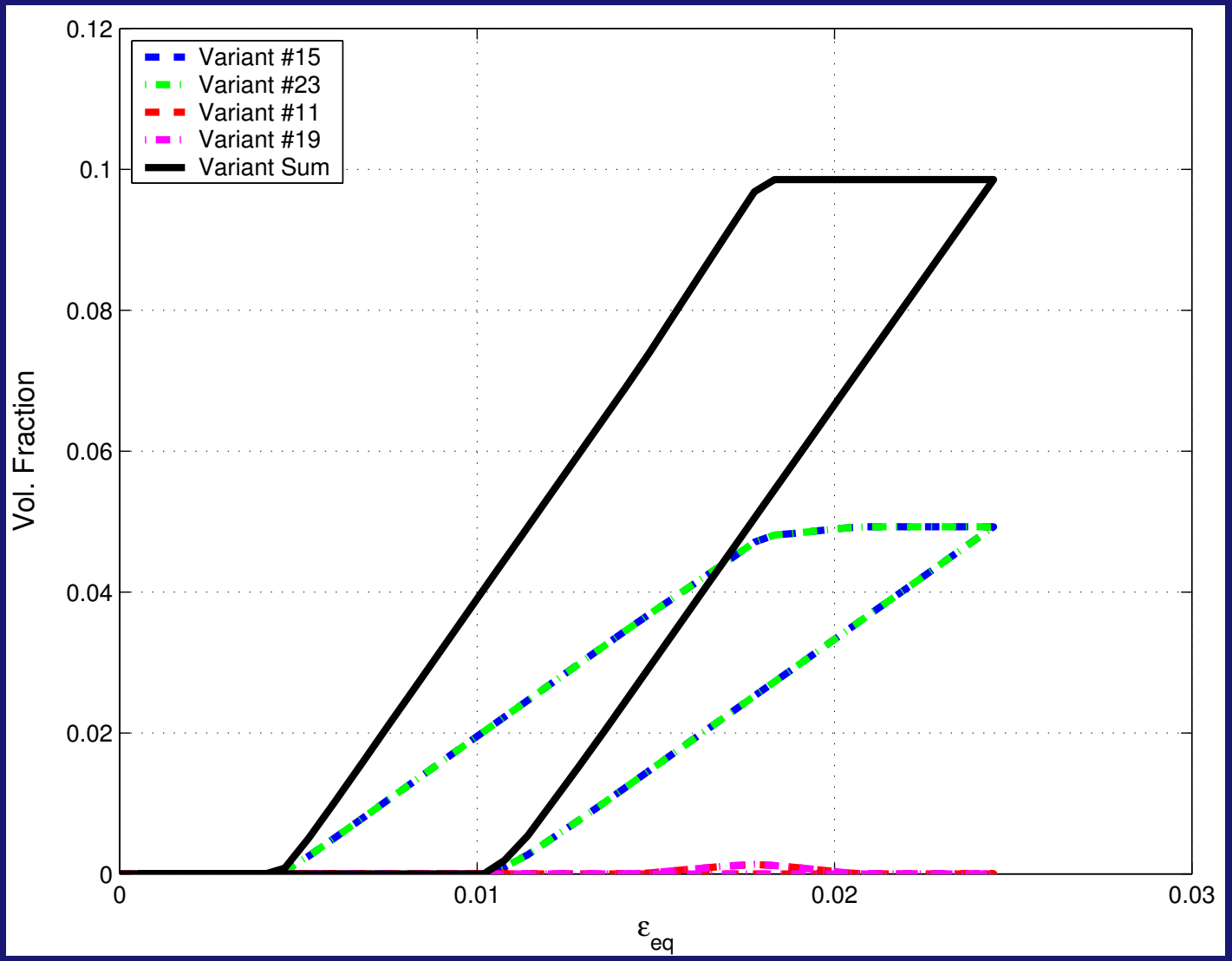

Volume fraction vs. equivalent strain for pure torsion

Numerical simulations

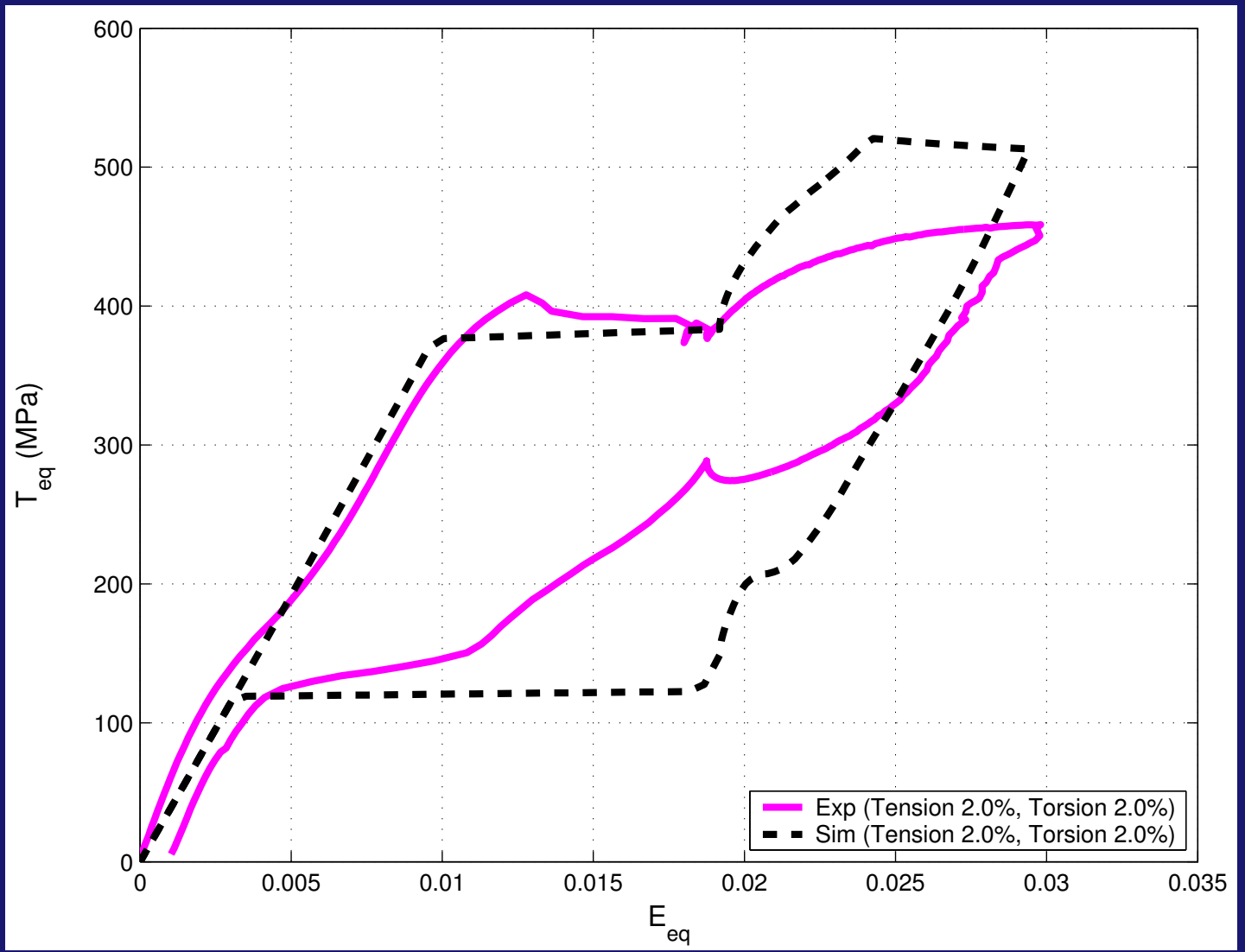

Equivalent stress-strain plot for tension followed by torsion (TYPE I)

Numerical simulations

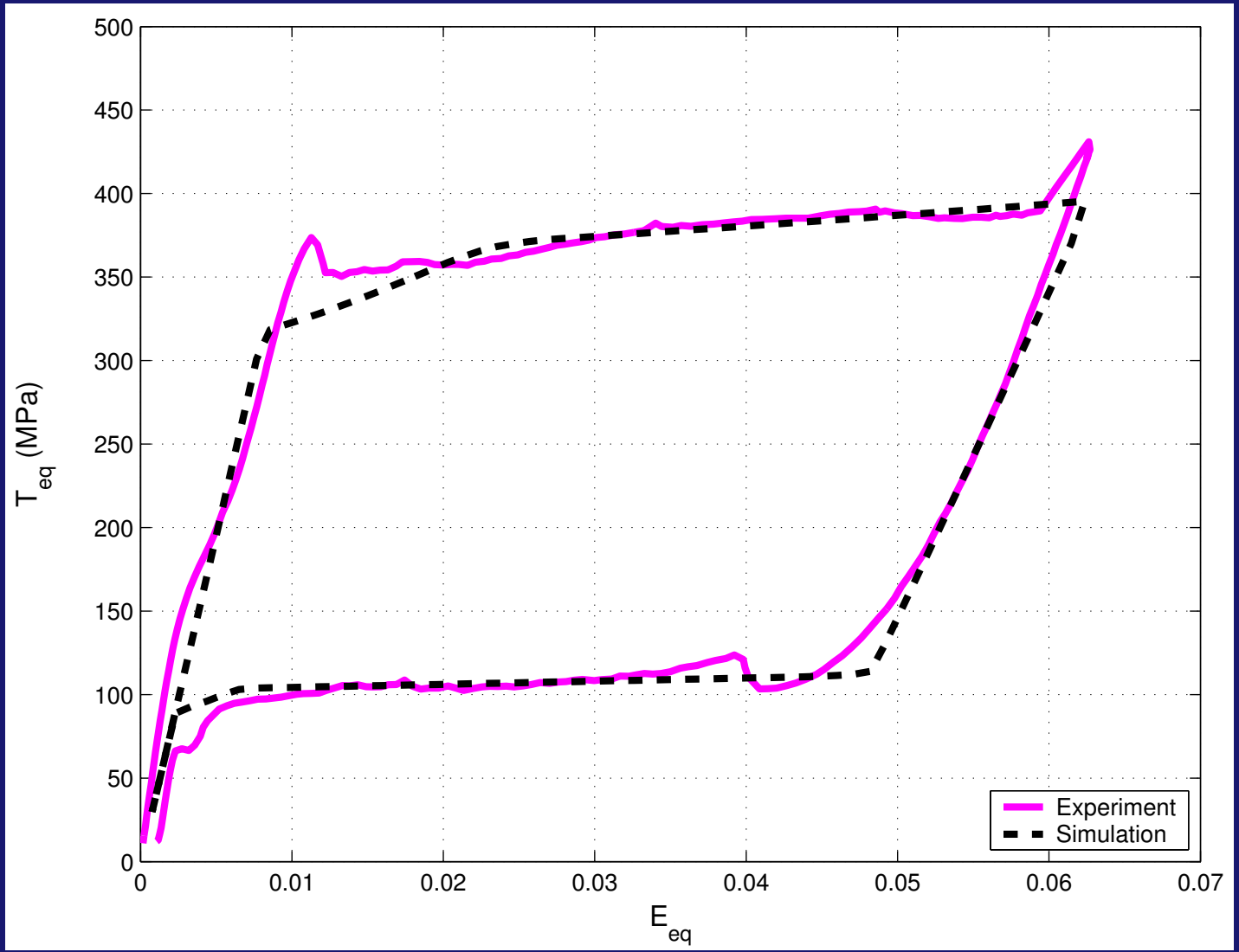

Equivalent stress-strain plot for simultaneous tension/torsion (TYPE III)

Numerical simulations

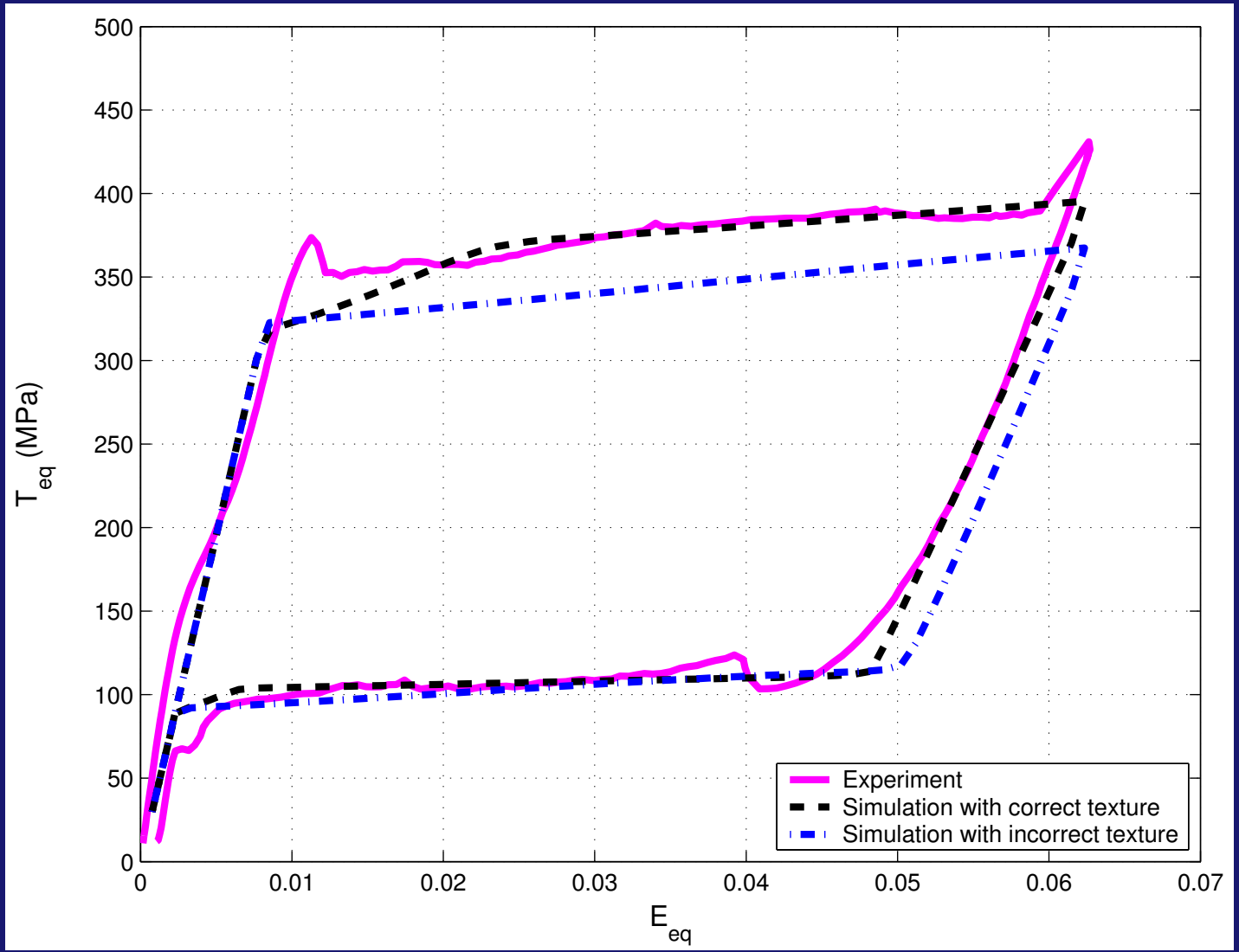

Effect of texture on equivalent stress-strain response

Numerical simulations

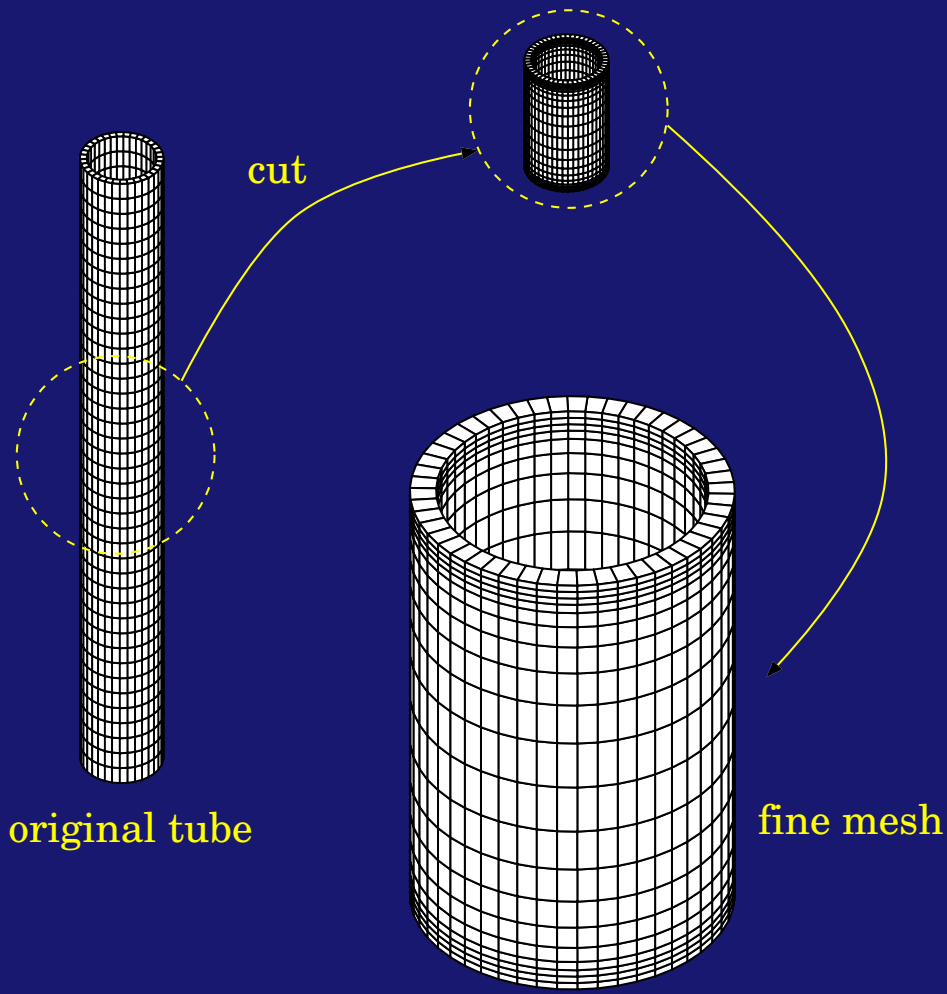

Schematic of stent manufacturing

Numerical simulations

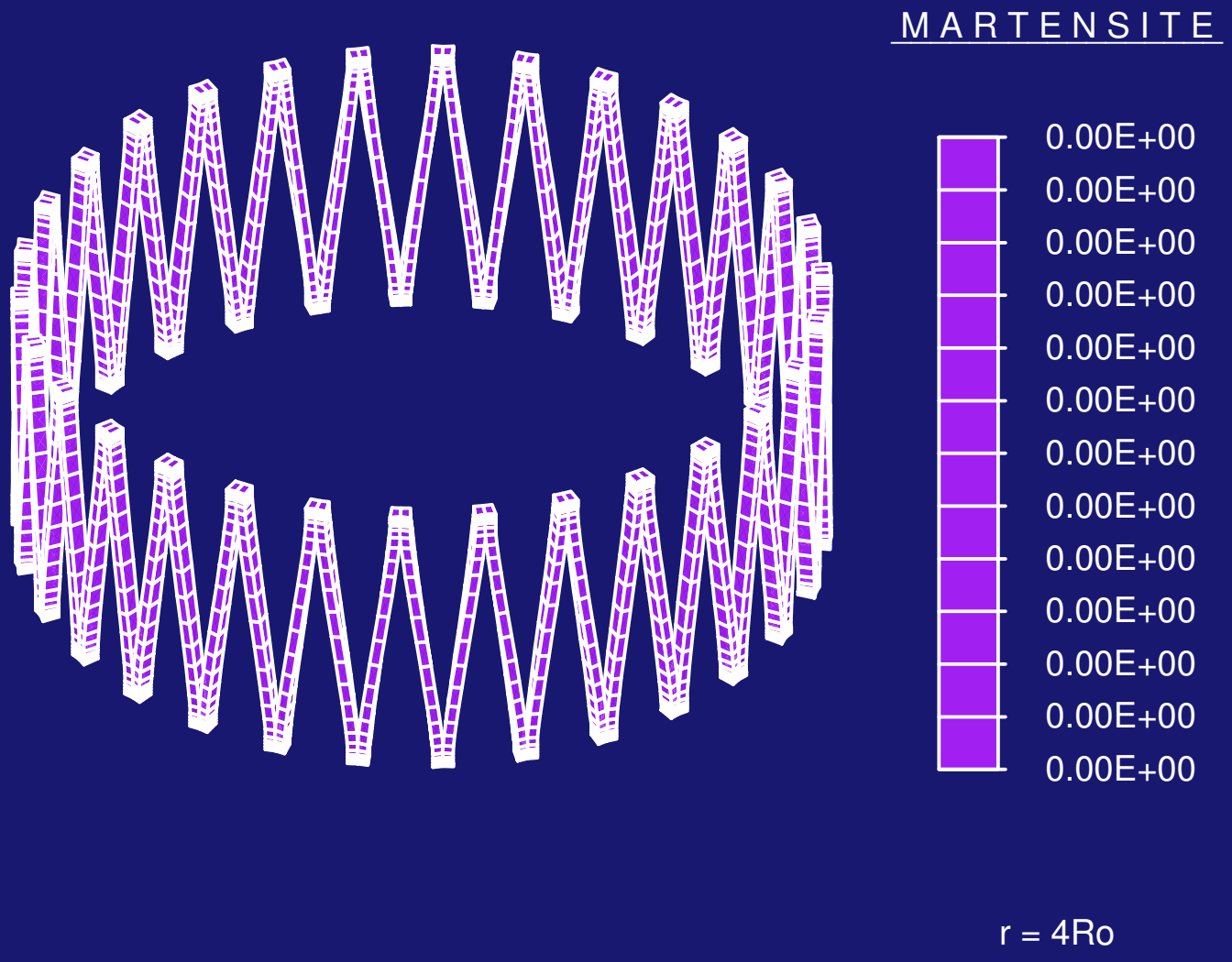

Martensite distribution on a stent in compression/tension cycle

Numerical simulations

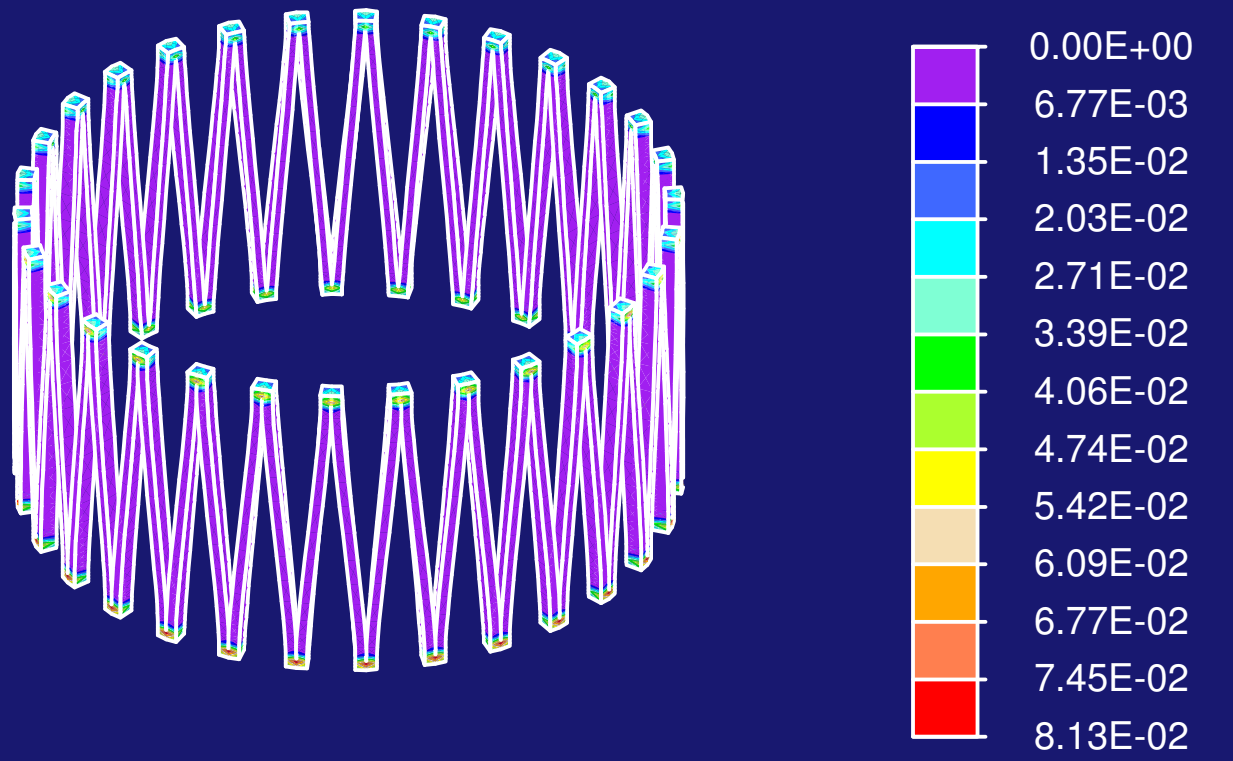

Martensite distribution on a stent in compression/tension cycle

Numerical simulations

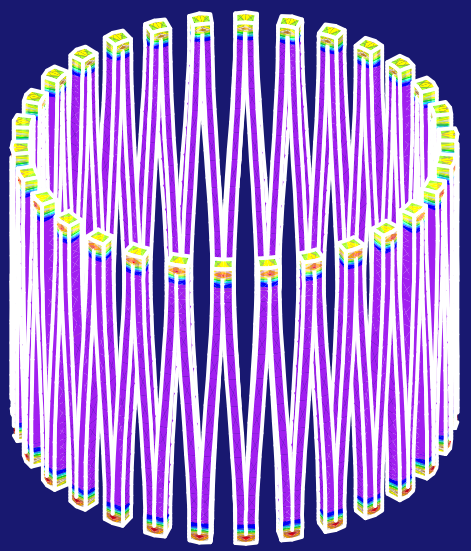

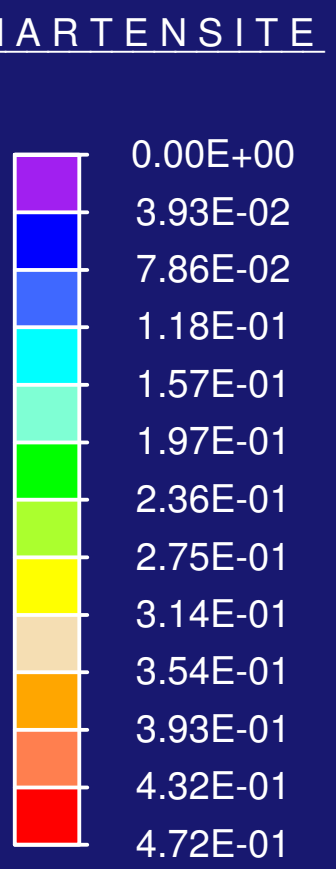

r = 2Ro

Martensite distribution on a stent in compression/tension cycle

Numerical simulations

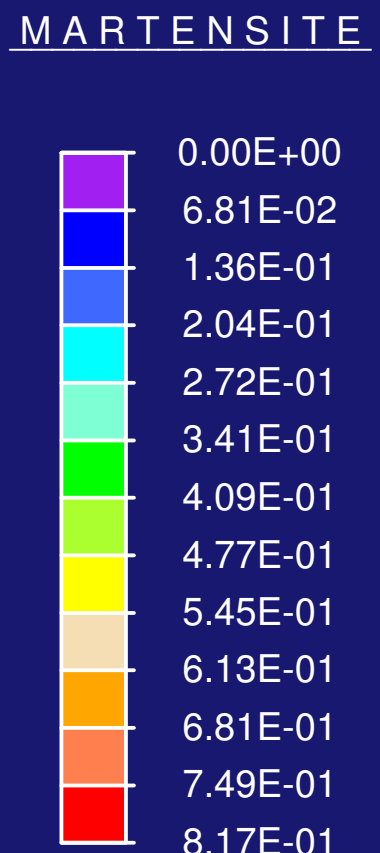

r = Ro

Martensite distribution on a stent in compression/tension cycle

Numerical simulations

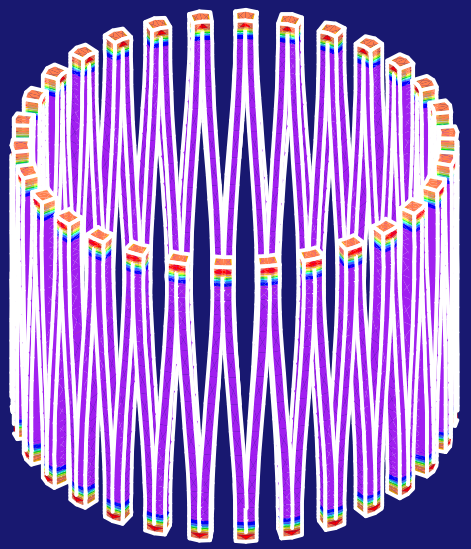

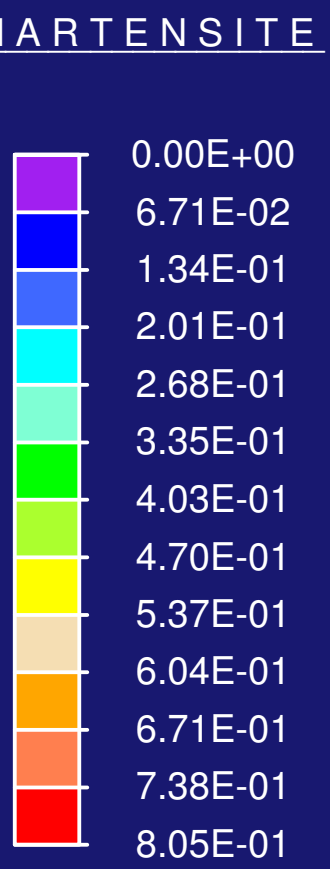

r = 2Ro

Martensite distribution on a stent in compression/tension cycle

Numerical simulations

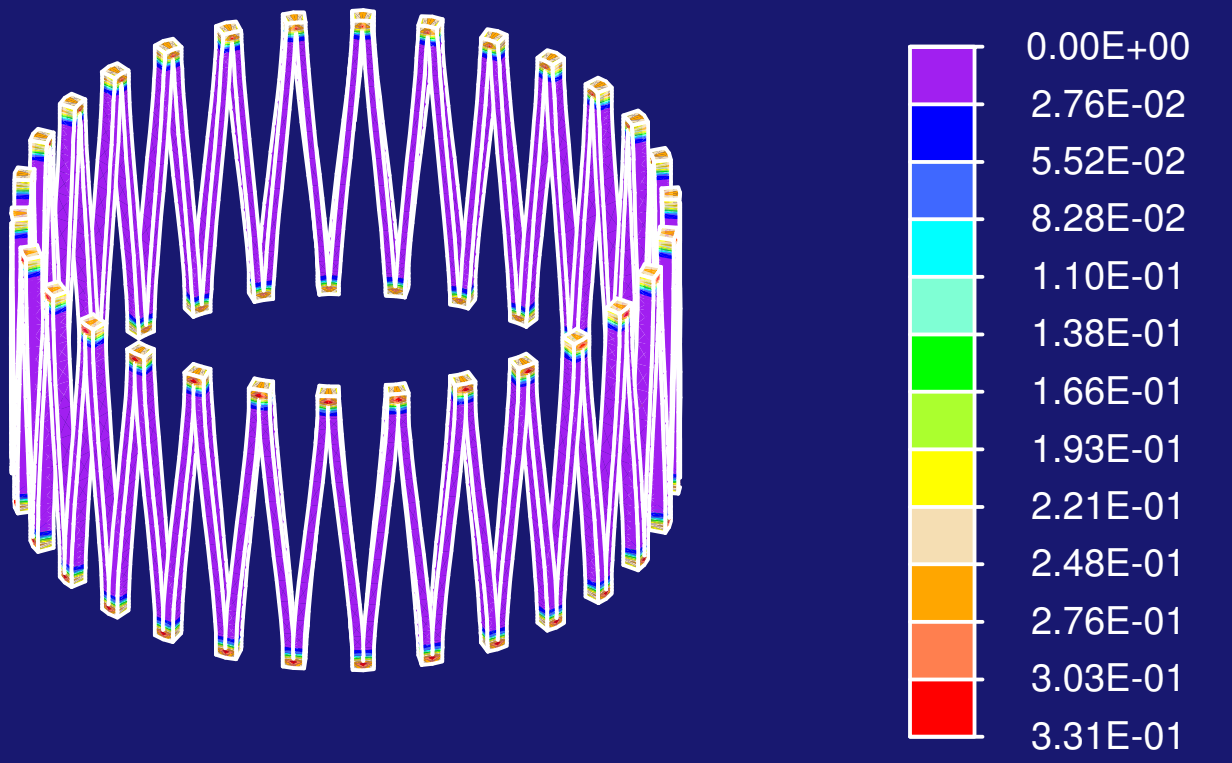

Martensite distribution on a stent in compression/tension cycle

Numerical simulations

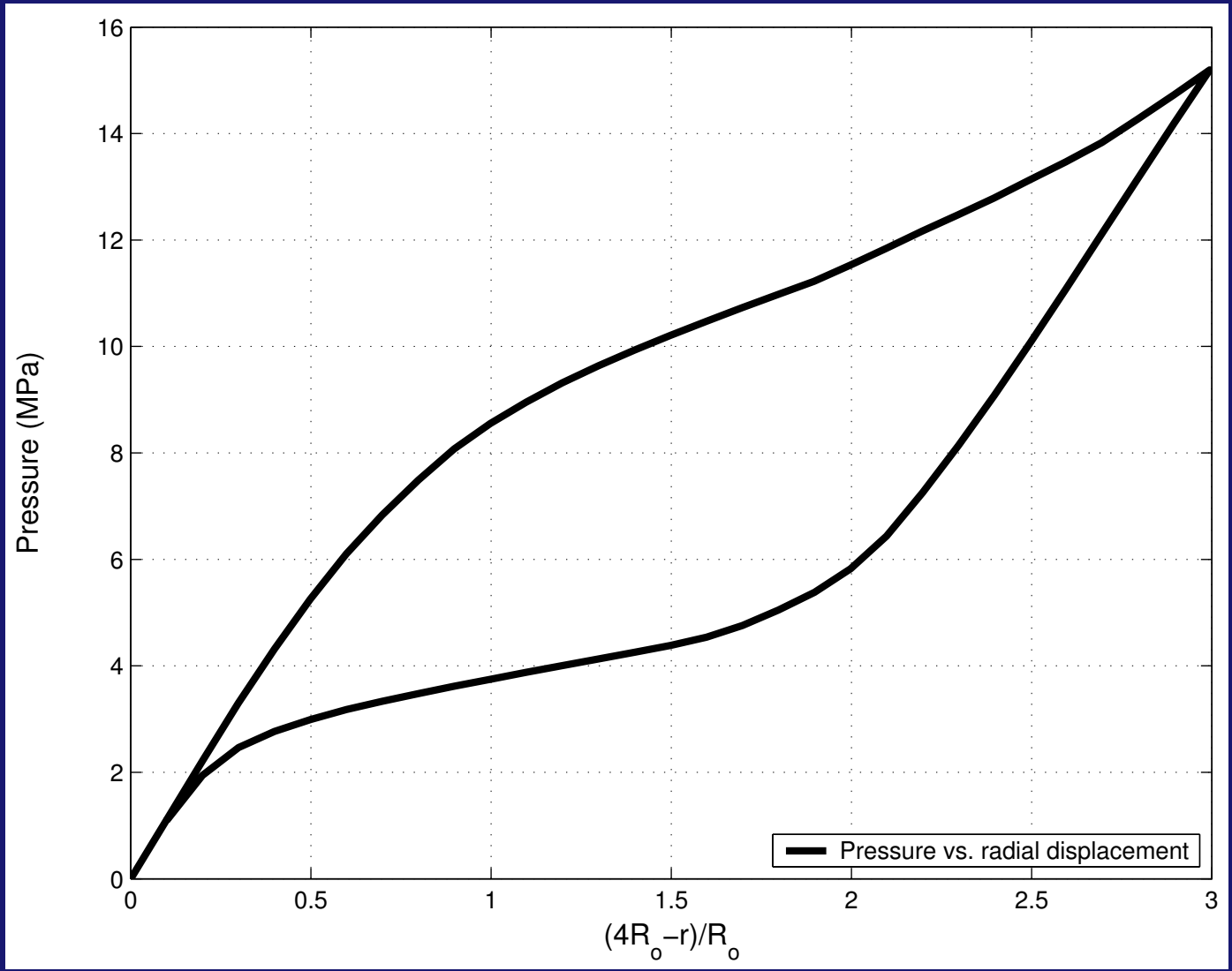

Pressure-radial displacement plot for a stent

Numerical simulations

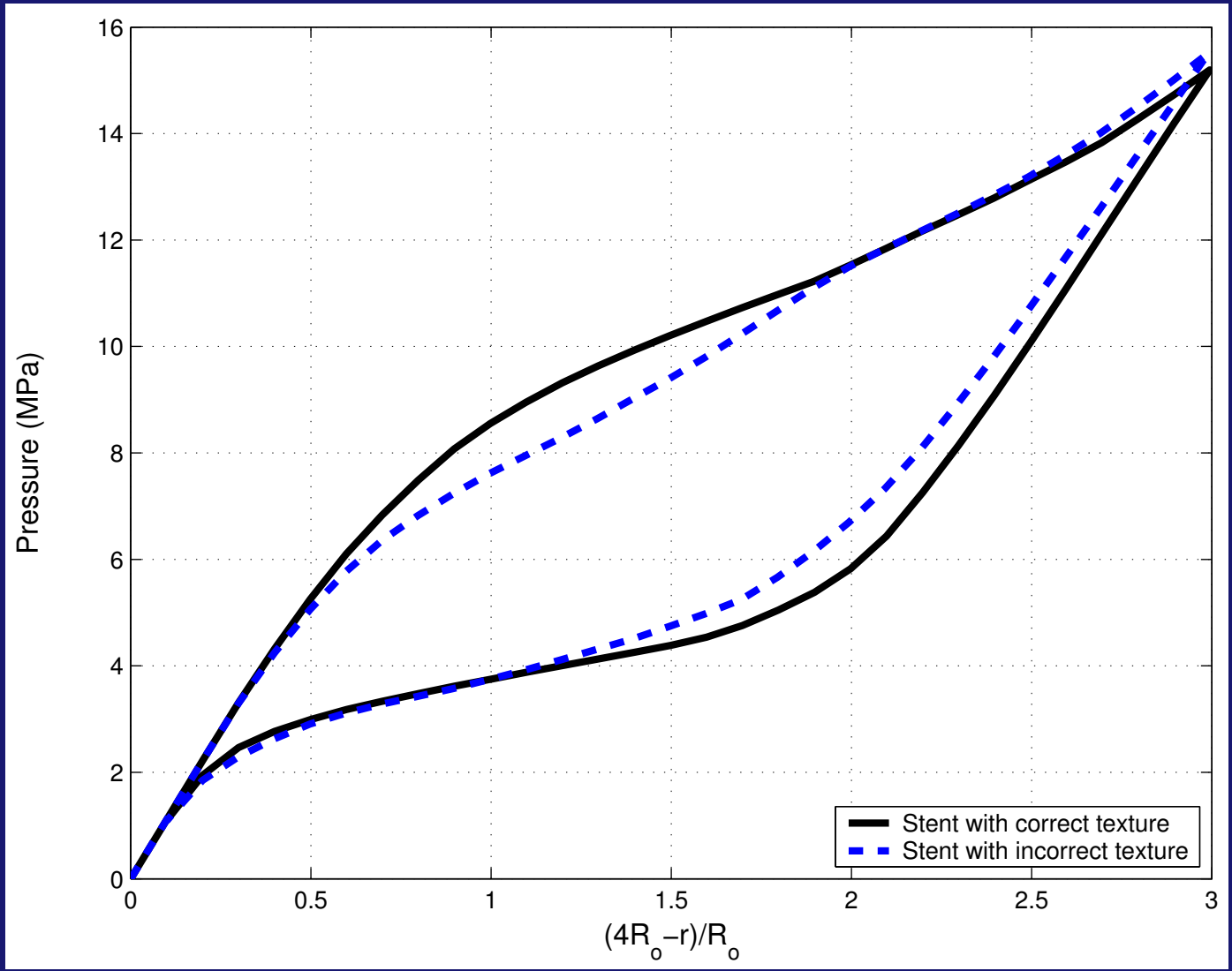

Effect of texture on stent response

Numerical simulations

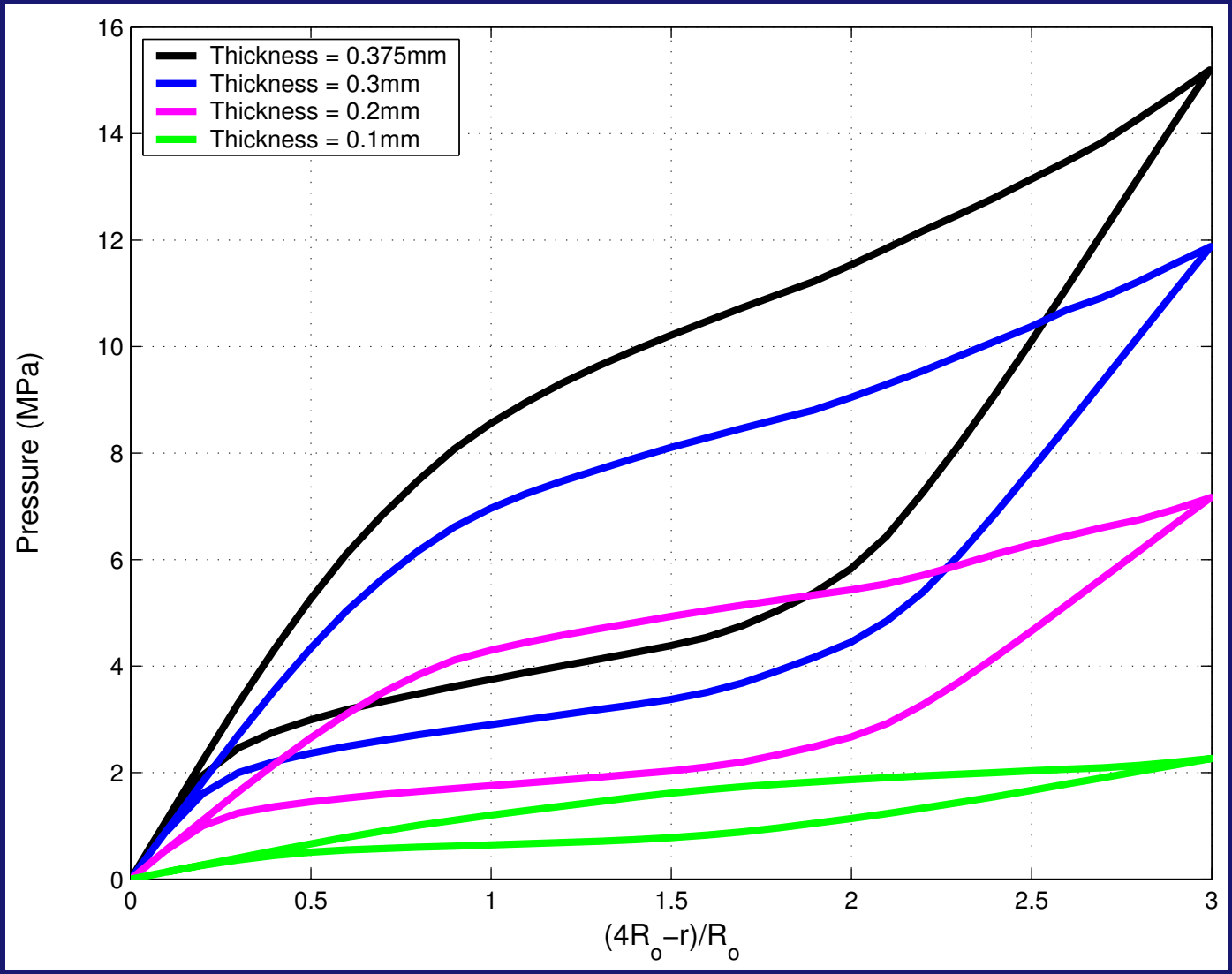

Effect of wall-thickness on stent response

Numerical simulations

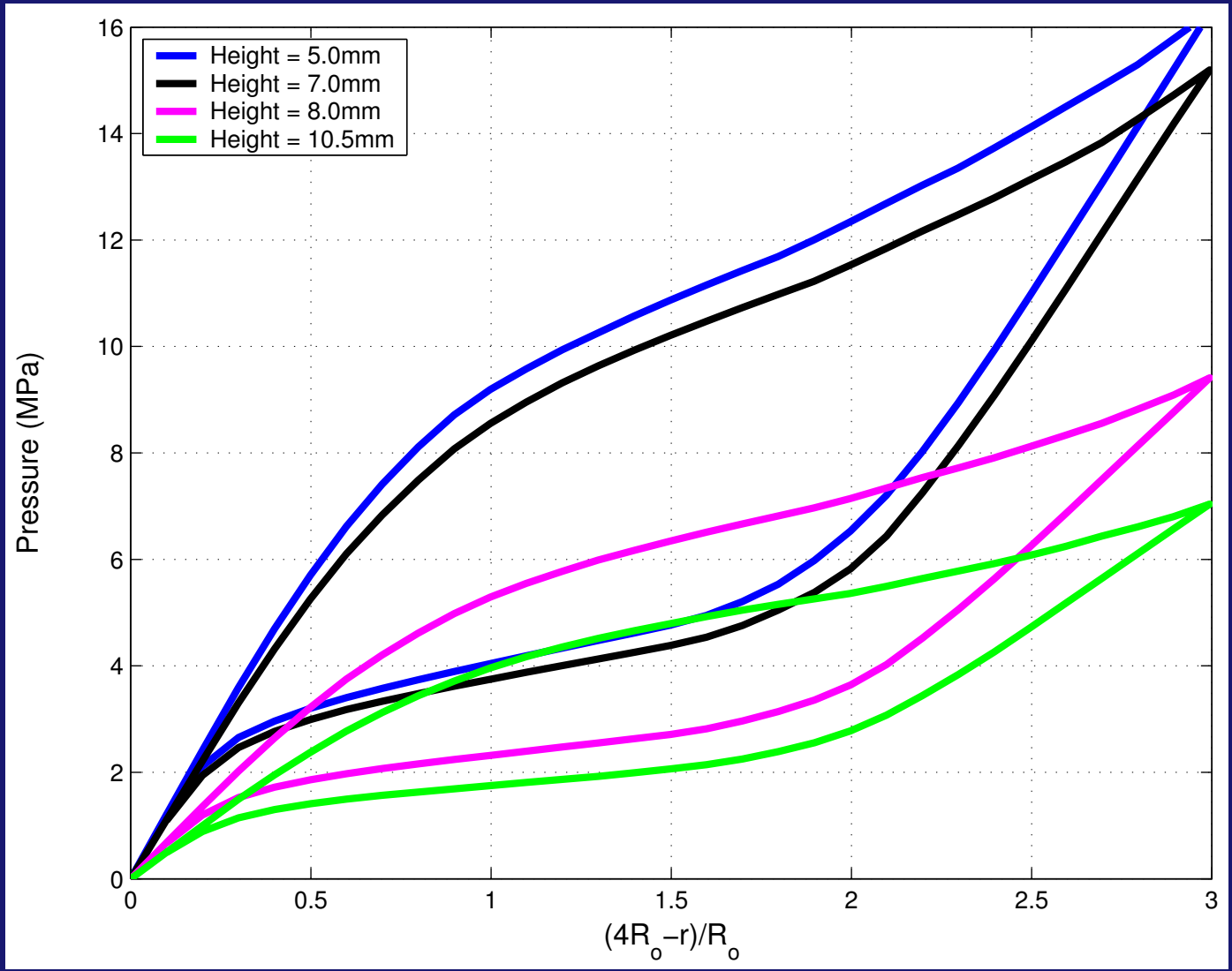

Effect of cascade-height on stent response

Closure

- Superelasticity may be algorithmically tackled either as a multi-phase elasticity problem or as a plasticity-like problem.
- The multi-phase elasticity problem (unified approach) makes no algorithmic distinction between elastic loading and forward transformation.
- The plasticity-like problem introduces an element of new physics in the flow-like rule for the evolution of the variant volume fractions.
- Texture can be incorporated either via direct simulation or by two-scale modeling.

References

1. M.A. Qidwai and D.C. Lagoudas, *Int. J. Numer. Meth. Engrg.*, **47**, pp. 1123-1168, (2000) [Plasticity-like algorithmic development for phenomenological theory].

2. S. Govindjee and C. Miehe, *Comp. Meth. Appl. Mech. Engrg.*, **191**, pp. 215-238, (2001) [Plasticity-like algorithmic development for microstructural theory].

3. Y. Jung, P. Papadopoulos and R.O. Ritchie, *Int. J. Numer. Meth. Engrg.*, **60**, pp. 429-460, (2004) [Elasticity-based algorithmic development for microstructural theory].

4. U.F. Kocks, Chapter 2 of **Texture and Anisotropy**, Cambridge UP, (2000) [Background on texture measurement].